UNIVERSITY OF CALIFORNIA

Santa Barbara

Patient-Derived Induced Pluripotent Stem Cells for Modeling Splicing Factor Retinitis Pigmentosa in Retinal Pigmented Epithelial Cells and Retinal Organoids

A Dissertation submitted in partial satisfaction of the

requirements for the degree Doctor of Philosophy

in Biochemistry and Molecular Biology

by

Leah Priscilla Foltz

Committee in charge:

Professor Dennis Clegg, Chair

Professor Peter Coffey

Professor Stuart Feinstein

Professor Megan Valentine

Professor Carol Vandenberg

June 2018

The dissertation of Leah Priscilla Foltz is approved.

_____

Peter Coffey

_____

Stuart Feinstein

_____

Megan Valentine

_____

Carol Vandenberg

_____

Dennis Clegg, Committee Chair

June 2018

Patient-Derived Induced Pluripotent Stem Cells for Modeling Splicing Factor Retinitis Pigmentosa in Retinal Pigmented Epithelial Cells and Retinal Organoids

by

Leah Priscilla Foltz

ACKNOWLEDGEMENTS

I would like to acknowledge my scientific advisor, Dr. Dennis O. Clegg, for providing guidance for the past five years. I would also like to thank the graduate students who mentored me in my early years, especially Lyndsay Leach, Tracy Clevenger, and Roxanne Croze, as well as the current Clegg lab members who make every day at work a collaborative and enjoyable experience.

Thank you to my committee members, Dr. Pete Coffey, Dr. Stu Feinstein, Dr. Megan Valentine, and Dr. Carol Vandenberg. Pete's depth of knowledge in the retinal field helped me refine my experimental design. Stu's ability to make me think beyond the methods and surface level results helped me achieve a more in-depth analysis. Megan's insights into the importance of negative results and developing tools helped me frame my publications and presentations. Finally, Carol's concise scientific writing and constructive criticism pushed me to mature my scientific thinking.

I would like to acknowledge our collaborators at the University of Wisconsin-Madison and Harvard University. Dr. James Thomson and Dr. Sara Howden generously provided the cell lines that served as the foundation of my thesis. Dr. Eric Pierce, who originally isolated the cells from a patient, and Dr. Revital Bronstein, who assisted in the RNA sequencing experiments. Finally, Dr. Ken Kosik and Elmer Guzman, who assisted in RNA sequence analysis.

The Laboratory for Stem Cell Biology and Engineering, Neuroscience Research Institute Microscopy Facility, and the Biological Nanostructures Genetics Core were critical to the completion of this work. My appreciation goes to the principal

investigators who establish and maintain high quality, state-of the art core facilities. I would like to personally thank the directors and associate directors of these shared core facilities whose level of knowledge and expertise provided an invaluable resource. Specifically, Michelle Maloney and Cassidy Arnold for training me to perform stem cell culture, Mary Raven and Ben Lopez for aiding in confocal imaging, and Jennifer Smith for answering my many questions regarding sequencing.

Thank you to my parents who have supported me both emotionally and financially through my career as a graduate student. You have believed in my ability to complete this journey from day one. It was this unwavering support that got me through long days, failed experiments, and self-doubt. I would also like to thank my siblings, both by blood and by marriage: David, Kelsey, Gavin, Alyssa, and Brendan. It is your curiosity and genuine interest in my work that kept me motivated to hone my skills in scientific communication. Especially to my sister, Kelsey, whose acting tips helped me refine my presentations and kept me calm on stage at my Grad Slam and TEDx endeavors.

Finally, and most of all, I would like to thank my partner, John Eliot Macy. Your dedicated work ethic is infectious and your passion for your company has inspired me to find passion in what I do. Thank you for listening to my rehearsals countless times, providing a fresh perspective, and for believing in my ability as a scientist.

VITA OF LEAH PRISCILLA FOLTZ

as of June 2018

EDUCATION

2013-2018 **Ph.D. in Biomolecular Science and Engineering** (expected)

Biomolecular Science and Engineering program

University of California at Santa Barbara

Dissertation: **Patient-Derived Induced Pluripotent Stem Cells for Modeling Splicing Factor Retinitis Pigmentosa in Retinal Pigmented Epithelial Cells and Retinal Organoids**

2013-2018 **Certificate in Technology Management** (expected)

Technology Management Program

University of California at Santa Barbara

2009-2013 **B.S. in Biochemistry and Molecular Biology**

Molecular, Cellular, and Developmental Biology

University of California at Santa Barbara

PUBLICATIONS

Foltz, L.P., Howden, S.E., Bronstein, R., Guzman, E., Pierce, E.A., Thomson, J.A., Clegg, D.O., 2018. Transcriptome Analysis and Functional Assessment of Patient-Derived Retinal Cells as Corrected by CRISPR/Cas9. (in preparation)

Foltz, L.P., Clegg, D.O., 2018. Patient-Derived Induced Pluripotent Stem Cells for Modelling Genetic Retinal Dystrophies. Prog. Retin. Eye Res. (in revision)

Foltz, L. P., Clegg, D. O. Rapid, Directed Differentiation of Retinal Pigment Epithelial Cells from Human Embryonic or Induced Pluripotent Stem Cells. *J. Vis. Exp.* (128), e56274, doi:10.3791/56274 (2017).

RESEARCH EXPERIENCE

2015-2018 **Ph.D. Candidate,** Dennis Clegg Lab, UCSB

Biomolecular Science and Engineering program

Developed an *in vitro* disease model for splicing factor retinitis pigmentosa.

2014- 2015 **Graduate Student Researcher,** Dennis Clegg Lab, UCSB

Developed a project to qualify as a Ph.D. candidate.

Spring 2014 **Graduate Student Researcher,** Pete Coffey Lab in collaboration with Dennis Clegg Lab, UCSB

Studied the effects of titanium substrates on retinal pigmented epithelial cells.

Winter 2014 **Graduate Student Researcher,** Ken Kosik Lab

Optimized a protocol for developing cerebral organoids from stem cells. Achieved neuronal cell expression.

Fall 2013 **Graduate Student Researcher,** Dennis Clegg Lab, UCSB

Characterized the directed differentiation of keratinocytes into retinal pigmented epithelial cells.

2011-2013 **Undergraduate Student Researcher,** Cherie Briggs Lab, UCSB

Performed genetic analysis of Rana Sierrae frog populations with relation to their microbiome and fungal infections.

Investigated the cause of differences in fungal infections across lakes in the Sierras.

AWARDS & HONORS

2018	New Venture Competition Finalist and Honorable Mention
2017	UC Grad Slam People's Choice Award Winner
2017	UCSB Grad Slam Grand Prize Winner (Best 3-minute Talk)
2017	Neuroscience Research Institute Travel Award
Summer 2015	Breaux Fellowship
2015	Nominee for Excellence in Teaching Award Spring 2015
2014-2015	Crossroads Fellow
2014	Garland Scholar
2013	Distinction in the Major, UCSB
2012	Worster Award for Undergraduate Research Assistant

SCIENTIFIC COMMUNICATION EXPERIENCE

February 2018	Invited Speaker at Braille Institute
November 2017	Speaker at TEDx Santa Barbara
June 2017	Invited Speaker at Stanford Blood Center, Cafe Scientifique
March 2017	Society for Developmental Biology West Coast Annual Meeting, Poster Presentation

Summer 2015	UC Systemwide Bioengineering Conference, UCSF
	Poster Presentation
June 2015	UC Systemwide Bioengineering Conference, UCSC
	Poster Presentation

ABSTRACT

Patient-Derived Induced Pluripotent Stem Cells for Modeling Splicing Factor Retinitis Pigmentosa in Retinal Pigmented Epithelial Cells and Retinal Organoids

by

Leah P. Foltz

Retinitis pigmentosa is the leading cause of inherited blindness, affecting 1 in 3,000 individuals throughout the world. Advancements in genetic screening have helped the field identify the vast range of genetic mutations that can result in the retinal dystrophy observed in retinitis pigmentosa patients, but the underlying pathogenic mechanisms of these mutations are not well understood. Two major questions remain in understanding the pathology of this disease. First, the degree to which certain cell types are affected remains undetermined, namely the photoreceptors and their supportive retinal pigment epithelial cells. Second, the molecular mechanisms by which these diseases take place are not fully elucidated. In addition to being costly, animal models have limitations in recapitulating the pathology of these ocular diseases, especially with regards to patient-specific retinitis pigmentosa mutations. Induced pluripotent stem cells hold significant potential to elucidate the mechanisms of disease. This work characterizes the pathology of autosomal dominant retinitis pigmentosa and autosomal recessive retinitis pigmentosa using *in vitro* disease models with human cells. A point mutation in PRPF8, a ubiquitously expressed splicing factor, causes autosomal dominant retinitis

pigmentosa. This dissertation presents a novel cellular model of splicing factor retinitis pigmentosa using patient-derived, gene-corrected induced pluripotent stem cells. By differentiating both diseased and corrected cells into retinal pigmented epithelial cells and retinal organoids, genetic and functional analyses were performed to identify the differences between diseased and healthy retinal cells. Previously identified defects in murine retinal pigmented epithelial cell function were not identified in human retinal pigmented epithelial cells. By using unbiased RNA sequencing analysis, differences have been identified in the retinal pigmented epithelial cells at the level of long noncoding RNA and cell cycle regulation. Taken together, these finding highlight the importance of using human cells for disease modeling of the retina and the role of long noncoding RNA and cell cycle regulation in the pathology of splicing factor retinitis pigmentosa.

Table of Contents

LIST OF FIGURES AND TABLES

I. Patient-Derived Induced Pluripotent Stem Cells for Modeling Inherited Retinal Dystrophies

ABSTRACT

The human retina is a highly complex tissue that makes up an integral part of our central nervous system. It is astonishing that our retina works seamlessly to provide one of our most critical senses, and it is equally devastating when a disease destroys a portion of the retina and robs people of their vision. After decades of research, scientists are beginning to understand retinal cells in a way that can benefit the millions of individuals suffering from inherited blindness. This understanding has come about in part with the ability to culture human embryonic stem cells and the discovery of induced pluripotent stem cells, which can be cultured from patients and used to model their disease. In this chapter, we highlight the successes of specific disease modeling studies and resulting molecular discoveries. The greatest strides in cellular modeling have come from mutations in genes with established and well-understood cellular functions in the context of the retina. We believe that the future of cellular modeling depends on emphasizing reproducible production of retinal cell types, demonstrating functional rescue using site-specific programmable nucleases, and shifting towards unbiased screening using next generation sequencing.*

A. Genetic Heterogeneity of Retinitis Pigmentosa

The human retina consists of not just a few types of neurons, but rather is made up of around 55 different cell types[1]. Masland et al. 2001 describes the added complexities of the primate retina, which unlike some simpler mammals, consists of two types of horizontal cells, twenty-nine types of amacrine cells, between ten and fifteen different retinal ganglion cells, and so on. In the context of disease modeling, it is hard to imagine that it is possible to recapitulate the highly complex, fundamental plan of the retina. The success of existing disease models suggests it is not necessary to produce all of these cell types in a way that mimics the positions and proportions they are found *in vivo.* Instead, the research produced thus far has elucidated molecular pathology by focusing on two of the most commonly affected cell types: photoreceptors and retinal pigmented epithelial cells (RPE).

Inherited retinal dystrophies such as retinitis pigmentosa and Leber congenital amaurosis, cause degeneration of the retina and result in a loss of vision[2]. The pathology of these diseases has been documented in patients and animal models, which provide a limited amount of information about the cellular mechanisms of disease[3,4]. The retina makes up the posterior portion of the eye and consists of an inner and outer layer of neurons. The inner layer, consisting of ganglion, amacrine, bipolar, and horizontal cells, is generally less affected by retinal dystrophies than the outer layer, consisting of light-sensing photoreceptor cells and supportive retinal pigmented epithelial cells[5].

Retinitis pigmentosa is the most commonly inherited retinal dystrophy, affecting approximately 1 in 3,000 individuals[2]. This disease is inherited in both autosomal dominant, autosomal recessive, and X-linked patterns and can be caused by a mutation in any one of more than 60 genes[6,7].

The disease begins with a loss of night vision, followed by peripheral vision, and in some cases results in complete blindness. While hyperpigmentation of the retina is a hallmark of the disease, the cellular and molecular mechanisms underlying this phenotype remain unclear. The most accepted hypothesis is that retinitis pigmentosa is a rod-cone dystrophy, with degeneration of rods preceding cones and later atrophy of retinal pigmented epithelial cells. There are some studies that suggest the retinal pigmented epithelial cells are predominantly affected in splicing factor mutations, such as pre-mRNA processing factors: PRPF3, PRPF8, and PRPF31[8]. These data are based on a mouse model of the disease, and the results have yet to be replicated in a human cellular model.

The first report of a disease model using patient-derived induced pluripotent stem cells (iPSCs) to study the pathology of retinitis pigmentosa in retinal cell types examined five patient cell lines spanning four known causative mutations: RP1, RP9, PRPH2, RHO[9]. The same researchers published a follow-up study in which they demonstrated rod degeneration in addition to the reported ER stress[10].

Several groups have been successful in modeling rhodopsin mutations in early disease models using two-dimensional photoreceptors. Jin et al. 2011 and 2012 examined a G188R point mutation in RHO. A E181K point mutation in RHO resulted

in ER stress and was rescued in the two-dimensional photoreceptors using helper-dependent adenoviral vector gene transfer[11].

One of the earliest studies using a three-dimensional multi-layer retinal organoid examined the pathogenicity of mutations in usherin (USH2A)[12]. While mutations in USH2A are commonly known to cause a syndromic Usher syndrome I, it is also known to cause non-syndromic retinitis pigmentosa[13]. The patient-derived photoreceptor precursors revealed ER stress, as was shown in the rhodopsin mutants.

In addition to identifying cellular stress caused by pathogenic mutations, stem cell disease modeling is also useful for identifying novel mutations. Early work with two-dimensional retinal progenitor cells demonstrated the pathogenicity of a novel Alu insert into male germ cell-associated kinase (MAK)[14]. More recent research identified novel variants in receptor expression-enhancing protein 6 (REEP6) in iPSC derived three-dimensional retinal organoids[15].

Several disease models have examined pathology in RPE rather than photoreceptors. Membrane frizzled-related protein (MFRP) is an RPE-specific membrane receptor that resulted in actin disorganization in iPSC-derived RPE from two patients[16]. Researchers were able to rescue the actin organization and restore apical microvilli using an AAV8 vector containing MFRP.

Later work introduced the use of translational read through inducing drugs (TRIDs) to show functional rescue in the case of premature stop codons. TRIDs were first used to rescue RPE with nonsense mutations in RP2 (ARL3 GTPase activating

protein)[17]. This work was expanded upon to show restoration of RP2 and rescue of cilia function in three-dimensional retinal organoids[18].

Another case of RPE-specific disease modeling showed known causative mutations in MER receptor tyrosine kinase (MERTK) result in phagocytic defects in patient-derived RPE[19]. This work was expanded upon by again using TRIDs to restore the MERTK and functional rescue of phagocytosis[20].

tRNA nucleotidyl transferase CCA-adding 1 (TRNT1) and X-linked retinitis pigmentosa GTPase regulator (RPGR) are the most recent additions to the growing list of iPSC disease models. In both studies, three-dimensional retinal organoids were produced from multiple patients using age or sex-matched controls, respectively. Various indels in TRNT1 resulted in autophagy defects and oxidative stress[21]. Deletions in RPGR resulted in abnormal actin polymerization and rhodopsin mislocalization and proposed a novel model for RPGR mediated actin regulation[22].

Future studies should focus on reproducing these findings in other patients with the mutations reported here and expanding to include other mutations that have yet to be modeled using iPSC. Any research that was conducted in two-dimensional retinal precursors should be repeated in three-dimensional retinal organoids, which more closely mimic the *in vivo* environment of photoreceptors.

B. Patient-Derived Induced Pluripotent Stem Cells

Induced pluripotent stem cells (iPSC) were initially produced from adult fibroblasts[23,24]. Fibroblasts are relatively accessible via a minimally invasive skin biopsy. There are now cases of iPSC production from other sources, including blood

and urine, which require even less invasive or entirely noninvasive procedures, respectively. Mononuclear blood cells or renal tubular cells are isolated from the blood or urine and used for reprogramming[25,26]. For example, activated T-cells were isolated from a routine peripheral blood sample to derive iPSCs and subsequently study a point mutation in visual homeobox 2 (VSX2)[27]. The same researchers had previously demonstrated that activated T-cell derived cells had the capacity to produce retinal cells and retinal organoids[28].

There is not currently a consensus on the preferred somatic cell source for producing iPSCs. In deciding upon which cell type is best going forward, the field considers the invasiveness of the procedure, the plasticity of the resulting stem cells, and the ability to differentiate into various retinal cell types. Research has shown that stem cells may retain cellular memory of the somatic cell source[29]. More research is needed to systematically determine the benefits and shortcomings of each potential cell source.

Induced pluripotent stem cells, which were first described in 2007, are an essential tool in modeling inherited retinal dystrophies[23,24]. Reprograming methods have been reviewed thoroughly with regards to integrating versus non-integrating vectors[25,30]. The disease models described here use retroviral transduction, lentiviral transduction, non-integrating Sendai virus, or non-integrating episomal vectors (Table 3-7). More recent modifications have focused on adapting reprogramming methods to adhere to good manufacturing practices (GMP)[31].

C. Gene-Correction Using CRISPR/Cas9

Site-specific programmable nucleases include zinc-finger nucleases (ZFNs), transcription activator-like effector nucleases (TALENs), and most recently RNA-guided engineered nucleases (RGENs), which have been thoroughly reviewed[32]. Kim and Kim et al. 2014 use the term RGENs to avoid confusion with the original CRISPR type II. Clustered regularly interspace short palindromic repeats (CRISPR)/CRISPR associated systems (Cas) were first described in the context of adaptive bacterial immunity[33]. All three of these nucleases are capable of creating double-stranded, site-specific breaks in DNA, which triggers the endogenous DNA repair systems in eukaryotic cells. Although they share a similar mechanism of action, ZFNs, TALENs, and RGENs differ in terms of their success rate, mutation rate, target site length, off-target effects, cytotoxicity, and size[32].

The first several years of disease modeling for retinal dystrophies have relied on viral or drug mediated rescue of patient-derived cells. These techniques are limiting due to the packaging size limits of viruses or the need for a known drug target, respectively. For example, translation read-through inducing drugs have been useful for disease models of RP2, but this is only applicable to cases of premature stop codons[17]. The genetic heterogeneity of retinal dystrophies makes these diseases ideal candidates for precise gene editing by deciphering between subtle pathological differences caused by specific point mutations. Editing the genomic DNA allows the gene to remain under control of the endogenous regulatory elements, more accurately mimicking the disease state.

Notably, Burnight et al. 2017 used CRISPR/Cas9 to generate gene-corrected iPSCs for multiple patient cell lines[34]. This work targeted three mutations in proteins previously studied in disease models: male germ cell-associated kinase (MAK), centrosomal protein 290kDa (CEP290), and rhodopsin (RHO). Early work with iPSCs and retinal progenitors derived from two retinitis pigmentosa patients revealed a pathogenic Alu insert in MAK[14]. The IVS26 cryptic splice mutation in CEP290 has been studied in fibroblasts and three-dimensional retinal organoids, demonstrating functional rescue of cilia via lentiviral transduction or antisense oligonucleotides[35–37]. Early interest in ZFN allowed researchers to engineer the nuclease to repair a common Pro23His rhodopsin mutation known to cause retinitis pigmentosa[38]. These three mutants were selected to demonstrate the efficacy of CRISPR for exonic mutations (MAK), intronic mutations (CEP290), and dominant gain-of-function (RHO)[34].

While most of the retinal disease models discussed in this chapter do not use CRISPR, there are many non-retinal disease models that have successfully used CRISPR[39]. Researchers have started to provide gene-corrected iPSC lines as a lab resource, which will accelerate the use of CRISPR in retinal disease modeling as well as improve reproducibility between studies[40]. To address the concerns of line to line variability with passage of stem cells, Howden et al. demonstrated the ability to reprogram and gene edit iPSC simultaneously[41].

Although CRISPR/Cas9 has received a lot of attention as revolutionary gene-correction technique, there is mounting concern about off-target effects. In the least, the intended gene target should be sequenced to confirm the desired effects, either

disruption or correction. Whole-genome sequencing allows for detection of insertion or deletions elsewhere in the genome. For both CRISPR and TALEN nucleases, WGS has revealed a low incidence of off-target mutations in human stem cells[42]. Improvement of CRISPR techniques have allowed development of Cas9 endonucleases that are efficient without creating insertions and deletions (indels)[30]. Of some concern is the discovery that *in vivo* gene-correction results in single nucleotide variants in addition to indels[43]. Moving forward, researchers should be aware of any off-target effects when using RNA-guided engineering nucleases.

D. Differentiation Methods: RPE and Retinal Organoids

Prior to the discovery of induced pluripotent stem cells (iPSC), researchers had been developing spontaneous and directed differentiation of retinal cell types from embryonic stem cells. The first report of the spontaneous appearance of RPE was described in 2004, three years prior to production of human iPSC[23,24,44]. Spontaneous differentiation methods include any protocol in which the cell type of interest arises without addition of exogenous growth factors or small molecules. These protocols have the advantage of being technically easier than their directed counterparts.

Directed differentiation methods involve the addition of growth factors and small molecules to mimic the *in vivo* developmental process of the retina. Various methods for directing differentiation of RPE in both suspension and adherent cultures has been thoroughly reviewed from 2008 through 2014[45]. In 2015, a novel small-molecule approach was developed using an unbiased approach to screen for RPE-differentiation promoting factors[46]. It has been demonstrated that both spontaneous

and directed differentiation methods give rise to functional RPE across several embryonic and induced pluripotent stem cell lines[47]. Most recently, RPE differentiation that recapitulates normal development without the need for manual dissection, embryoid bodies, or suspension culture was developed[48].

In addition to RPE methods, other protocols have been developed to produce portions of the neural retina, including photoreceptors. Production of neural retina has been approached in both two-dimensional[49,50] and three-dimensional methods[51-54]. Various methods for directing differentiation of neural retina in both two-dimensional and three-dimensional cultures for human and mouse stem cells has been thoroughly reviewed from 2006 through 2017[55].

Capowski et al. 2016 demonstrated the patterning of iPSC-derived optic vesicles closely mimics development of the vertebrate eye. In that study, iPSCs were produced from a patient with a mutation in VSX2 (R200Q), which is known to cause microphthalmia[27]. The optic vesicles from the mutated cells had proliferation defects and a disproportionate amount of RPE differentiation when compared to the unaffected sibling. RNA sequencing experiments revealed a significant effect on the expression of WNT genes, identifying a role for VSX2 and highlighting the usefulness of next generation sequencing in identifying novel roles for transcription factors[56]. The ability to mimic *in vivo* development of retinal tissue has also been confirmed in mouse stem cell lines[57]. Functional characterization by live imaging of retinal organoids further demonstrates the recapitulation of human development[58].

E. Next generation sequencing

In the simplest terms, a disease model is a causal model that investigates a cell or tissue with a defect that results in disease symptoms. In the case of retinal dystrophies, a patient harbors a mutational defect that results in blindness. A medical doctor must first identify the physical defects of the retina, properly diagnose the disease, and identify the genetic mutation. The identification of the underlying mutation requires a skin biopsy or blood sample from the patient, which can be used for subsequent gene sequencing and/or isolation of fibroblasts or mononuclear blood cells for production of iPSCs. These stem cells can then be provided to research laboratories for further analysis. Ideally, it would be possible to differentiate the induced pluripotent stem cells into a retinal cell type and notice an obvious defect when compared to a control. For reasons that will be discussed, stem cell disease models are not always able to immediately capture the molecular pathology of the underlying pathogenic mutation. For example, the study of rhodopsin mutations for retinitis pigmentosa have been revisited and refined over several years[9–11]. Causative mutations in another protein, CEP290 provides yet another example of a disease model that has evolved[35–37,59]. The purpose of identifying these research "stories" is to highlight the noticeable diversity of cellular disease models and the need for rigorous evaluation of each model.

When discussing and evaluating stem cell disease models, it is important to identify the controls used for comparison to a patient-derived cell line. There are three models that are frequently employed for investigating IRDs. These involve

comparison of patient-derived cells to 1) wild-type cells, 2) age-matched, sex-matched, or sibling cells, or 3) genome-edited patient-derived cells. In earlier work, wild-type iPSC lines were generally accepted as controls, but with a deeper understanding of line-to-line variability, models are strengthened by the use of sibling controls, or age and sex matched controls in the very least[60].

We believe a criterion standard of cellular disease models would fulfill at least four basic criteria: (1) the model would include stem cell lines from multiple patients harboring the same mutation, (2) the model would compare the diseased patient cells to a gene-corrected version, (3) in addition to the gene-corrected cells, an additional age-matched, sex-matched wild-type control would be included, and (4) any functional rescue would be connected to the function of the mutated gene in some way (**Figure 1**). In practice, it is not always feasible to attain this level of control in every cellular model and a study shouldn't necessarily be disregarded if it does not obtain one or more of the criteria.

With regards to the first criterion, researchers may not have access to patient-derived cell lines and instead introduce the mutation into a wild-type cell line. If this model recapitulates the disease phenotype, it can be said with a reasonable degree of certainty that the mutation is sufficient. Researchers may have access to a patient,

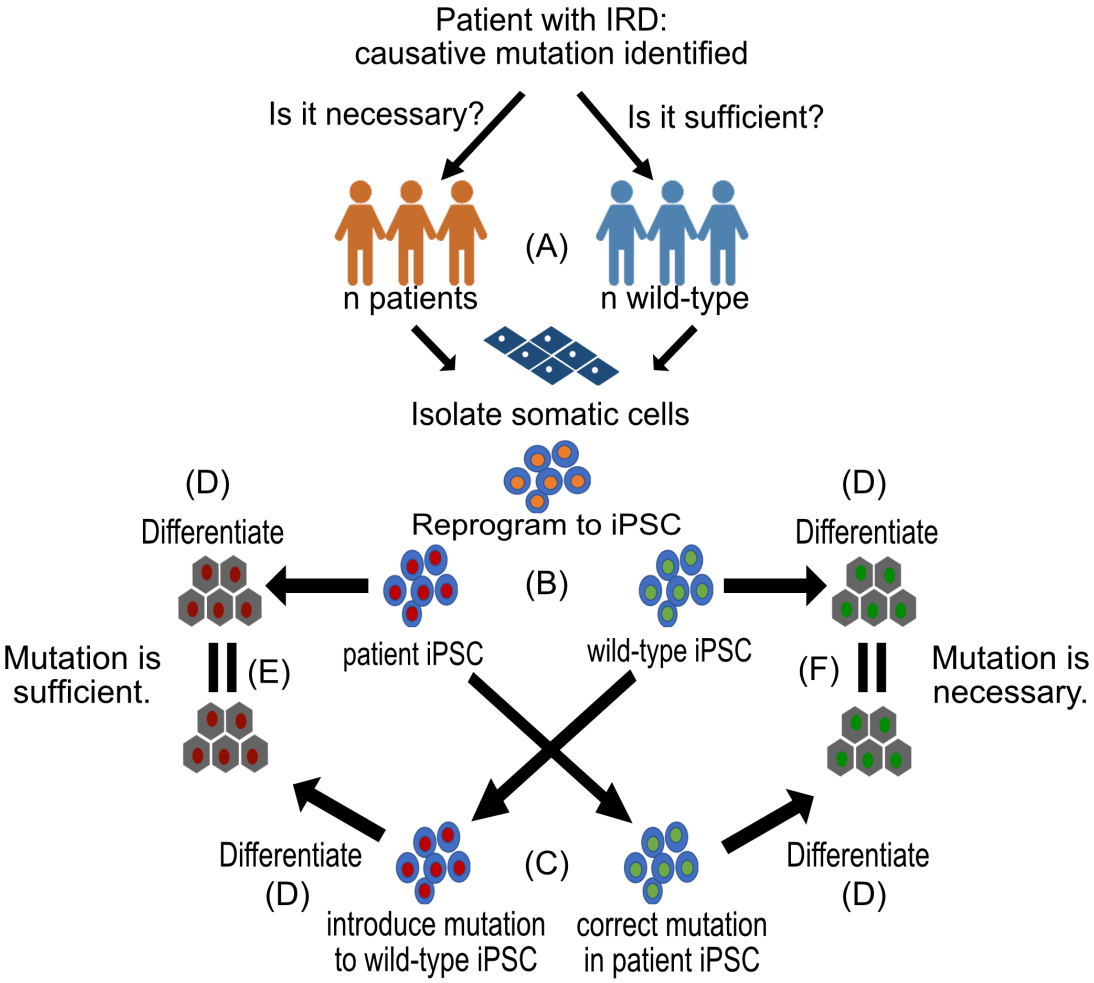

Figure 1. Overall workflow for designing and implementing an iPSC disease model.

(A) One or multiple (n) patients and one or multiple (n) wild-type individuals are identified for isolating somatic cells and producing iPSC. (B) Upon reprogramming, patient cells will harbor the mutation, as indicated in red, and wild-type cells will not, as indicated in green. (C) Site-specific programmable nucleases can be used to correct the patient mutation or introduce the patient mutation in the wild-type samples. (D) After differentiation, cells with and without the mutation can be genetically and functionally analyzed. (E) if the introduction of the mutation mimics the patient-derived cells, the mutation is sufficient to cause the observed disease phenotype. (F) If the correction of the mutation mimics the wild-type cells, the mutation is necessary to cause the observed disease phenotype.

but due to the heterogeneity of retinal dystrophies, it may not be feasible to locate multiple patients with the same mutation.

Regarding the second criterion, precise gene editing requires a level of expertise that is not always available to researchers. Genome editing may introduce off target effects that confound results, again highlighting the approach of introducing a mutation into a wild-type cell line to prove sufficiency[5]. Overexpression of disease causing genes in non-retinal cell types has had some success, but this method does not recapitulate endogenous regulation[61,62].

The third criterion is relatively easy to satisfy now that numerous iPSC lines are commercially available based on age, sex, disease state, etc. With regards to the fourth criterion, there are a limited number of functional assays that have been established for retinal cell types. The underlying molecular pathology for a specific mutation may not be connected to a function that can be easily measured *in vitro.* For example, it is more convincing to demonstrate the role of CEP290 in ciliogenesis rather than demonstrating a general decrease in cell viability or increase in cellular stress[35–37,59]. As the field of stem cell disease modeling progresses, it is critical to reassess our criteria for a convincing model and will need to be done on a case-by-case basis.

F. Future Directions

From the existing studies, it is reasonable to state that disease modeling inherently involves several layers of heterogeneity. The diseases themselves result from numerous different mutations across dozens of different genes. There are several sources of somatic cells for stem cell production by a variety of different

reprogramming methods. Each of those resulting stem cell populations can then undergo a plethora of differentiation protocols for producing retinal cell types. This inherent heterogeneity is important to consider because it may affect the reproducibility of disease models. As the field moves forward, it will be vitally important to provide thorough protocols to allow other researchers to repeat and build upon findings.

Clinical trials using RPE are already underway for other degenerative diseases, such as age-related macular degeneration, and trials using photoreceptors or other retinal cell types are on the horizon. The field of disease modeling is critical to the success of these trials because functional findings will inform researchers as to which cell types are primarily affected.

With the promise of cellular therapies, it is important to work towards using protocols that adhere to good manufacturing practice, which includes the development of xeno-free protocols for differentiation of retinal cell types[31,63,64].*

G. Conclusions

The following chapters demonstrate the application of iPSC disease modeling to splicing factor autosomal dominant retinitis pigmentosa (RP13) and autosomal recessive retinitis pigmentosa (RP12). Chapter II is a detailed protocol for the production of retinal pigmented epithelial cells for subsequent disease modeling and was originally published in the Journal of Visualized Experiments. Chapter III summarizes the findings in retinal pigmented epithelial cells differentiated according to the protocol in chapter II, using patient-derived, gene-corrected stem cells as a starting material. Finally, Chapter IV explores the use of retinal organoids for modeling two forms of retinitis pigmentosa: autosomal dominant RP13 as caused by a point mutation in pre-mRNA processing factor 8 (PRPF8) and autosomal recessive RP12 as caused by a point mutation in crumbs 1 (CRB1).

*This chapter was published as Foltz, L. P. & Clegg, D. O, "Patient-derived induced pluripotent stem cells for modelling genetic retinal dystrophies," *Progress in Retinal and Eye Research,* 2018.

II. Rapid, Directed Differentiation of Retinal Pigment Epithelial Cells from Human Embryonic or Induced Pluripotent Stem Cells

ABSTRACT

This protocol describes how to produce retinal pigment epithelial cells (RPE) from pluripotent stem cells. The method uses a combination of growth factors and small molecules to direct the differentiation of stem cells into immature RPE in fourteen days and mature, functional RPE after three months. We describe a robust method to direct the differentiation of pluripotent stem cells into retinal pigment epithelial cells (RPE). The purpose of providing a detailed and thorough protocol is to clearly demonstrate each step and to make this readily available to researchers in the field. This protocol results in a homogenous layer of RPE with minimal or no manual dissection needed. The method presented here has been shown to be effective for induced pluripotent stem cells (iPSC) and human embryonic stem cells. Additionally, we describe methods for cryopreservation of intermediate cell banks that allow long-term storage. RPE generated using this protocol might be useful for iPSC disease-in-a-dish modeling or clinical application.*

A. **Introduction**

The retinal pigment epithelium is a monolayer of pigmented cells that provide crucial support for photoreceptors. Retinal pigment epithelial cells (RPE) have numerous functions in vision, including light absorption, nutrient and ion transport, the retinoid cycle, phagocytosis of photoreceptor outer segments, and growth factor secretion[65]. There are a variety of retinal dystrophies that affect the function of RPE and result in a loss of vision, including age-related macular degeneration and retinitis pigmentosa. Generation of RPE from pluripotent stem cells may facilitate research to understand these eye diseases, and can provide an unlimited source of RPE for cell therapies[45]. In fact, multiple clinical trials are underway using RPE derived from pluripotent stem cells[66].

This differentiation protocol was originally described by Buchholz et al. 2014 and was based on the previously published method from Clegg[67,68]. The procedure mimics the normal *in vivo* developmental process to direct undifferentiated pluripotent stem cells towards an RPE fate via manipulation of the IGF, FGF-2 (FGF-basic), TGF-beta, and WNT pathways[67,68]. The protocol was significantly improved by addition of a WNT pathway agonist late in the protocol, which yielded 97.77% ± 0.1% PMEL (pre melanosome protein) positive cells, and has been adapted to xeno-free conditions[69,70]. The resulting RPE have been shown to express RPE markers at the transcript and protein levels, to secrete known RPE growth factors with appropriate polarity, and carry out phagocytosis of photoreceptor outer segments[47]. This protocol is more rapid and reliable than "spontaneous" protocols of differentiation

that involve simple removal of basic fibroblast growth factor[47]. Furthermore, RNA sequencing data show that RPE obtained using this protocol are very similar to those obtained using the more common spontaneous approach[47]. The 14-day method generates RPE that fit the "5 P's" mentioned by Mazzoni et al. 2014 (pigmented, polarized, phagocytic, post-mitotic, polygonal)[71]. Several additional directed differentiation methods have been published in recent years[46,48,72,73].

B. Materials and Methods

1. Preparation of reagents for day 0 to day 14 of the protocol.

1.1. Prepare the following medium components:

1.1.1. Make 100 mL of Retinal differentiation medium (RDM) by adding 1 mL of 100X N2 supplement, 2 mL of 50X B27 supplement, and 1 mL of 100X NEAA (non-essential amino acids) to 96 mL of DMEM/F12 (Dulbecco's modified essential medium, nutrient mixture F12).

1.1.2. Make 10 mL of 1 M Nicotinamide (NIC) by dissolving 1.221 g of NIC in 8 mL of sterile water, vortexing, and bringing the volume to 10 mL with sterile water. Sterile filter the solution.

1.2. Prepare the following growth factors and small molecules:

1.2.1. Reconstitute recombinant mouse noggin, human DKK-1 (dickkopf WNT signaling pathway inhibitor 1), and IGF-1 (insulin-like growth factor 1) to 100 µg/mL in 0.1% BSA in PBS. Aliquot as needed and store at -20 °C for up to 3 months.

1.2.2. Reconstitute FGF-basic (fibroblastic growth factor-2) to 10 µg/mL and recombinant human/mouse/rat Activin A to 100 µg/mL in 0.1% BSA in PBS. Aliquot as needed and store at -80 °C for up to 1 year.

1.2.3. Reconstitute SU 5402 (FGFR-specific tyrosine kinase inhibitor) and CHIR99021 (GSK-3β inhibitor) in DMSO to 10 mM each. Aliquot and store at -20 °C for up to 1 year or 6 months, respectively.

1.3. Obtain the following for day 0 and/or day 14: 1X EDTA solution (0.2 g ethylenediaminetetraacetic acid per liter of PBS), 1X PBS -/- (phosphate-buffered saline without calcium or magnesium, pH 7.4), 1X trypsin-like dissociation enzyme (TDE), DPBS (Dulbecco's phosphate-buffered saline), any RPE supporting medium (RSM), and Y-27632 dihydrochloride (use at 10 µM).

2. Day 0: Day of pluripotent stem cell passage for differentiation.

2.1. Grow stem cell colonies in feeder-free, serum-free conditions to approximately 80% confluence before passaging.

Note: See discussion for details on optimizing this step.

2.2. Coat a 12-well plate with non-growth factor reduced natural extracellular matrix-based hydrogel (ECM) as per manufacturer recommendations. Allow to set for 1 h at room temperature or overnight at 4 °C.

2.3. Aliquot the volume of RDM and PBS -/- needed for day 0 and warm in a water bath to 37 °C before adding growth factors**.** Bring EDTA to room temperature.

2.4. Add the growth factors necessary for day 0 to the warmed RDM with 10 mM NIC, 50 ng/mL noggin, 10 ng/mL DKK-1, 10 ng/mL IGF-1. From the stocks described in step 1.2, add 100 µL of NIC, 5 µl of noggin, 1 µL of DKK-1, and 1 µL of IGF-1 to 10 mL of RDM.

2.5. Pick to remove all differentiated colonies based on morphology from the stem cells that will be passaged for differentiation. Use a P10 pipet tip to manually remove the differentiated cells.

Note: Fibroblastic cells between colonies as well as the opaque cells within colonies indicate differentiated cells to be removed. See discussion for details about differentiated cells.

2.6. Passage a single well of a 6-well plate into 4 wells of a 12-well plate (1:4).

Note: See discussion for details on passaging stem cells at this stage.

2.6.1. Aspirate the stem cell medium from the stem cells and wash the wells once with pre-warmed PBS -/-.

2.6.2. Aspirate PBS -/- and rinse each well three times with 1 mL of EDTA per well of a 6-well plate.

2.6.3. Gently tilt the plate and aspirate the EDTA. Do not agitate the plate in any way to avoid prematurely lifting the cells.

2.6.4. After the third wash, add 1 mL of EDTA and incubate at room temperature in the hood for 3-5 min. Do not disturb the plate during this incubation.

2.6.5. Aspirate the EDTA and add 1 mL of RDM per well that will be seeded with 0.5 mL of extra medium. For example, wash 1 well of a 6-well plate with 4.5 mL of RDM to plate on 4 wells of a 12-well plate.

2.6.6. Use a cell scraper to gently detach the cells. Collect all cells in a conical tube and triturate the cells in RDM by pipetting up and down 5 times. Dissociate large clumps of cells but do not triturate to single cell suspension. Distribute the cells evenly in the pipet. Complete this step quickly to prevent reattachment to the plate.

2.6.7. Seed cells on the ECM-coated 12-well plates (1 mL of cell suspension per well).

2.6.8. Tilt the plate back and forth and gently place in a cell culture incubator at 37 °C and 5% CO_2 to remain in culture until the next medium change. Distribute the cells evenly throughout the wells.

2.6.9. Note the exact time. Change medium at the same time each day.

3. Day 1 to 14 of the 14-day differentiation protocol.

3.1. Day 1: Change the medium on all wells (1 mL per well) using RDM with the growth factor composition for day 0.

3.2. Day 2: Change the medium using RDM (1 mL per well) with 10 mM NIC, 5 ng/mL FGF-basic, 10 ng/mL noggin, 10 ng/mL DKK-1, 10 ng/mL IGF-1. From the stocks described in step 1.2, add 100 µL of NIC, 5 µL of FGF-basic, 1 µL of noggin, 1 µL of DKK1, and 1 µL of IGF1 to 10 mL of RDM.

3.3. Day 4: Change the medium using RDM (1 mL per well) with 100 ng/mL activin A, 10 ng/mL DKK-1, 10 ng/mL IGF-1. From the stocks described in step 1.2, add 10 µL of activin A, 1 µL of DKK1, and 1 µL of IGF-1 to 10 mL of RDM.

Note: Observe that cells are confluent at this stage.

3.4. Day 6: Change the medium using RDM (1 mL per well) with 100 ng/mL activin A, 10 µM SU 5402. From the stocks described in step 1.2, add 10 µL of activin A and 10 µL of SU 5402 to 10 mL of RDM.

3.5. Days 8, 10, and 12: Change the medium using RDM (1 mL per well) with 100 ng/mL activin A, 10 µM SU 5402, 3 µM CHIR99021. From the stocks described in step 1.2, add 10 µL of activin A, 10 µL of SU 5402, and 3 µL of CHIR99021 to 10 mL of RDM.

4. Day 14: Day of enrichment to passage 0 RPE.

4.1. Coat a 6-well plate with growth factor reduced ECM as per manufacturer recommendations. Allow to set for 1 h at room temperature or overnight at 4 °C.

4.2. Aliquot the volume of DPBS needed and 1 mL of RDM per well of enrichment and warm in a water bath to 37 °C. Bring the TDE to room temperature and warm necessary volume of RSM (+0.5X antimicrobial reagent, +/- Y-27632) to 37 °C.

4.3. Add Y-27632 to RSM to obtain a 10 µM composition. Use this medium for the first 4-7 days to improve attachment.

4.4. Aspirate spent medium from all wells and add 1 mL per well of pre-warmed RDM (no growth factors required).

4.5. Using a dissecting microscope, manually dissect and scrape away all non-RPE cells using a P10 pipet tip.

Note: See the representative results section for examples.

4.6. After dissection, aspirate RDM and all cell debris. Wash twice with 1 mL of pre-warmed DPBS per well.

4.7. Add 0.5 mL of TDE per well of a 12-well plate and incubate at 37 °C for 5 min. Use a cell scraper to gently remove the cells from the plate. Use a P1000 pipet to gently triturate the cell/TDE suspension 3-4 times to create a uniform suspension.

4.8. Dilute the cell/TDE suspension 1:10 in pre-warmed RSM, without Y-27632. Centrifuge cell suspension at 173 x g for 5 min at room temperature.

4.9. Aspirate the medium from the cell pellet and resuspend the cells in RSM with 10 µM Y-27632 (1 mL per enriched well).

4.10. Strain the cells using a nylon mesh cell strainer with 40 µm pores. Count the number of cells in a specified volume using a hemocytometer and calculate the concentration of cells in the strained solution.

4.11. Seed cells on the growth factor reduced ECM-coated plates at $1x10^5$ cells/cm^2.

4.12. Change the RSM with 10 μM Y-27632 48 h after cell seeding. Remove the 10 μM Y-27632 between days 4-7.

4.13. Allow the cells to mature for 28 to 35 days at 37 °C and 5% CO_2. Continue to change the RSM every 3-4 days (e.g. on Mondays and Thursdays).

5. Maturing the RPE: Passage 0 to passage 1/passage 1 to passage 2;

Note: volumes are indicated for 1 well of a 6-well plate or a T75 flask as indicated by parentheses.

5.1. Between days 28 to 35 of passage 0, coat a 6-well plate (or T75 flask) with non-growth factor reduced ECM as per manufacturer recommendations.

5.2. Aliquot the volume of DPBS and RSM needed and warm in a water bath to 37 °C. Bring TDE to room temperature.

5.3. Aspirate spent medium from wells and wash each well twice with 2 mL (10 mL) of pre-warmed DPBS.

5.4. Aspirate DPBS and add 1mL (5mL) of TDE. Place in incubator at 37 °C and 5% CO_2 for 5 min. After incubation, view cells on an inverted microscope to confirm the cells are contracting and detaching.

5.5. Using an appropriately sized cell scraper, gently remove the cells from the bottom of the well or flask.

5.6. Use a P1000 tip (10mL serological pipet) to gently triturate the cell/TDE suspension 3-4 times to create a uniform suspension.

5.7. Dilute cell suspension 1:10 in RSM. Reserve 2mL (5mL) of RSM to rinse the well/flask and add to the diluted cell suspension. **Do not allow enzyme exposure time to exceed 25 min.**

5.8. Centrifuge the cell suspension at 173 x g for 5 min at room temperature.

5.9. Aspirate the medium from the cell pellet and resuspend the cells in RSM

Note: Only use 10 µM Y-27632 at passage 0, not at passage 1 and beyond.

5.10. Strain the cells using a nylon mesh cell strainer with 40 µm pores. Count the number of cells in a specified volume using a hemocytometer and calculate the concentration of cells in the strained solution.

5.11. Seed cells on the ECM-coated plates at $1x10^5$ cells/cm^2.

5.12. Allow the cells to mature for 30 days. Continue to change the RSM every 3-4 days.

5.13. Repeat the above procedure at day 30 to passage the cells from passage 1 to 2.

6. Creating an intermediate cell bank: Cryopreservation of passage 2 day 3-5 RPE.

Note: Cryopreserve cells while they are subconfluent (~50%) and have not regained pigment.

6.1. Based on the number of cells, calculate the volume of animal component-free, defined cryopreservation medium with 10% DMSO (dimethyl sulfoxide) needed to resuspend the cells at a concentration of $3x10^6$ cells/mL.

6.2. Follow steps 5.2 to 5.8. Resuspend the cell pellet in the cryopreservation medium and transfer 1mL of the cell suspension to 1.2 mL cryogenic vials.

6.3. Place cryogenic vials in a freezing container designed to cool at -1 °C/min and place at -80 °C overnight. Transfer to liquid nitrogen for long-term storage.

Note: These cells will be passage 3 upon thawing. Culture the cells for 30 more days before characterization. Seed passage 3 RPE at $1.5x10^5$ per cm^2 upon thawing.

C. Results

This method results in the production of a homogeneous, pigmented, and cuboidal monolayer of RPE. The timeline in Figure 2 corresponds to the images depicted in A-F. As shown in Figure 2A, the stem cell colonies are tightly packed with defined edges and no fibroblastic cells between colonies or opaque cells within colonies.

Figure 2B provides a representation of immature RPE that are subconfluent. If the cells are already confluent at this stage, they cannot extend projections that are critical to the differentiation process. However, if cells are severely subconfluent, they will not be able to begin forming tight junctions characteristic of epithelial cells. Details on how to optimize this confluence are outlined in the discussion section.

Figure 2C shows the morphology of the two most common types of non-RPE that may come about during this differentiation process: neural ribbons and defined patches. It is important to note that these neural ribbons appear especially opaque on a dissecting microscope whereas the defined, fibroblastic-like patches are nearly translucent on a dissecting microscope. It can be helpful to mark these areas on a tissue culture plate with an ethanol-proof lab pen to more easily identify them on both a compound microscope and dissecting microscope.

Figures 2D-F show the characteristic bright borders, cobblestone morphology, and pigmentation that indicate a healthy, maturing culture of RPE.

Figure 3 is a higher magnification image to show the different appearance of fully mature RPE depicted by phase contrast and bright field microscopy. At passage 3 day 30, the cells are ready for the characterization that has been described in previous publications, including RNA expression, protein expression, growth factor secretion, and phagocytosis[45,67,69,70]. These characterizations show that the cells represented in these images are not only pigmented and cuboidal, but also phagocytic, post-mitotic, and polarized.

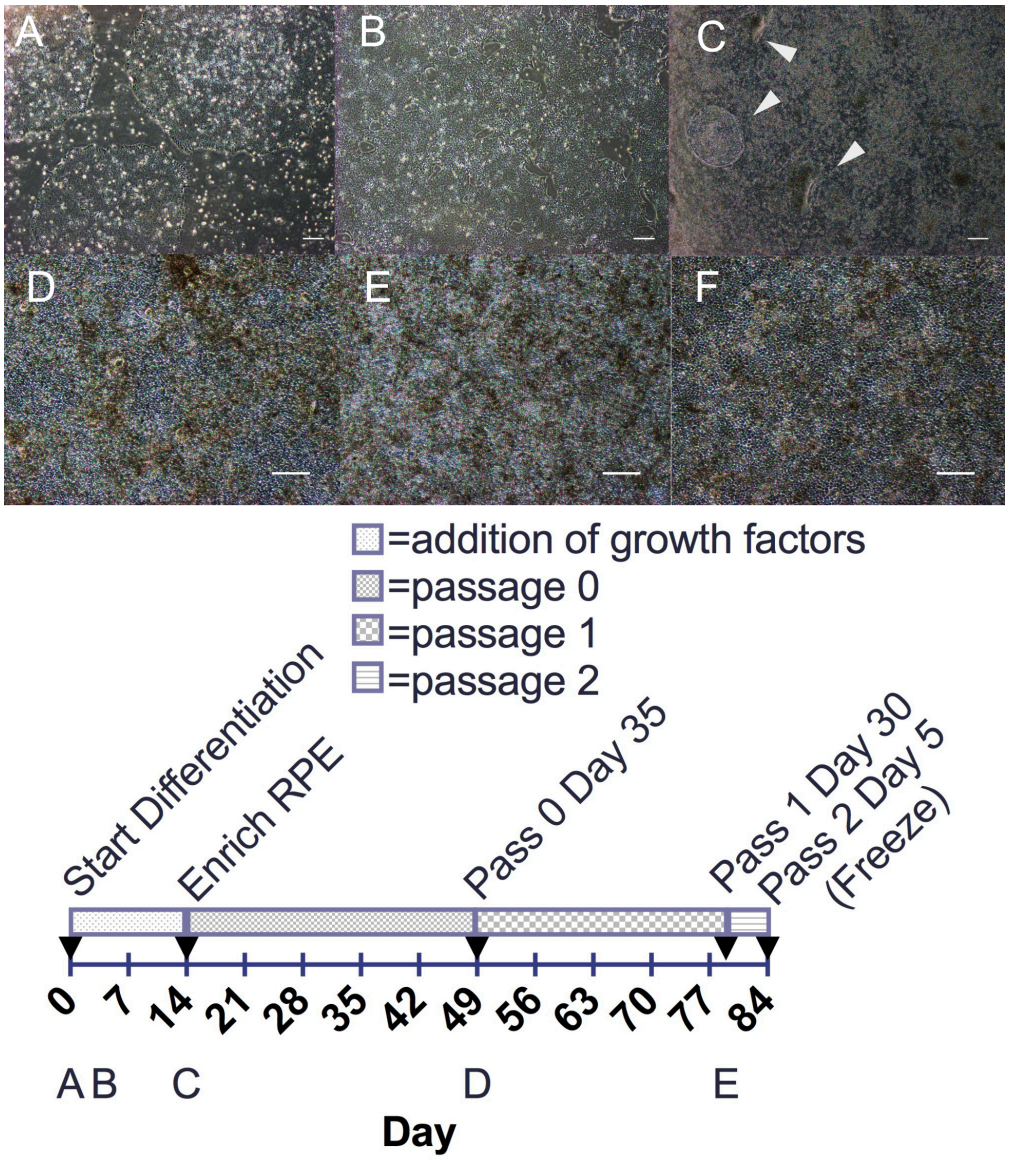

Figure 2. Timeline for the addition of growth factors and maturation of RPE Representative morphology and confluence of maturing RPE.

Growth factors are added to 12-well plates from day 0-14. Maturing RPE are cultured in 6-well plates or T75 flasks from day of enrichment to 30 days post-thaw (passage 3 day 30). Arrows indicate enzymatic cell passaging. A-E below the timelines correspond to the images. Induced pluripotent stem cells immediately before passaging for differentiation (A). Immature RPE cells subconfluent at day 2 (B) and before pick-to-remove enrichment on day 14; non-RPE patches (indicated by white arrows) appear as patches or opaque "ribbons" (C). RPE at passage 0, 1, and 3 on day 30 (D, E, and F). Scale bar equals 200 μm.

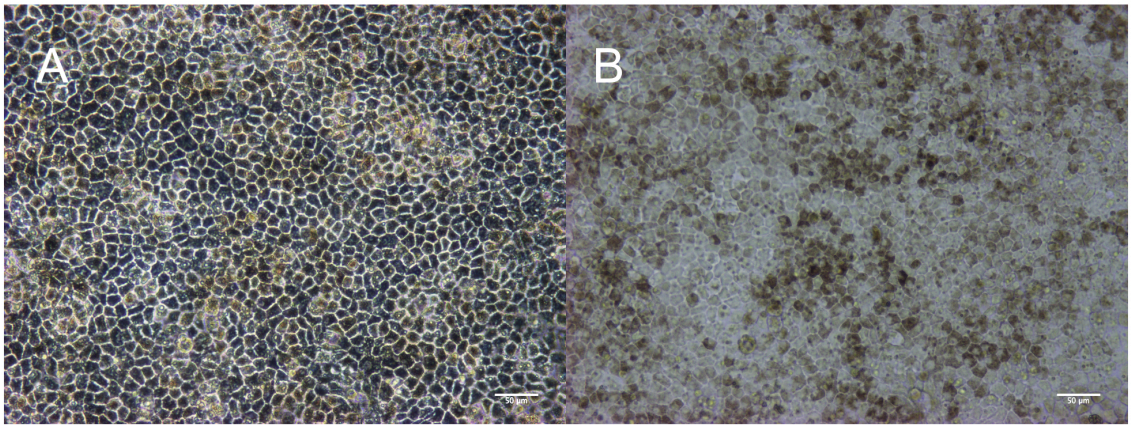

Figure 3. Mature RPE at passage 3 day 30

Cuboidal morphology depicted in phase contrast (A) and pigmentation depicted in bright field (B). Scale bar equals 50 µm.

D. Discussion

This protocol describes how to produce retinal pigment epithelial cells from pluripotent stem cells. The method was optimized using both human embryonic and iPSC from a feeder-free, serum-free culture method. Since the initial isolation of human embryonic stem cells in 1998 and the derivation of induced pluripotent stem cells (iPSC) in 2007, scientists have developed a multitude of stem cell culture methods[23,24,74,75]. These methods should be sufficient for producing stem cell colonies that are susceptible to this differentiation. There are no known limitations to the applicability of this method to properly derived and maintained pluripotent stem cells.

The most critical steps are the passaging of stem cells to day 0 of differentiation (step 2.4-2.5) and the potential need for manual dissection at day 14 of the process (step 4.5). When picking to remove differentiated cells from the stem cell colonies (step 2.4), it is helpful to refer to the images in Kent et. al. 2009. As indicated, the fibroblastic cells between colonies as well as the opaque cells within colonies indicate differentiated cells and need to be removed before beginning this protocol[76]. Only undifferentiated, tightly packed colonies with defined edges should be passaged for differentiation.

The number of stem cells seeded per well is complicated by the fact that the stem cells cannot be triturated into a single cell suspension upon passage and cannot be accurately counted using a hemocytometer. The approximation of 80% confluent stem cells is indicated for passaging 1 well of a 6 well plate into 4 wells of a 12-well

plate. Differences between stem cell lines, such as growth rate, can affect how quickly the immature RPE reach confluence between days 0 to 4. The stem cells will produce RPE regardless of precise confluence; however, the cell yield will be negatively affected if the cells are too sparse early in the protocol. The immature RPE cells should be approximately 40-50% confluent on day 1 and nearly 100% confluent by day 4. If the cells are not producing a confluent monolayer by day 4 or 6, the protocol should be repeated at a higher seeding density at day 0. For example, if one well of a 6-well plate was passaged to 4 wells of a 12-well plate at day 0 and the immature RPE are not 100% confluent at day 4, reduce the seeding to a 1:3 or 1:2 passage on day 0 or allow the stem cells to become more confluent before passaging. It is critical to establish a consistent seeding density when comparing multiple cell lines.

The manual dissection step at day 14 is only necessary when non-RPE are present in culture (**Figure 2C**). Since the addition of CHIR99021 to the protocol, many pluripotent stem cell lines require little to no manual dissection. Some preparations have a higher incidence of neural patches and it is critical to remove those cells. If the RPE are not viable at passage 0 and beyond, it is possible to repeat the differentiation protocol taking sufficient time to remove all non-RPE cells. This does not happen often, but it is mentioned here to note that the dissection step on day 14 can be optimized when needed.

There are a variety of RPE differentiation protocols that vary in cost as well as culture methods, efficiency, quantification, and functional assessment, the latter of which has been reviewed thoroughly[45]. We prefer the 14-day method detailed here

because of its efficacy, adaptability, and applicability to a wide range of cell lines[47,67,70]. The cryopreservation step in this protocol also provides a major advantage in creating an intermediate cell bank for future use, avoiding lot-to-lot variability in experiments. Starting with only 4 wells of a 12-well plate, it is possible to expand into 6 well plates at passage 0 and T75 flasks at passage 1 and 2. At passage 2 day 3-5, when the cells are still subconfluent and have not regained pigment, it is possible to cryopreserve tens of millions of cells and then thaw the mature RPE, designated passage 3 day 30, to check RNA expression, protein expression, growth factor secretion, phagocytosis, etc. We have also established protocols to expand RPE for up to 13 passages[77].

Looking forward, this method will be useful for iPSC modeling of ocular disease and for generation of RPE for cellular therapy. With regards to iPSC disease modeling, this protocol is currently being used in the lab to produce RPE from CRISPR-corrected lines with non-corrected controls from the same patient. Furthermore, this protocol is adaptable to synthetic substrates and xeno-free conditions that are useful for adhering to the good manufacturing practices required for a cellular therapy.*

E. Conclusions

The protocol described in this chapter was used to produce a homogeneous population of RPE from multiple patient-derived gene-corrected iPSC lines for subsequent disease modeling. The purpose of providing a detailed protocol is to highlight the importance of a robust differentiation method. The cells produced by this method are shown to be similar in their morphology, gene expression, protein localization, and functional ability. The striking similarity of the cells produced by this method allows for a robust disease model that can identify and explore minute differences between cells as described in chapter III. By publishing this method in great detail, we have enabled other scientists to apply this technique to their own disease models, which will further our collective knowledge surrounding the effect of retinal dystrophies on retinal pigmented epithelial cells.

*This chapter was published as Foltz, L. P. & Clegg, D. O. Rapid, Directed Differentiation of Retinal Pigment Epithelial Cells from Human Embryonic or Induced Pluripotent Stem Cells. *J. Vis. Exp.* **9,** 2–7 (2017).

III. Transcriptome Analysis and Functional Assessment of Patient-Derived Retinal Cells Edited by CRISPR/Cas9

ABSTRACT

We demonstrate that retinal pigmented epithelial cells (RPE) produced from patient-derived induced pluripotent stem cells (iPSC) are morphologically and functionally similar to wild-type RPE *in vitro*. RPE produced by directed differentiation methods from three diseased and three gene-corrected induced pluripotent stem cell lines were analyzed in terms of gene and protein expression, apicobasal polarity, and phagocytic ability. Functionally, the diseased and gene-corrected RPE were able to establish apicobasal polarity and phagocytose photoreceptor outer segments at the same capacity as wild-type RPE. These data suggest that patient derived diseased and gene-corrected iPSC are able to differentiate into RPE, thus allowing for the establishment of a well-controlled disease model. In this study, we performed RNA-sequencing for patient-derived retinal pigmented epithelial cells and retinal organoids to identify differentially expressed genes. The RPE that were studied were purified populations of cells, which allows for reduction of background based on cell-to-cell variability. We identified differentially expressed genes in RPE and demonstrated the up-regulation of a lncRNA and REC8 in the diseased RPE, implicating the role of lncRNA and cell cycle regulation in pathogenesis. These data showed that there is minimal line-to-line variability from a single patient, allowing for identification of differentially expressed genes that relate to a genetic mutation.

A. Introduction

Retinitis pigmentosa is the most common form of inherited blindness and can be caused by a multitude of different genetic mutations that lead to the same phenotype. Specifically, mutations in ubiquitously expressed splicing factor proteins are known to cause an autosomal dominant form of the disease, but the retina specific pathology of these mutations is not well understood. In this study, we examined the cellular pathology of splicing factor autosomal dominant retinitis pigmentosa (RP13).

Mutations in ubiquitously expressed proteins provide a unique challenge for understanding pathology. In the case of RP13, it is known that the retina is the specifically affected tissue, but the cellular specificity has not been determined. The two most commonly affected retinal cells are photoreceptors and their supportive retinal pigmented epithelial cells (RPE). To investigate the effect of a patient-specific point mutation in a specific retinal cell type, it is critical to produce a homogenous cell population. In this study, we have produced a purified population of RPE to investigate the molecular pathology.

Mutations in three pre-mRNA processing factors are known to cause autosomal dominant retinitis pigmentosa: PRPF3, PRPF8, and PRPF31. Early investigation of 150 Spanish families positively identified specific point mutations in PRPF3, PRPF31, and PRPF8[92]. RP13 is used to refer to the form of the disease caused by one of several known causative mutations in PRPF8. The mechanism by which a mutation that affects alternative splicing causes retinitis pigmentosa is unknown[6,90,91].

The human pre-mRNA processing factor 8 (PRPF8) gene encodes a protein that is ubiquitously expressed and is one of the largest and most highly conserved nuclear proteins[80]. PRPF8 was first identified as the 220kDa mammalian homolog of the yeast PRP8 protein, a component of the U5 small nuclear ribonucleotide complex in the spliceosome[65–67]. The role of PRPF8 in pre-messenger (pre-mRNA) splicing has been a topic of investigation for nearly twenty years and has been investigated by a variety of methods to help elucidate the function of this protein in the context of RNA splicing[84–86]. Pre-mRNA splicing is critical for the proper removal of introns to allow for subsequent protein translation[87]. Crystallographic studies in yeast have shown that mutations in PRFP8 disrupt protein-protein interactions, but these results have not been confirmed in human protein models[88,89].

RPE are highly polarized cells and their function depends heavily on their apical basal polarity. In a functioning retina, the apical microvilli bind and internalize the photoreceptor outer segments. It is possible to assess this function *in vitro* and will prove to be relevant to modeling RP13. Animal models have shown that the RPE cells of splicing factor knockout mice are unable to phagocytose rod-outer segments efficiently[8]. Specifically, RPE from PRPF8 knockout mice were subjected to a rod-outer segment phagocytosis assay, and the researchers found a 37-48% decrease in phagocytosis. Using established imaging techniques, it was shown that the cells were deficient in binding of the outer-segments rather than internalization[78]. Further examination by immunofluorescence showed that the localization of some adhesion and phagocytosis proteins was perturbed in the PRPF8 knockout mice. For example,

although the αV integrin was correctly expressed on the apical membrane, the β5 integrin and MerTK were expressed throughout the RPE cell in the mutant. Additionally, it was shown that the focal adhesion kinase (FAK) was localized to the basal side rather than throughout the RPE cells. These findings have led to the hypothesis that RPE cells are the specific cell type affected and the molecular mechanism might involve improper splicing of trafficking proteins[79].This PRPF8 mutant phenotype has not yet been shown in humans and does not provide mutation-specific information.

The patient mutation investigated here is a 6901 C→T missense mutation leading to a proline to serine substitution (P2301S) located in the Jab1/MPN domain in exon 42 of the C-terminal of PRPF8. A missense mutation at the same nucleotide position (P2301T) had previously been reported to cause RP13[93]. P2301S was first identified in a study of 43 Italian families and was later investigated in the context of the clinical phenotype of one Italian family[94,95]. The pedigree depicts a deceased male that had RP13 with two out of five children suffering from RP13, one of which was deceased and one of which harbored the P2301S mutation. Both of these individuals had children and grandchildren carrying the P2301S mutation, all exhibiting an RP13 phenotype. The disease began with night blindness at an average age of 10.3 years (±6.4 SD). Fundus examination revealed atrophy of the retinal pigmented epithelium (RPE) in four living patients, but not in the two younger living patients. Testa et. al. concluded that this mutation results in a mild phenotype with partial preservation of cone photoreceptors, absence of rod photoreceptors, and atrophy or RPE[94]. It is

difficult to draw any conclusions about the precise cellular pathology from clinical phenotypes, but it is critical to note that both the RPE and rod photoreceptors are affected. Cellular modeling of RP13 is necessary to elucidate the cellular and molecular pathology of the disease.

For the purpose of cellular modeling, the Pierce Lab of Harvard Eye and Ear Institute generously gifted RP13 patient fibroblasts to the Thomson lab of University of Madison, Wisconsin. The fibroblasts served as the somatic cell source for producing induced pluripotent stem cells via the Thomson factors: OCT4, SOX2, NANOG, and LIN28[23]. The patient harbors a P2301S mutation in the gene encoding the splicing factor PRPF8. To investigate the role of this mutation, Howden et. al. performed simultaneous reprogramming and correction of the missense mutations using CRISPR/Cas9 editing[41,96,97]. The aim of this research is to produce RPE from the diseased and gene-corrected patient iPSC in order to investigate the cellular pathology.

Next-generation sequencing can be used to perform non-Sanger, high-throughput DNA and RNA sequencing, which is useful for screening multiple samples in parallel. In the context of retinitis pigmentosa, there are limitations to traditional methods of gene expression analysis, such as quantitative polymerase chain reaction (qPCR). Specifically, qPCR is limited to measuring the RNA expression of particular genes of interest; however, the genes needing to be investigated may be unknown in a novel disease model. RNA sequencing allows for the screening of diseased and gene-corrected patient-derived cells to identify genes of interest as well

as noncoding transcripts. Long noncoding RNA (lncRNA) or more specifically long intergenic non-coding RNA (lincRNA) are recently discovered RNA molecules. To narrow down the potential roles of lncRNA, these molecules are generally classified by their genomic context: (1) stand alone, (2) natural antisense transcripts, (3) pseudogenes, (4) long intronic ncRNA, or (5) divergent transcripts, promoter-associated transcripts, and enhancer RNA[98]. Recent studies demonstrate that various lncRNA molecules may play a role in a healthy retina and contribute to retinal degenerative disease[99–101].

In addition to identifying non-coding transcripts, next-generation sequencing can help cluster differentially expressed genes based on their known functional role, such as a pathway analysis. Looking at the limited amount of differences in gene expression, we were able to identify REC8 and IRX5 which both have been shown to play a role in cell cycle regulation. Given the relationship between cell cycle regulation and ciliogenesis, we investigated this difference further.

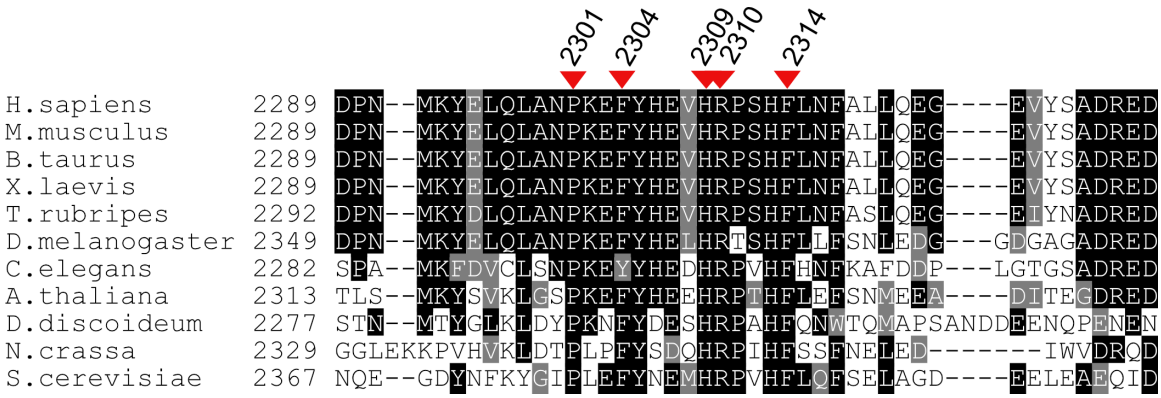

Figure 4. RP13 causative mutations in conserved Jab1/MPN domain of PRPF8**.**

Missense mutations at amino acid positions P2301S and H2309P have been identified in patients with splicing factor RP13.

B. Materials and Methods

Sample Acquisition and Pluripotent Cell Line Maintenance

Patient-specific human iPSC lines clone 3, clone 3.5, clone 3.80, clone 3.16, clone 3.5, and clone 3.86.1 (gifts from S. Howden, collectively referred to as PRPF8 lines) were maintained in TeSR™-E8™ (StemCell Technologies, Vancouver, BC, Canada, http://www.stemcell.com) and passaged using an Versene (0.2g EDTA(Na_4) per liter PBS) (Thermo Fisher) passaging protocol[102]. No manual dissection of undifferentiated colonies was necessary. All six PRPF8 lines were derived from fibroblasts isolated from the skin biopsy of one patient (gift from E. Pierce to J. Thomson). The fibroblasts were reprogrammed using enhanced episomal vectors and corrected using Cas9 protein and PRPF*-specific sgRNA[41].

H9 hESC (WiCell Research Institute, Madison, WI, http://www.wicell.org) and MyCell iPSC line no. 1013.201 (Cellular Dynamics International MyCell iPSC Services, Madison, WI, http://www.cellulardynamics.com) were adapted from mTESR™1 (StemCell Technologies) and manual passage to TeSR™-E8™ and Versene passage with manual dissection of differentiated colonies. All pluripotent cell lines were maintained on hESC-Qualified BD Matrigel (BD Biosciences, Sparks, MD, http://www.bdsciences.com) with daily medium changes and Versene passaging every 4-7 days. All cell lines were cryopreserved in 10% DMSO in TeSR™-E8™ at approximately $2x10^6$ cells per mL.

Maintenance of immortalized and primary cell lines

Primary human retinal microvascular endothelial cells (RMEC; Cell Systems, *https://cell-systems.com/*) were obtained at passage 4 and expanded to an intermediate cell bank at passages 7 and 9. RMEC were maintained on Matrigel (BD Biosciences) in microvascular endothelial cell media and passaged with trypsin (0.05%; Millipore Sigma, St. Louis, MO, http://www.sigmaaldrich.com) between days 3 to 5 before cells reached confluence. Immortalized human RPE, ARPE-19, were maintained in ARPE-19 media: DMEM/F12 with sodium pyruvate and 1X GlutaMAX (Gibco), 10% fetal bovine serum (Atlanta Biologicals, , Flowery Branch, GA, http://www.atlanta-bioloigicals.com/), and 15 mM HEPES butter. Human fetal RPE (fRPE) (gift from P. Coffey) were maintained on Matrigel in RPE media[103]: MEM - alpha modification (Millipore Sigma) supplemented with fetal bovine serum (5%, 15% for the first 3 days after seeding; HyClone), N1 (1X; Millipore Sigma), NEAA (1X), GlutaMAX-I (2 mM; Invitrogen), taurine (250 μg/mL; Millipore Sigma), triiodothyronine (0.013 μg/L; Millipore Sigma), hydrocortisone (20 ng/mL; Millipore Sigma).

Differentiation of pluripotent cells to retinal pigmented epithelial cells

PRPF8 iPSC lines and wild type iPSC MyCell and hESC H9 were seeded onto Matrigel-coated 6 well plates (Corning, Corning, NY, https://www.corning.com/) and cultured for 3 to 7 days before passage by Versene. Directed differentiation was initiated by Versene passage of undifferentiated stem cells to 12 well plates (Corning). Undifferentiated stem cells are left in small clumps rather than single cells, thus an exact seeding density of cells per cm^2 is not possible. Instead, optimization of passage

was completed by a serial dilution of stem cells into a 12 well plate and examined for neural projections at day 4 of differentiation.

Growth factors and small molecules were added over the course of fourteen days as previously described[69]: DMEM/F12 with 1X B27, 1X N2, 1X NEAA (Invitrogen, Carlsbad, CA, http://www.invitrogen.com), 50 ng/mL Noggin, 10 ng/mL Dkk1, 10 ng/mL IGF1, 5 ng/mL bFGF (R&D Systems, Minneapolis, MN, http://www.rndsystems.com), 10mM nicotinamide (Millipore Sigma), 100 ng/mL Activin A (Peprotech, www.peprotech.com), 10μM SU5402 (Santa Cruz Biotechnology, www.scbt.com), and 10 μM CHIR99021 (Stemgent, www.stemgent.com). If necessary, cells with non-RPE morphology were manually dissected and removed at day 14. All remaining cells with RPE morphology were passaged using TrypLE (Invitrogen) for 5 minutes at 37 ˚C and 5% CO_2 and passed through a strainer with 30 μm pores. Immature RPE were seeded on Matrigel-coated plates at density ($1x10^5$ cells per cm^2) and allowed to mature for 4 to 5 weeks. RPE were matured and cryopreserved to create an intermediate cell bank as previously described[104].

Immunofluorescence

iPS-derived RPE cells were thawed and seeded onto Matrigel-coated Permanox-treated 8-chambered slide. On day 30, cells were washed with phosphate-buffered saline (PBS) and fixed in 4% paraformaldehyde (PFA) in 0.1M sodium cacodylate buffer, pH 7.4, for 15 minutes at 4 ˚C. Cells were washed twice with cold PBS then blocked with 5% bovine serum albumin (BSA) (Millipore Sigma) with 0.2%

Triton X-100 (Millipore Sigma) to permeabilize the cell membrane. After blocking, cells were incubated overnight at 4 ˚C with primary antibody. Cells were washed three times with cold PBS, incubated with the corresponding secondary antibody conjugated to AlexaFlour (1:300) (Invitrogen) or Cy2, 3, or 5 (1:200) (Jackson-Immuno) for 1 hr at 4 ˚C, incubated with Hoechst (2 μg/mL)(Invitrogen) for 5 min at room temperature, washed three times with PBS, mounted with 80 μL Prolong Gold Mountant (Invitrogen) and coverslip, and imaged on Olympus IX70 Inverted Compound microscope, Olympus Fluoview 1000 Spectral Confocal microscope (Olympus, Tokyo, Japan, http://www.olympusamerica.com/), or Leica SP8 Resonant Confocal microscope (Leica, Wetzlar, Germany, www.leica-microsystems.com).

Western Blot Analysis

iPS-derived RPE were thawed and seeded at $1.5x10^5$ cells per cm^2 in duplicate on Matrigel-coated 6-well plates (Corning). RPE were allowed to mature for 30 days and then were passaged using TrypLE (Gibco). An average of $1.5x10^6$ cells were collected from each well and pelleted by centrifugation at 2500 x g for 5 minutes. The supernatant was discarded, and the cells were washed twice in cold PBS and pelleted by centrifugation. Cells were lysed using RIPA lysis buffer (Thermo Scientific) at a concentration of 1 mL of buffer for $5x10^6$ cells as per manufacturer's recommendations, with 1X final concentration of Halt Protease Inhibitor Cocktail and Halt Phosphatase Inhibitor Cocktail (Thermo Scientific). The cell buffer mixture was

shaken gently on an orbital shaker for 15 min at 4 ˚C and then centrifuged at 14,000 x g for 15 minutes. Supernatant was collected and stored at -80 ˚C.

Protein concentration was determined using a Pierce™ BCA Protein Assay Kit (Thermo Fisher Scientific) according to the manufacturer's microplate procedure (Synergy H1 Hybrid Multi-Mode Reader, BioTek, Winooski, VT, http://www.biotek.com/). Cell lysates (10-20 µg total protein per lane) were separated by sodium dodecyl sulfate polyacrylamide gel electrophoreses (SDS-PAGE) in Novex™ WedgeWell™ Tris-Glycine Gels (Invitrogen). Separated proteins were transferred to nitrocellulose membranes with 0.45 µm pore size (Life Technologies) using Pierce™ Power Blotter semi-dry transfer, blocked for 1 hour at room temperature in Blocking Buffer for Fluorescent Western Blotting (Rockland, Pottstown, PA, http://www.rockland-inc.com/), and incubated with primary antibodies overnight at 4 ˚C: monoclonal mouse anti-GAPDH loading control (0.5 µg/mL; MA5-15738); polyclonal rabbit anti-PRPF8 (1 µg/mL; ab87433 and ab79237). Membranes were washed with Tris-Buffered Saline Tween-20 (TBST) (Thermo Fisher Scientific), probed with secondary antibodies for 30 minutes at room temperature: donkey anti-mouse IgG (H+L) (IRDye® 680RD; 0.06 ng/mL; LI-COR Biosciences, Lincoln, NE, http://www.licor.com/) and donkey anti-rabbit IgG (H+L) (IRDye® 800CW; 0.06 ng/mL), and washed with TBST. Fluorescent signal was visualized on an Odyssey Imager (LI-COR Biosciences).

Quantitative PCR Analysis

Passage 3 iPS-derived RPE were thawed and seeded at $1.5x10^5$ cells per cm^2 onto Matrigel-coated 6-well plates (Corning). RPE were allowed to mature for 30 days and then were passaged using TrypLE (Gibco). Cells were collected by centrifugation at 2500 x g for 5 min. Cells were lysed using Buffer RLT (RNEasy Mini Kit, Qiagen) at a concentration of 350 μL per $1x10^6$ cells. cDNA was synthesized by two methods. Up to 1 μg of total RNA was used to synthesize cDNA using the iScript cDNA Synthesis Kit (Bio-Rad, Hercules, CA, http://www.biorad.com/). Alternatively, 30 ng of RNA was used to synthesis cDNA using AgPath-ID™ One-Step RT-PCR Reagents. Primers used were TaqMan Gene Expression Assays (Thermo Fisher). Quantitative real-time polymerase chain reaction was performed using CFX96™ Real-time PCR Detection System (Bio-Rad) using FAM detection. 20 μL reactions were run in triplicate in a 96-well plate. Data were normalized by two methods: the geometric mean of housekeeping genes SERF2, EIF2B2, and UBE2R2 or by the Livak method[105].

ELISA Assay for PEDF and MFG-E8

Passage 3 iPS-derived RPE, fetal RPE, ARPE-19, and RMECs were thawed and seeded at $1.5x10^5$ cells per cm^2 in triplicate onto Matrigel-coated 24-well Transwell® inserts (Corning). Cells were allowed to mature for 30 days and media was collected 48 hours after the last media change from the apical and basal compartments. Media samples were then flash frozen in liquid nitrogen and stored at -80 ˚C. Secreted protein was measured using enzyme-linked immunosorbent assays as per manufacturer's recommendations for pigment epithelial derived factor (Human PEDF ELISA Kit, BioProductsMD, Middletown, MD, http://www.bioproductsmd.com/) and milk-fat

globule-EGF factor 8 (Human MFG-E8 Quantikine ELISA Kit, R&D Systems, Minneapolis, MN, http://rndsystmes.com/). Optical density was measured using a fluorescent plate reader (Synergy H1 Hybrid Multi-Mode Reader).

Phagocytosis Assay

Passage 3 iPS-derived RPE, fetal RPE, ARPE-19, and RMECs were thawed and seeded at $1.5x10^5$ cells per cm^2 in quadruplicate onto Matrigel-coated 96 well plates (clear bottom, black walls) (Corning). Cells were allowed to mature for 30 days and then were challenged with approximately 10 FITC-labeled (Invitrogen) photoreceptor outer segments (POS) (InVision BioResources, Seattle, WA, http://www.invisionbio.com/) per cell for 5 hr. Excess POS were aspirated and the cells were washed for 1 min three times with room temperature PBS. Subsets of samples were treated with 0.4% Trypan blue (Fisher Scientific) for 10 min at room temperature to quench FITC fluorescence. All samples were washed twice with PBS, fixed with ice-cold 100% methanol (Millipore Sigma), and rehydrated with PBS for overnight incubation. Fluorescence was quantified using FITC detection (excitation 488 nm, detection 520 nm) (Synergy H1 Hybrid Multi-Mode Reader, BioTek, Winooski, VT, http://biotek.com/). All fluorescent detection was normalized to AREPE-19 controls.

RNA Sample Collection

Passage 3 iPS-derived RPE were thawed and seeded at $1.5x10^5$ cells per cm^2 onto Matrigel-coated 6-well plates (Corning). RPE were allowed to mature for 30 days and then were passaged using TrypLE (Gibco). Cells were collected by centrifugation at

2500 x g for 5 min. Cells were lysed using Buffer RLT (RNEasy Mini Kit, Qiagen) at a concentration of 350 μL per $1x10^6$ cells.

RNA-Sequencing Library Preparation

Total RNA was processed for library preparation using Illumina TruSeq® RNA Sample Preparation kit as per manufacturer's recommendations and sequenced on Illumina HiSeq 4000.

RNA-Sequencing Data Analysis

RNA-sequencing reads were aligned to the reference human genome (GRCh37) using Rsubread TopHat Alignment. The resulting count matrix was analyzed for differential expression in the Bioconductor package edgeR for differential expression[107].

siRNA knockdown of PRPF8 and LOC339975

Passage 3 iPS-derived RPE were thawed at seeded at 60-80% of confluence in Matrigel-coated 24-well plates. Each cell line was plated in duplicate. 24 hours post seeding 1pmol of siRNA in OptiMEM media (Gibco) with lipofectamine (Gibco) for each siRNA, specifically PRPF8 (Invitrogen), LOC339975, and a negative siRNA control were added to the cells. 72 hours post-seeding cells were harvested using TrypLE (Gibco) and total RNA was collected for qPCR analysis.

Cell Cycle Analysis

RPE were enzymatically passaged at various time points and fixed in 4%paraformaldehyde in sodium cacodylate buffer, pH 7.4. Cells were permeabilized and blocked in 0.1% Triton-X in 0.5% bovine serum albumin in PBS. Flow cytometry

samples were prepared with 1 x 10^6 cells in suspension. Samples were incubated for 30 min at room temperature in the dark with 0.5 mL of FxCycle™ PI/RNase Staining Solution (Life Technologies). Samples were analyzed without washing using 488-nm excitation on an Accuri C6 Flow Cytometer (BD Biosciences).

Statistical Analysis

For all experiments, two-way ANOVA tests were performed. Significance was determined at $p < 0.05$.

C. Results

Characterization of RPE

To validate the production of RPE from all patient-derived iPSCs, the characterization of the cells was performed by established methods[67,69]. The purity of the RPE population after differentiation was determined by quantifying PMEL17 expression via flow cytometry (**Figure 5**). To analyze the expression of retinal specific genes, quantitative polymerase chain reaction was performed for several genes. RPE cell genes included BEST1, RPE65, PMEL17, CRALBP, and MITF isoform 2. Undifferentiated stem cell genes and proliferation marker included REX1, SALL, and MKi67. Non-RPE genes included S100A4, ITGA2, MITF isoform 4+5, PECAM1, and MAP2. Housekeeping genes included EIF2B2, UBE2R2, and SERF2. All six patient-derived iPSC cell lines were differentiated into RPE that expressed all native RPE genes by passage 0 day 30 or sooner and no longer expressed stem cell or proliferation markers (**Figure 5**). Interestingly, the only non-RPE gene expressed after differentiation was low levels of S100A4, a calcium-binding protein specific to

fibroblasts[108]. This may be related to the use of patient fibroblasts as the origin of somatic cells for reprogramming.

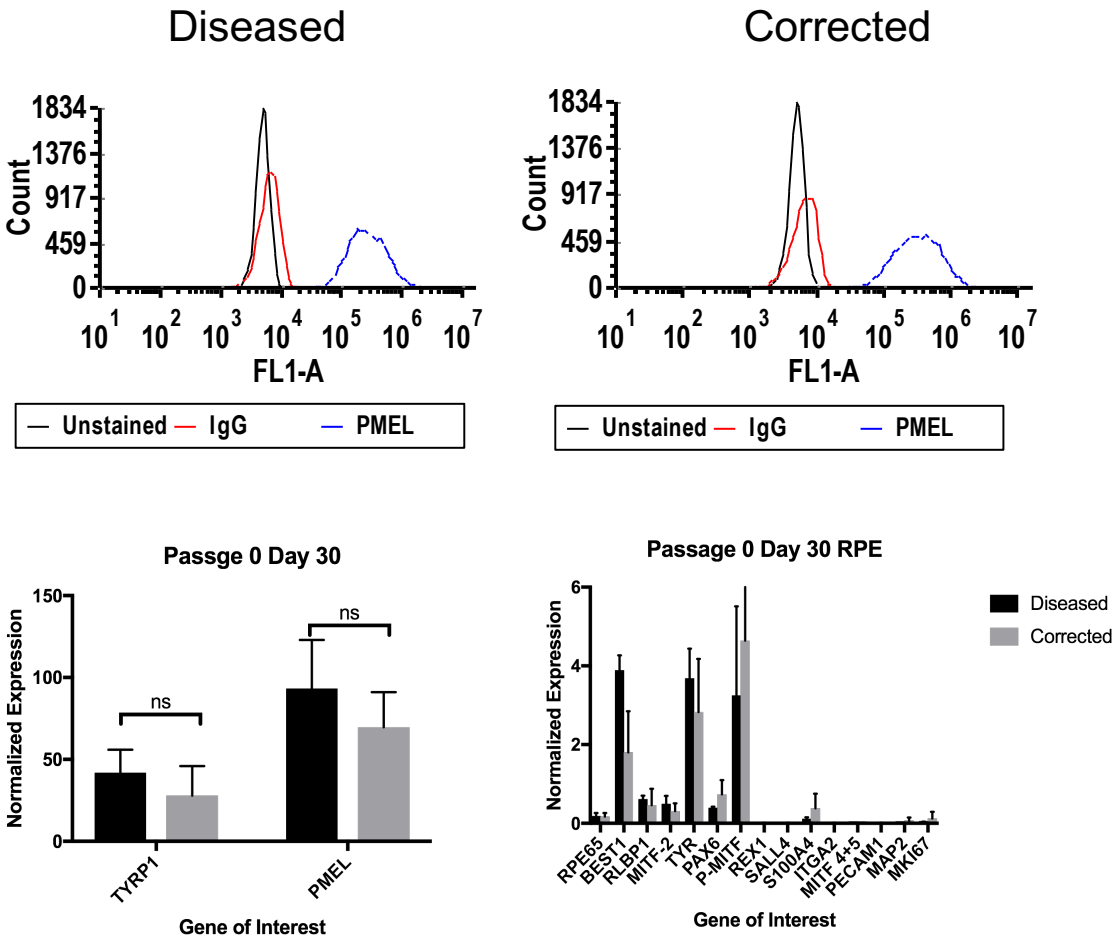

Figure 5. Purified population of PMEL+ RPE and relevant gene expression.

Flow cytometry analysis of RPE at passage 0 day 30 RPE reveal a population of PMEL+ cells compared to the unstained or IgG control. PCR analysis of relevant RPE genes reveal similar levels of expression relative to housekeepers and minimal expression of non-RPE genes.

To observe the localization of native RPE proteins, PMEL17, BEST1, and ZO-1 were examined by immunocytochemistry. Premelanosome 17 (PMEL17) is a transmembrane glycoprotein that is expressed early in pigmented cells and serves as an early marker of RPE differentiation[68]. Bestrophin 1 (BEST1) is an integral membrane protein that functions as a calcium-activated chloride channel in which mutations are known to cause retinal degeneration[109]. Zonula occludens (ZO-1) is a tight junction complex that helps establish the integrity of the epithelial monolayer. Diseased and corrected RPE expressed these RPE proteins in the proper locations (**Figure 6**). Localization of PRPF8 was also observed and confirmed to localize to the nucleus with some potential localization in speckles outside the nucleus.

The secretion of pigment epithelium-derived factor (PEDF) was measured by enzyme-linked immunosorbent assay (ELISA). The RPE are grown on Transwell® inserts to allow the separation of apical and basal media. For each of the six patient-derived lines, the apical media contained a significantly higher concentration of PEDF than the basal media, indicating the proper polarity of the iPSC-derived RPE (**Figure 7**). The secretion of milk-fat globule-EGF factor 8 protein (MFG-E8) was measured by ELISA and compared to the same positive and negative control cell lines used in the phagocytosis assay. There was no significant difference between diseased and corrected RPE, but both secreted significantly more MFG-E8 than the positive controls (fetal RPE and immortalized ARPE-19) and the negative control, retinal microvascular endothelial cells.

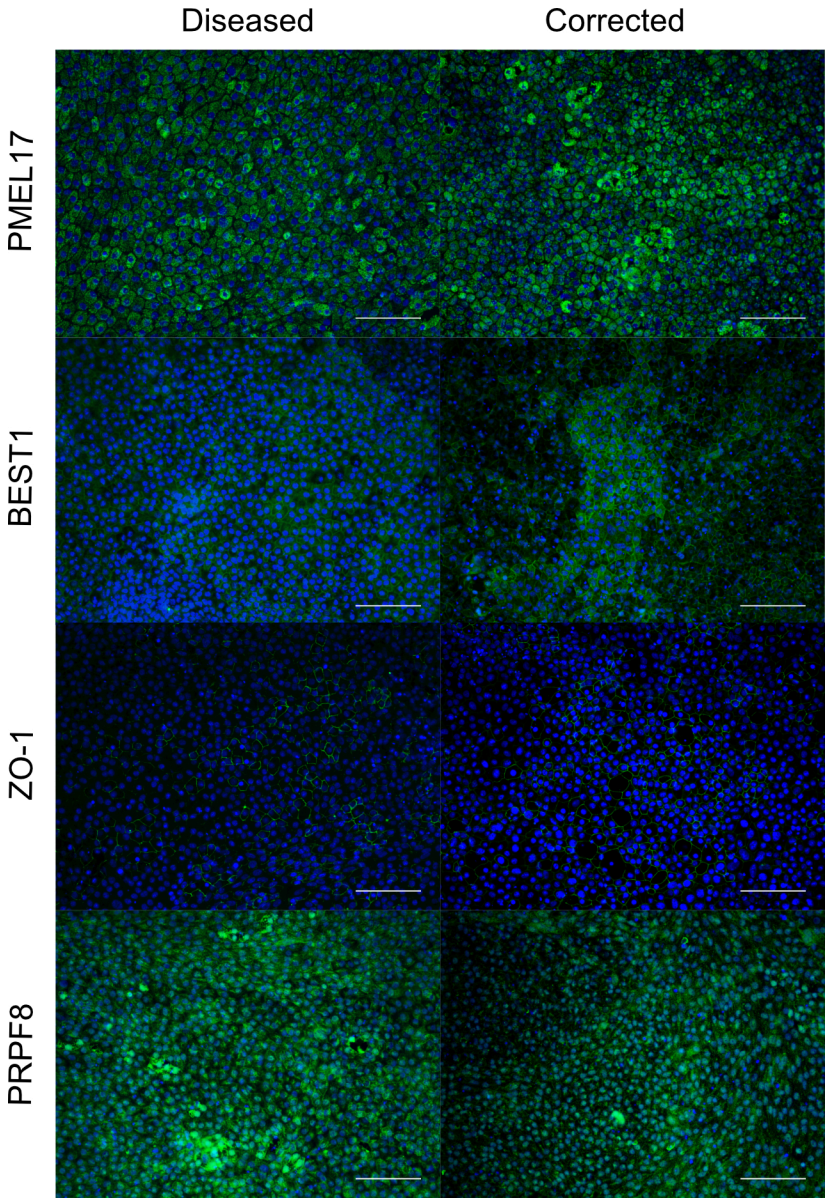

Figure 6. Localization of RPE-specific proteins.

Immunocytochemistry revealed proper localization of RPE-specific proteins (premelanosome 17, bestrophin 1, and zonula occludens). PRPF8 nuclear localization in both diseased and corrected cells. Scale bar equals 100 um.

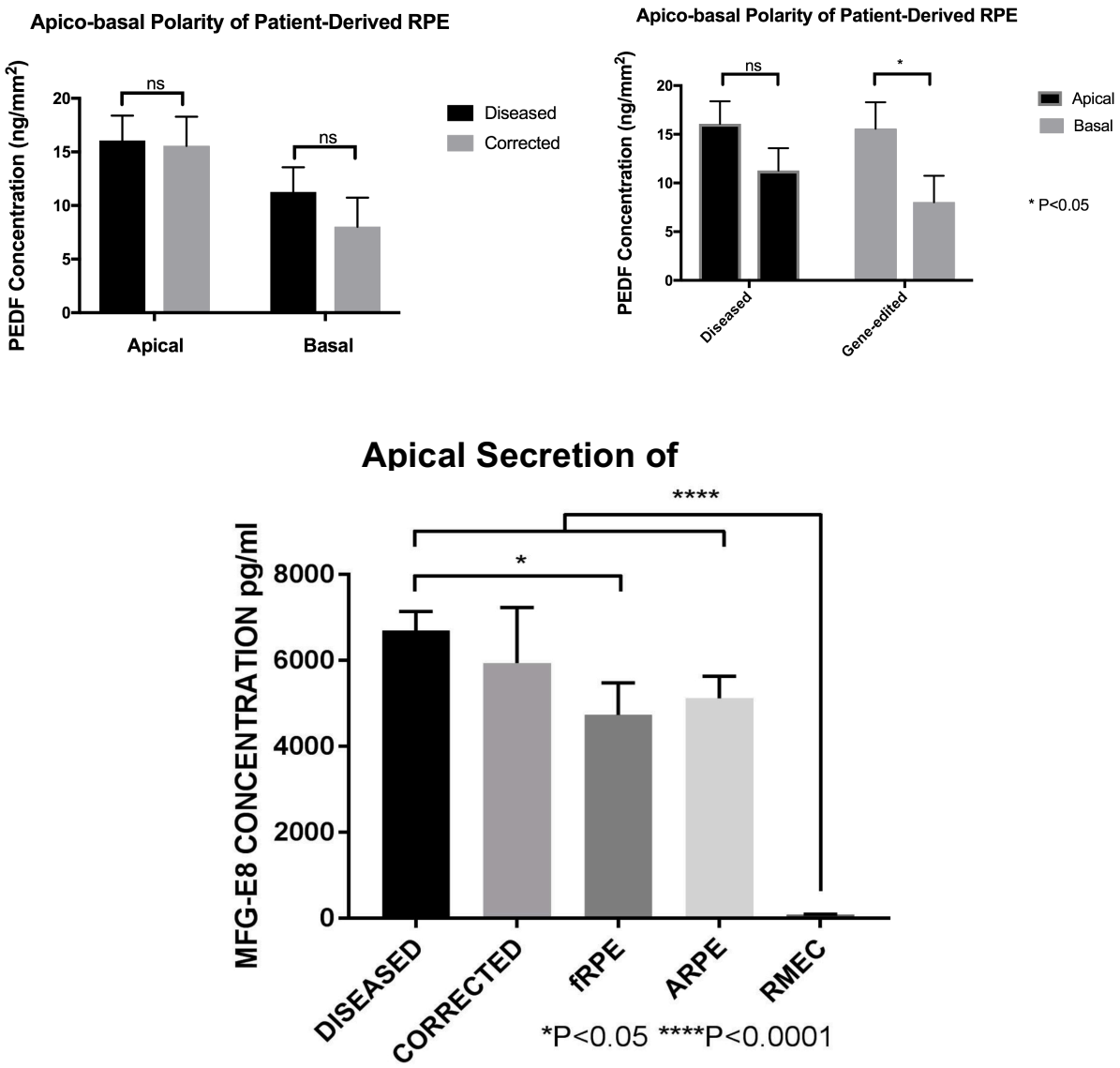

Figure 7. Secretion of functional proteins in RPE.

Diseased and corrected RPE establish apicobasal polarity as indicated by secretion of PEDF. Both diseased and corrected RPE secrete significantly higher levels of MFG-E8 than the positive and negative control cell lines.

Patient-derived RPE are not deficient in phagocytosis

Phagocytosis was measured by challenging the iPSC-derived RPE with fluorescently labeled photoreceptor outer segments and quantifying the fluorescence. Previous methods involved purification of outer segments from whole bovine eyes. The outer segments used in these experiments were purchased commercially to ensure the structural integrity and purity of the outer segments. After five hours of incubation, the relative fluorescent units were measured at an excitation of 488 nm. The total fluorescence is considered both the bound and ingested outer segments. A duplicate plate of cells was incubated with Trypan blue without permeabilization to quench fluorescence of any bound outer segments that were not ingested. The results indicate that the diseased and gene-edited cells were able to bind and ingest outer segments significantly more that the negative control line, retinal microvascular endothelial cells. Previous methods had required normalization of the data to show a significant difference from the negative control, which we attribute to endocytosis of sheared outer segments isolated from whole eyes. Since both lines bound and ingested significantly less than the immortalized ARPE-19, the assay was repeated in comparison to three wild-type stem cell-derived RPE. All six of the patient-derived lines and the three wild-type (H9 hESC, UCSF4 hESC, and MyCell iPSC) were produced from the same differentiation batch and are shown to phagocytose similar levels of outer segments (**Figure 8**).

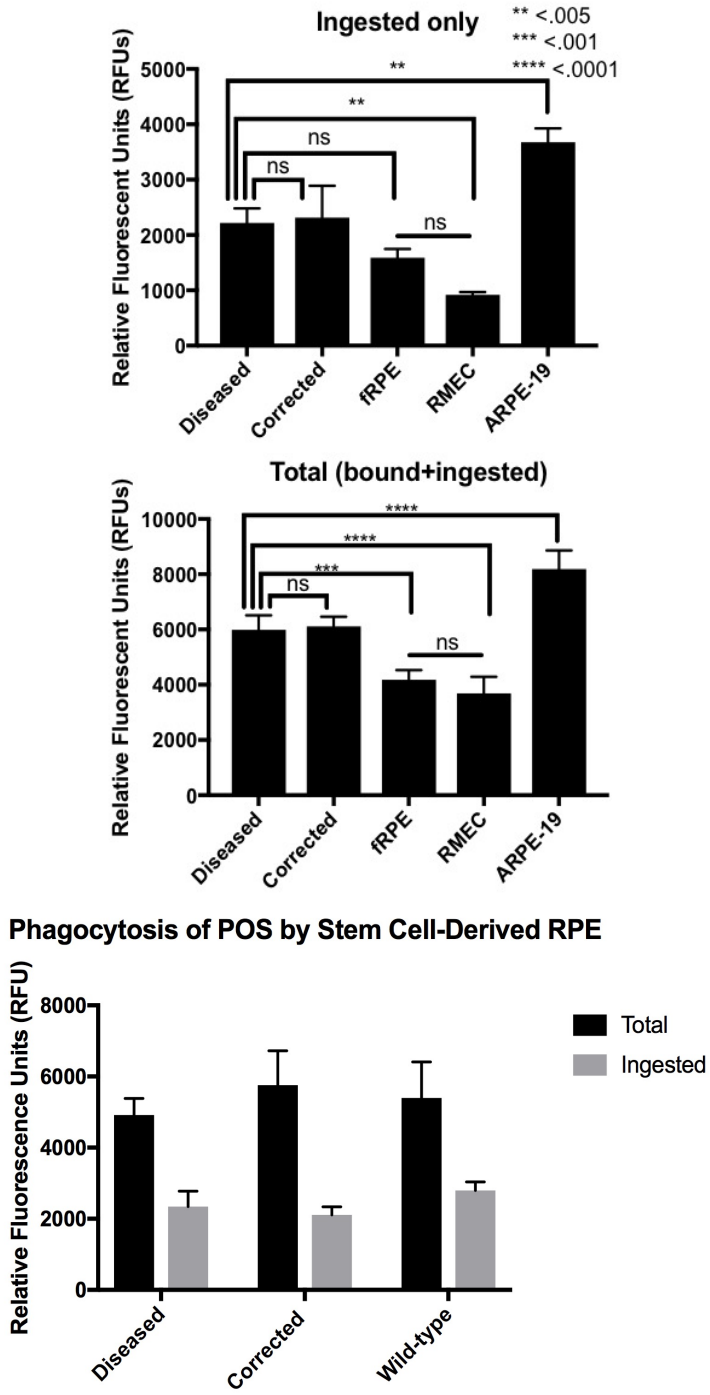

Figure 8. Phagocytosis of photoreceptor outer segments.

Diseased and corrected RPE were able to phagocytose outer segments in both binding and ingesting phases as well as fetal RPE and significantly more than endothelial cells (RMEC).

Atrophy of RPE upon extended passage

As a preliminary investigation of atrophy, RPE were passaged continuously for 100 days to observe the decline in the number of cells yielded per cm^2. After the initial seeding at 1 x 10^5 cells per cm^2, the RPE were able to reach a density of up to 3 x 10^5 cells per cm^2, indicating that the cells underwent approximately 1 to 2 divisions. After six passages, the cell yield started to decline to 2.5 x 10^5 cells per cm^2, and by day 100, the RPE maintained the initial seeding density, indicating that there was no proliferation occurring. We determine that within 100 days, there was no significant difference in the ability of the diseased and corrected RPE to proliferate (**Figure 9**).

Cells were imaged before passage to observe morphology and pigmentation (**Figure 10-11)**. As shown, diseased and corrected cells were able to maintain some level of cuboidal morphology and pigmentation throughout the passages. However, holes and fibroblastic cells started to appear after several passages and pigmentation was sparse (**Figure 9**). The images shown are meant to be representative, but an unbiased quantification of morphology and pigmentation would be required to draw any conclusions from the cell culture images. As a first estimation, we have relied on cell count to estimate proliferation and atrophy of RPE.

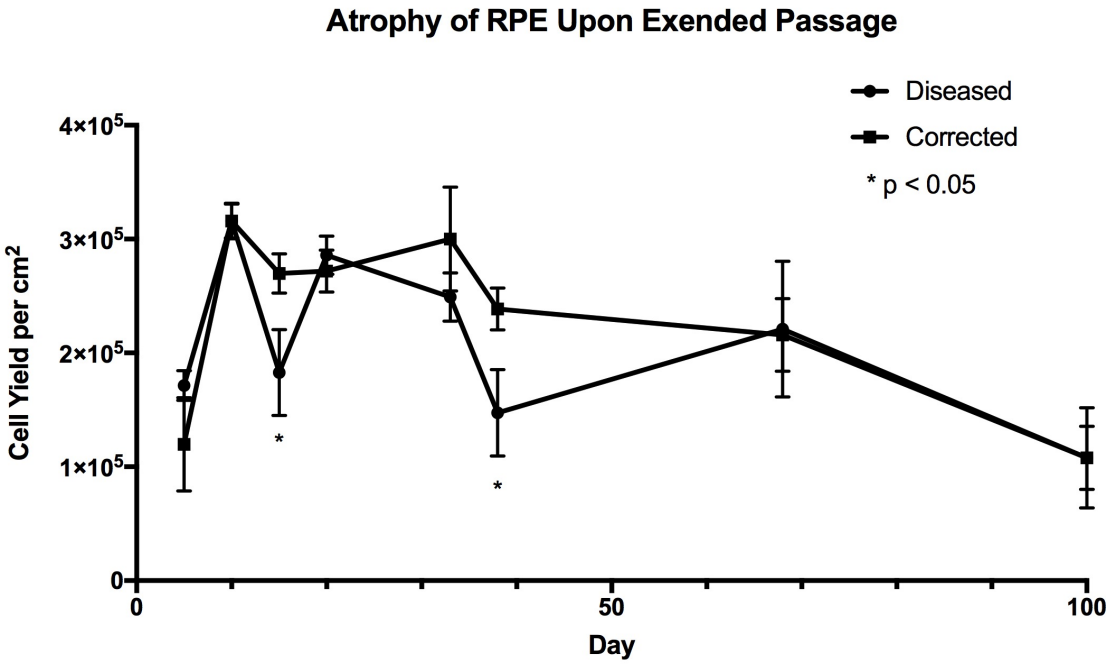

Figure 9. Atrophy of RPE upon extended passage.

RPE were passaged enzymatically at a seeding density of 1 x 10^5 cells per cm^2 and allowed to grow for 5 to 30 days. Both diseased and corrected RPE were able to proliferate until day 100. Each time point consists of two separate wells for all six cell lines.

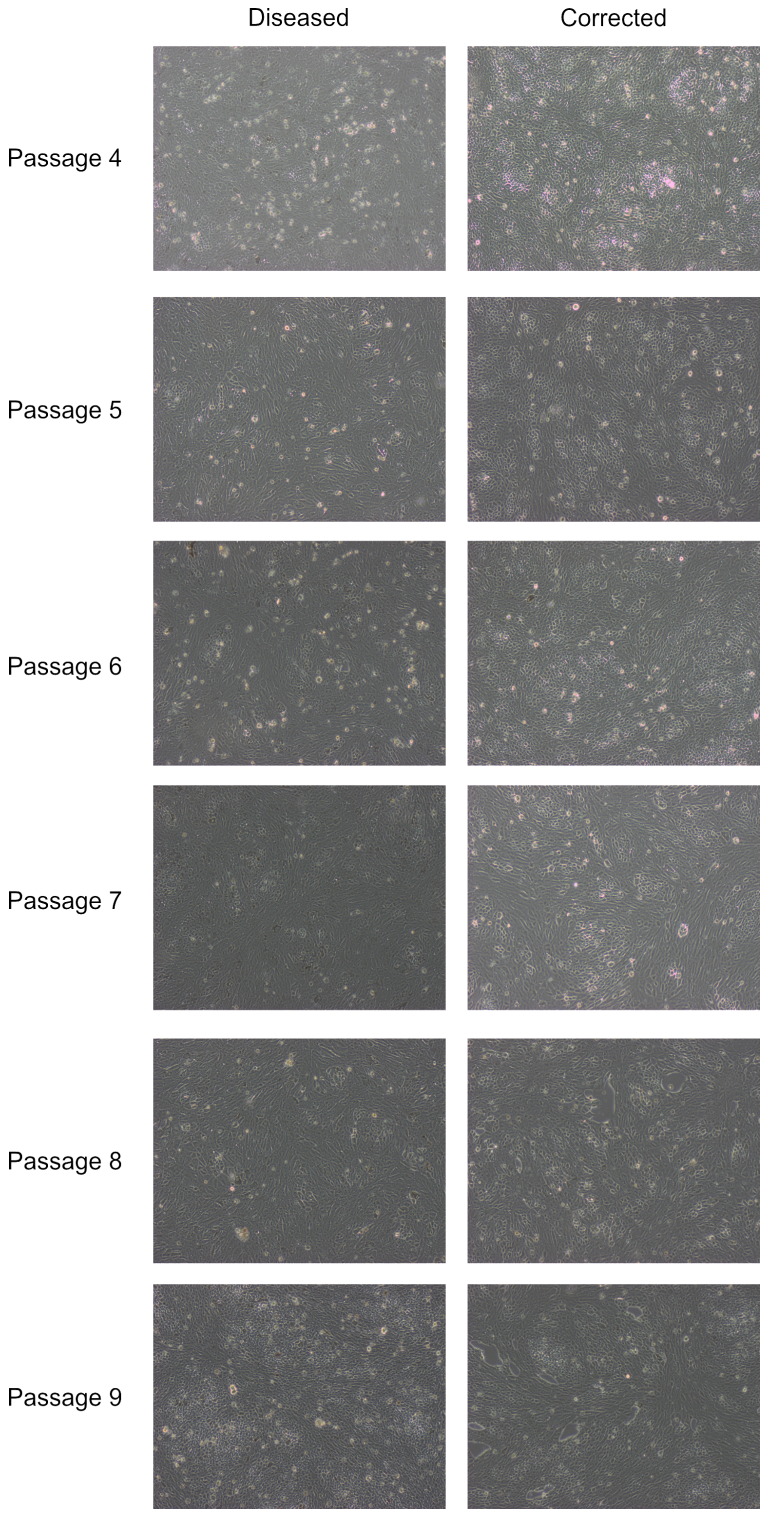

Figure 10 Extended passage RPE maintained epithelial morphology and confluence.

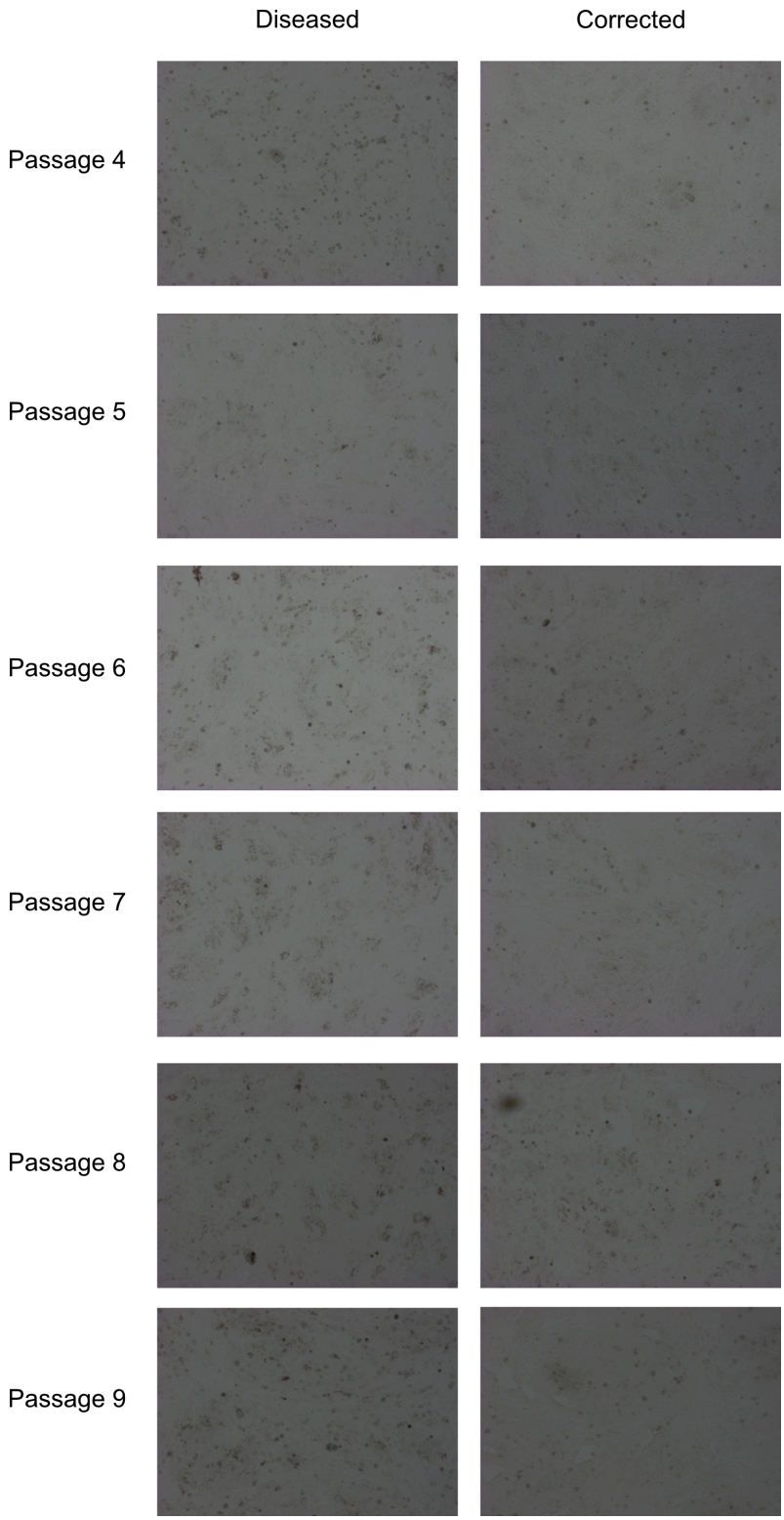

Figure 11. Extended passage RPE maintained pigmentation.

Confirmation of corrected point mutation in RPE

The mutated region of the PRPF8 gene was sequenced to confirm CRISPR/Cas9 correction of the P2301S point mutation. Figure 12 depicts the gene-corrected cell lines are homozygous for cytosine at position 6901 whereas the diseased cell lines are heterozygous for cytosine and thymine. The repair template contained silent mutations as indicated in the gene-corrected lines. These silent mutations, histidine(2306) and serine (2312) residues downstream of patient-specific mutation, aide in screening for off-target effects and prevent Cas9 re-cutting following gene repair and for confirming each cell line is derived from one clonal population. These silent mutations are predicted to be within a splice site

Minimal differentially expressed genes

Diseased and gene-corrected cell lines were grouped for analysis of differentially expressed genes using edgeR (**Figure 13-14**). Lowly expressed genes were filtered out by eliminating any sequences with less than 1 count per million (CPM) and the counts were normalized using a trimmed mean of M-values (TMM)[110]. Statistical dispersion was estimated using the quantile-adjusted conditional maximum likelihood (qCML) method. Biological coefficient of variation (BCV) was calculated and a multi-dimensional scaling (MDS) plot was produced to help identify outliers. Differential genes with a false detection rate (FDR) less than 0.05 were identified.

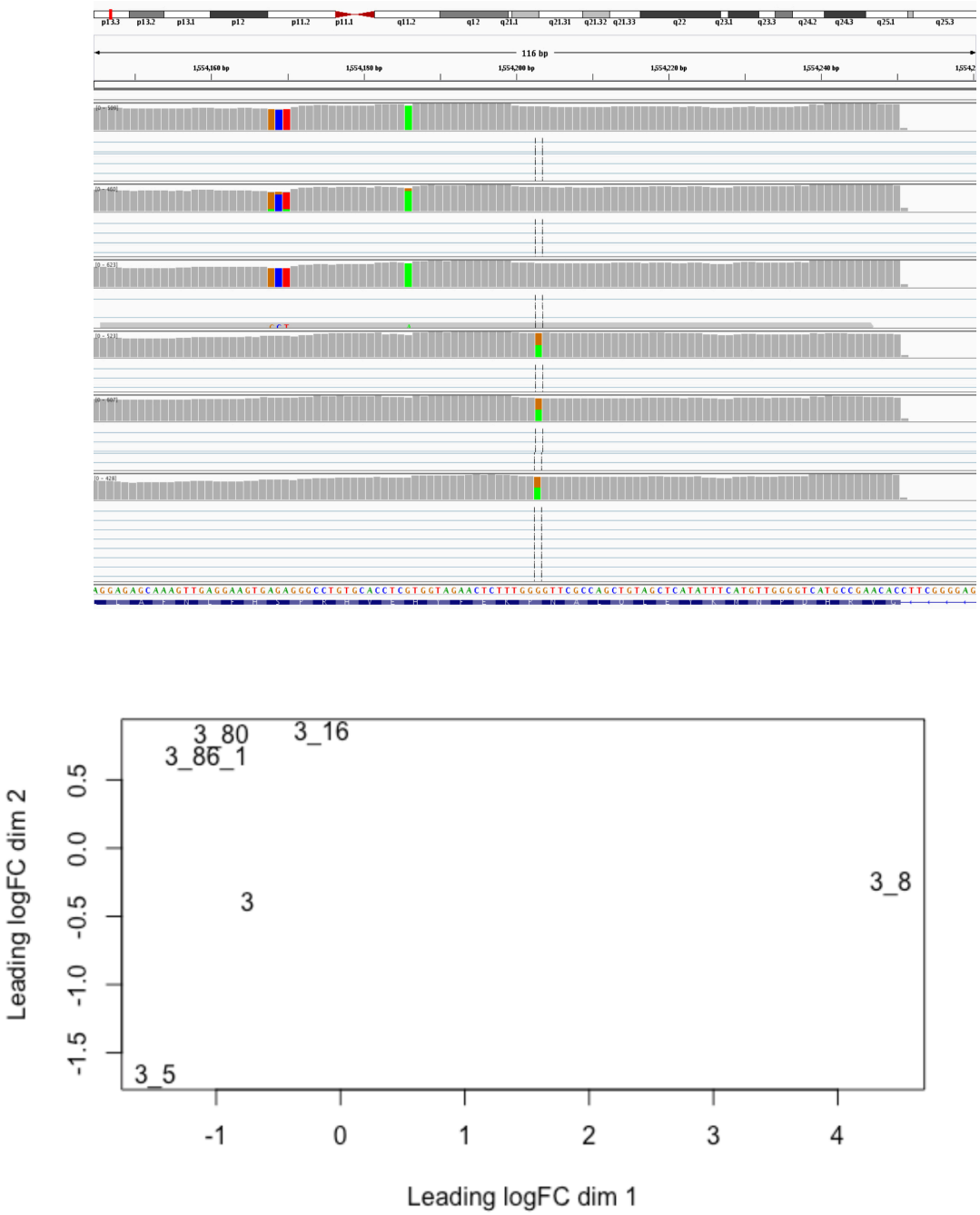

Figure 12. Confirmation of corrected point mutation in RPE and identification of outliers.

Sequencing of PRPF8 revealed the corrected genes received the point correction as indicated by the silent mutation (GCT) whereas the diseased lines retain different nucleotides on each chromosome (A and G). Corrected and diseased lines do not cluster but 3.8 and 3.5 are possible outliers. FC=fold-change, dim=dimension.

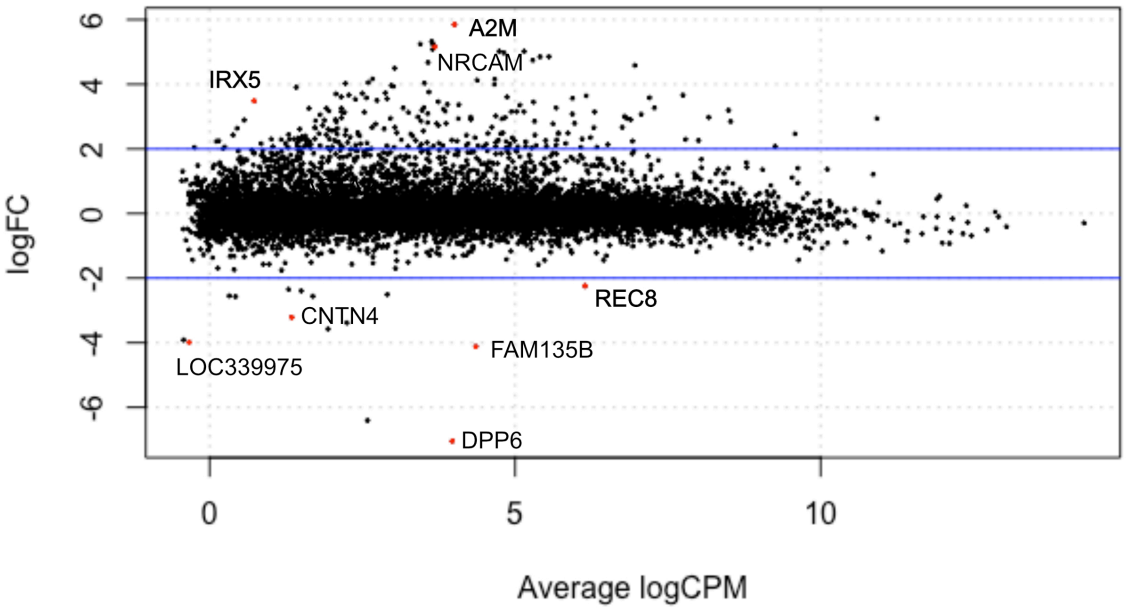

Figure 13. Differential expression of genes in passage 3 RPE from a single patient.

Eight genes identified with IRX5, A2M, and NRCAM more highly expressed in the corrected cells and LOC339975, CNTN4, DPP6, FAM135B, and REC8 more highly expressed in diseased cells. FC=fold-change, CPM=counts per million.

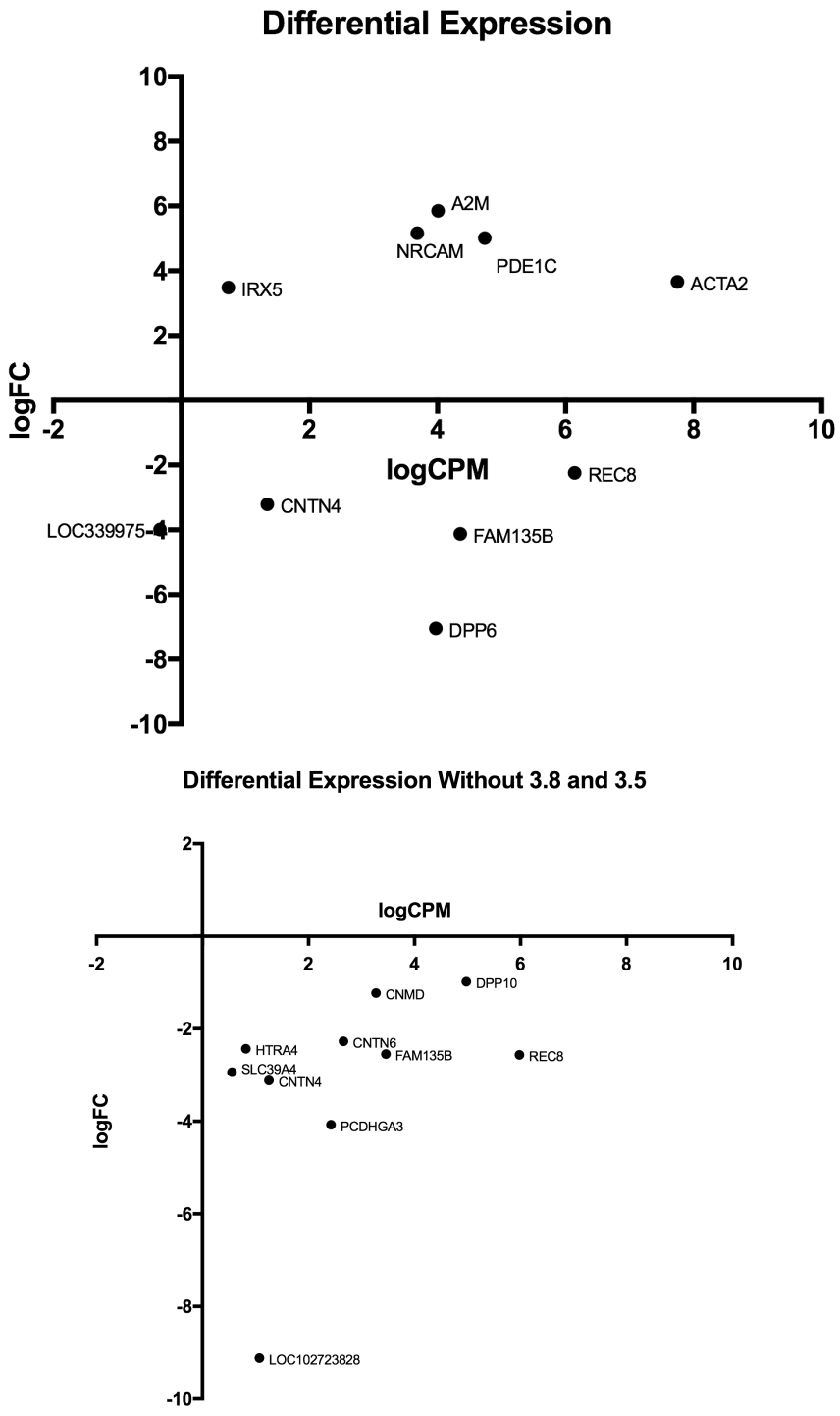

Figure 14. Differential expression of genes without outliers.

Differential expression analysis was repeated with and without clones 3.8 (corrected) and 3.5 (diseased). REC8 is identified in both analyses.

In the MDS plot, the distances between samples corresponds to the biological variation between those samples, which allowed for the identification of clone 3.8 as a possible outlier. There is no clear separation between the diseased lines (clone 3, 3.5, and 3.80) compared to the gene-corrected lines (clone 3.16, 3.8, and 3.86.1). In the log fold-change plot, the eight red points indicate the differentially expressed genes.

Upregulation of lncRNA in mutated retinal pigmented epithelial cells

In two RNA-sequencing experiments, LOC339975 was upregulated in the diseased retinal pigmented epithelial cells. In comparing the two groups, LOC339975 was expressed log fold-change of 4 higher in the mutated cell lines. This was confirmed by quantitative PCR analysis using probes for LOC339975.

To determine if LOC339975 is expressed in immature RPE and induced pluripotent stem cells, PMEL, TYRP1, and LOC339975 were measured in passage 0 day 30 RPE and SALL4, REX1, and LOC339975 were examined in passage 12 day 5 iPSC. In iPSC, immature, and mature RPE, the lncRNA is expressed at significantly higher levels in the diseased cells that the gene-corrected when compared to wild-type cells.

siRNA-mediated knockdown was performed to observe the effects of PRPF8 knockdown on the expression of lncRNA and to confirm aberrant expression of LOC339975 via RNA-specific targeting. PRPF8-siRNA decreased RNA expression in diseased and corrected cell lines when compared to a negative control-siRNA in the same cell lines. LOC339975-siRNA had no effect on PRPF8 expression and was

effective in decreasing expression of the lncRNA in diseased cells. There was no detection of LOC339975 in the corrected cell lines **(Figure 15)**.

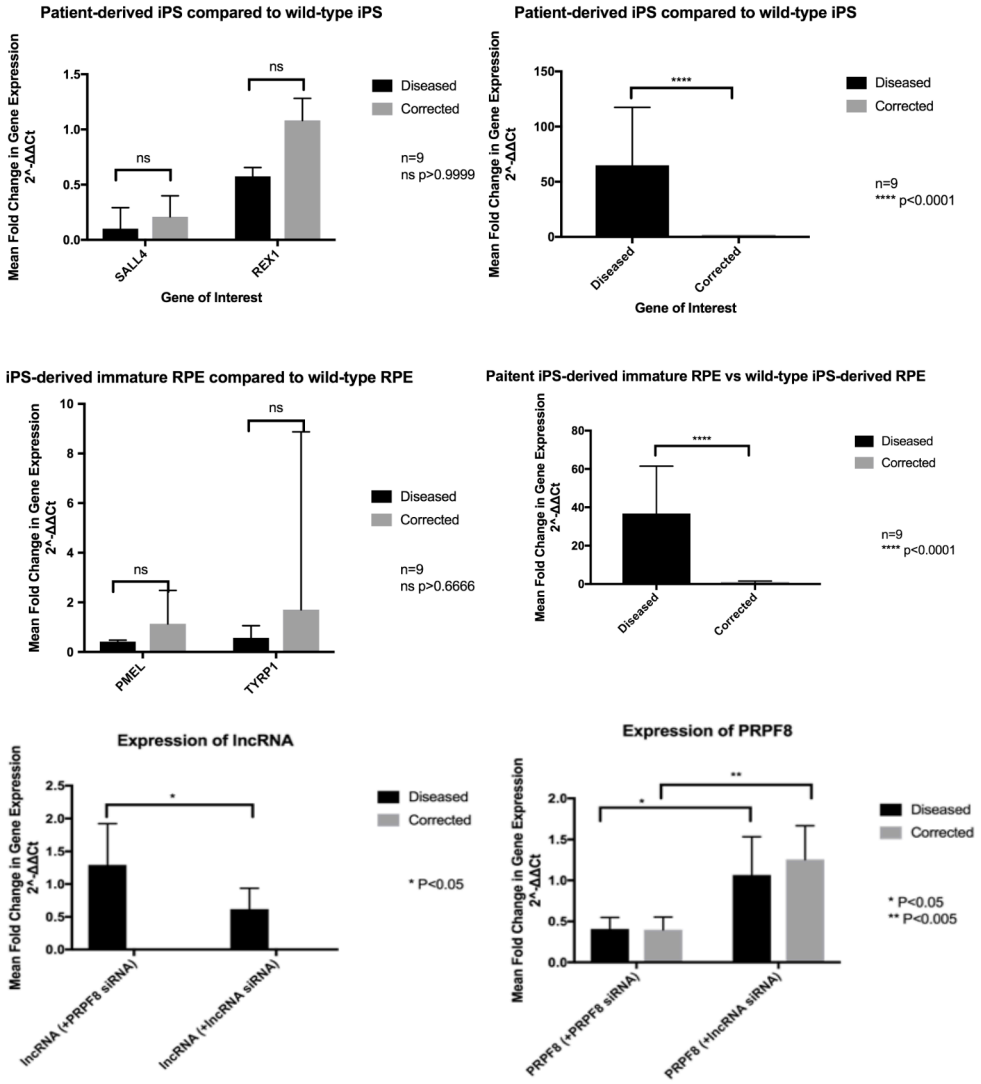

Figure 15. Detection of lncRNA in iPS and immature RPE.

PCR analysis of iPS and RPE from diseased and corrected lines reveal no significant difference of stem cell and RPE-specific genes but significant expression of lncRNA is observed in diseased cells when normalized to wild-type iPS and RPE. siRNA knockdown was successful for both lncRNA and PRPF8 when normalized to a negative control siRNA.

From this analysis, we demonstrate the lncRNA is upregulated in cells harboring a missense mutation in PRPF8 that is known to cause autosomal dominant retinitis pigmentosa. The role of lncRNA in splicing factor retinitis pigmentosa has not been reported prior to these studies.

The variation analysis as demonstrated that diseased clone 3.5 and corrected clone 3.8 were potential outliers, thus the differential expression analysis was performed with and without these outliers. In both analyses, REC8 was aberrantly expressed in the diseased RPE at a high level as indicated by logCPM (counts per million). Upon further investigation, it was found that REC8 inhibits the G0/G1 to S phase transition, and IRX5, a transcription factor more highly expressed in the corrected cells, promotes the G0/G1 to S phase transition. This led to the investigation of cell cycle arrest in the diseased cells.

The cell cycle analysis is based on the principal that the fluorescent intensity of propidium iodide at 488 nm is directly proportional to the mass of DNA present, which is expected to be higher in S phase and G2 phase than G0/G1 due to the replication of chromosomes. RNase is used to destroy RNA present to ensure fluorescence is only from the DNA. As expected, there are no cells in G2 phase at day 30, but the data revealed that a disproportionate number of cells were in the G0/G1 phase (**Figure 16**).

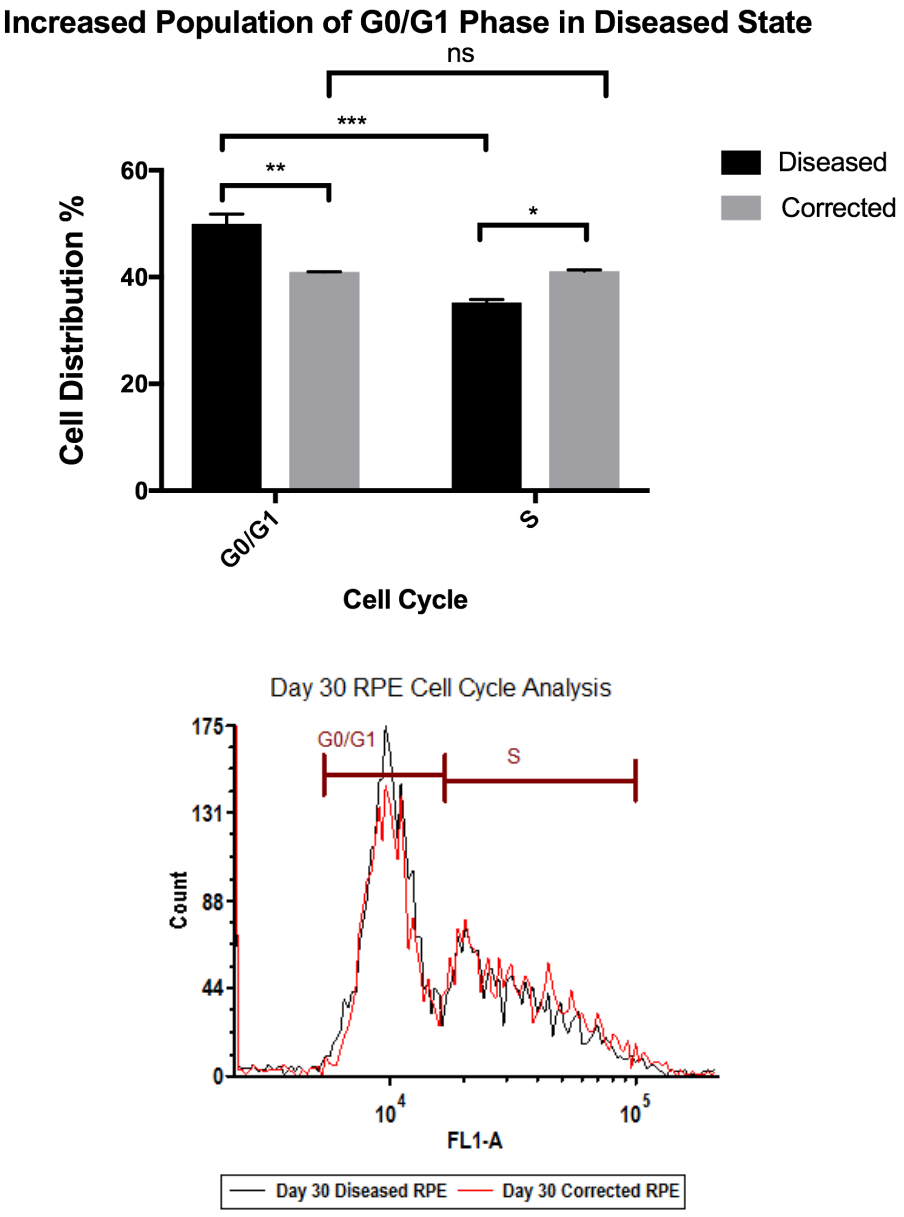

Figure 16. Increased population of G0/G1 phase in diseased state.

Flow cytometry analysis using propidium iodide and RNase reveal the proportion of cells in G0/G1 phase versus S phase. The same number of events were collected for each sample and the resulting counts were quantified in terms of cell distribution.

D. Discussion

With this work, we demonstrate that iPSC-derived RPE from a patient, with and without gene-correction, can produce a purified population of RPE that recreates the gene and protein expression of native RPE. In order to elucidate the pathology of splicing factor retinitis pigmentosa as caused by P2301S point mutation in PRPF8, it is important to ensure that the cells being examined recapitulate the *in vivo* cells.

After differentiation to a specific cell type, there are several general methods used to confirm the purity and functionality of the cell type of interest: 1) genetic analysis by polymerase chain reaction or next-generation sequencing, etc. 2) protein analysis by western blot, enzyme-linked immunosorbent assay, fluorescence assisted cell sorting, etc. 3) functional analysis such as photoreceptor outer segment phagocytosis. The same methods that have been used to confirm differentiation of a particular cell type may also be used to look for abnormalities in a disease state. While it would have been useful to find a difference between the diseased and corrected RPE, it is unsurprising that these assays did not reveal any distinction. There is no evidence that a mutation in PRPF8 affects the expression of RPE-specific genes or protein localization and secretion. There was a mouse model that argued that the protein localization of integrin subunits was affected in a knockout mouse for PRPF8, PRPF31, and PRPF3[8]. Specifically, they argue the αV integrin subunit, but note the β5, was mislocalized in the mutants. However, this result was a qualitative observation and the fluorescent images do not appear to support their argument.

The reproducibility of differentiation protocols is vitally important to the success of disease modeling. In order to draw conclusion from any observed differences between cells, there must be a strong indication that the cell populations are similar by other measurements, especially considering the concerns about line to line variability[47]. Once the gene expression and protein localization and secretion had been established, functional assays that have been shown to play a role in disease can be observed. RPE phagocytose POS on a daily basis, which is critical to the health of the retina[65]. The phagocytic relationship between RPE and photoreceptor outer segments was first observed by autoradiography over forty years ago[111]. Modern methods utilize the ability of RPE to phagocytose as a measurement of RPE health and differentiation efficiency *in vitro*[112]. RPE phagocytose via specific integrin subunits and are significantly more active in phagocytosis than most other cell types, allowing researchers to definitively identify RPE in culture[78,113]. Quantification of phagocytosis has been examined by several methods, including pixel detection and fluorescence plate reader[114].

Farkas et.al. argued that phagocytosis was deficient in the mutant RPE after isolation from the mice, which remained to be shown in human cells[8]. The mutation that was introduced in the mouse model (H2309P) was in the same domain as the patient cells (P2301S) (**Figure 4**). In fact, this sub region of the Jab1/MPN domain of PRPF8 is highly conserved across species and contains seven amino acids that have been recorded to have disease-causing point mutations[88,92,93]. The highly conserved nature of these residues suggests their critical role in the ill-defined function of PRPF8.

In order to assess phagocytosis, optimizations were required to observe a significant difference between the stem-cell derived RPE and the negative control cell line. Previous attempts of our phagocytosis assay were performed with preparations of photoreceptor outer segments that were isolated from whole bovine eyes in full light. The resulting preparations resulted in bleached outer segments, whereas commercially available outer segments retained the color of the tissue as it was isolated under low light conditions. Furthermore, the fluorescent labeling was performed at centrifugation speeds that have been reported to shear outer segments. By reducing the centrifugation speeds as described in the detailed protocol, outer segments were shown to retain their rod-like morphology. We believe this reduction in bleaching and shearing allowed there to be a significant difference between the negative cell line (retinal microvascular endothelial cells) and the stem cell derived RPE.

The secretion of pigment epithelium derived factor is frequently used as a measurement of apicobasal polarity and maturity of the RPE. We also wanted to investigate the secretion of MFG-E8, which is more closely related to the phagocytic function of RPE and had not been previously measured in stem cell-derived RPE. There was no significant difference in the ability of diseased and corrected RPE to secrete PEDF, and when compared to negative controls, stem cell derived RPE secreted significantly more MFG-E8, as expected. We believe that secretion of MFG-E8 and other proteins directly related to phagocytic function may help elucidate pathology of phagocytic defects in other disease models.

In addition to requiring robust differentiation procedures to produce a homogeneous population of RPE and optimization of functional assays, the initial reprogramming of the patient fibroblasts into iPSC must also be robust. Due to the relative simplicity and high efficiency, CRISPR/Cas9 has been used increasingly for genetic modifications in stem cells. Howden et. al. has developed an efficient protocol for the generation of gene-corrected cells lines that undergo the more precise homology directed repair pathway (HDR) rather than the predominate yet more mutative non-homologous end joining (NHEJ)[30,115]. The CRISPR/Cas9 system developed by Howden et al. and used to edit the cells in this study relies on two key factors related to the cell cycle: (1) cells prefer NHEJ in G1 phase and HDR in S phase, and (2) fusion of Cas9 endonuclease and geminin protein (Cas9-Gem) can be used to degrade Cas9 in the beginning of G1 phase. This allows the simultaneous reprogramming and gene editing of patient fibroblasts with a two to three-fold decrease in NHEJ and a reduction of insertion/deletion mutations in the healthy allele[115].

In disease modeling, it is critical to precisely edit a gene in order to compare the diseased and gene-corrected cells in a way that recapitulates the cellular and molecular mechanisms of the disease. The simultaneous reprogramming and gene-correction method allowed for the production of six passage-matched clones from one biological replicate. Due to the robust reprogramming and differentiation procedures, the next-generation sequencing transcriptome analysis revealed minimal differentially expressed genes. In two repeated RNA sequencing experiments, it was

found that a long-noncoding RNA (LOC339975, henceforth referred to as lncRP13) was expressed in the diseased cells but not the gene-corrected cells. As shown in the BCV analysis, clone 3.8 was identified as an outlier and was the most difficult to differentiate based on morphological assessment during the 14-day protocol. In examining the raw data, clone 3.8 was usually an outlier in the differentially expressed genes with the exception of lncRP13. Aberrant expression of lncRP13 was confirmed by quantitative polymerase chain reaction for all six of the patient-derived clones and normalized to passage-matched healthy control induced pluripotent stem cell line.

We hypothesized that knockdown of PRPF8 in gene-corrected cell lines may induce expression of lncRP13. Our results indicate that upon small interfering RNA (siRNA) knockdown of PRPF8, there is no detectable expression of lncRP13. These data suggest that the aberrant expression of lncRP13 is a result of the patient-specific mutation and is not due to a decrease in PRPF8 expression. Furthermore, we demonstrate that siRNA-mediated knockdown of lncRP13 in the diseased cells provides further evidence of the expression of this lncRNA. Future studies may demonstrate the functional role of lncRP13 in splicing factor retinitis pigmentosa, and siRNA-mediated knockdown may provide a tool for investigating the pathology or development of a drug therapy.

LncRNA has been implemented in its role in the normal function of the retina as well as in disease states[99–101]. lncRP13 specifically has remained uncharacterized. LncRNA has been shown to interact with proteins in involved in several different pathways[116]. Given the RNA binding ability of PRPF8, we hypothesize that there may

be a direct interaction between PRPF8 and lncRP13; however, understanding the RNA biology of lncRNA has proven difficult[117]. Future studies examining the interaction of lncRNA with pre-mRNA processing factors may help elucidate the role of lncRP13 in the molecular pathology of autosomal dominant retinitis pigmentosa.

Our RNA sequencing analysis also revealed that the diseased cells were more highly expressing REC8, which had been shown to inhibit cell cycle progression in other cell types but had not been studied in RPE[118]. Further investigation of the role of cell cycle arrest in inherited retinal degenerations led us to a body of literature pertaining to cell cycle, ciliogenesis, and ciliopathies.

Ciliopathies are a growing class of inherited retinal diseases that result in atrophy of the photoreceptors and the retina[119]. An siRNA-based functional genomics screen identified 112 candidate genes for their involvement in growth and maintenance of primary cilium[120]. Among these candidates were three pre-mRNA processing factors: PRPF6, PRPF8, and PRPF31, mutations in which can cause autosomal dominant retinitis pigmentosa. A more recent siRNA study investigated the connection between ciliogenesis and cell cycle progression, finding that PRPFs function in disassembly of the primary cilium and progression of cell cycle[121]. Together these data led us to hypothesize that PRPF8 may function beyond splicing in the disassembly of cilium and cell cycle progression.

Our results demonstrate that a larger proportion of diseased cells are arrested in the G0/G1 phase as compared to corrected cells. This work is the first report of cell cycle arrest in patient-derived cells as compared to those subjected to siRNA

knockdown of PRPFs. Future work should be directed towards identifying the precise functional role of PRPF8 and the other pre-mRNA processing factors in cell cycle regulation and ciliogenesis. Researchers have shown that RPE and retinal organoids can be used to examine the morphology of primary cilium in both photoreceptors and RPE[36,59]. This work pertained to mutations in CEP290, which had previously been shown to cause fewer cilia in fibroblasts from patients[35]. Given the role of CEP290 in ciliogenesis and the potential role of PRPFs in cilia disassembly, future studies will need to determine how to quantify abnormal cilia morphology depending on the patient-specific pathogenesis.

E. Conclusions

Our findings demonstrate that mature, functional RPE can be differentiated reproducibly from six induced pluripotent stem cells lines. This work shows that previous reports of phagocytic defects in mouse RPE are not detected in a human model of RP13. This is the first report that PRPF8 diseased RPE aberrantly express the lncRNA LOC339975 that is susceptible to siRNA. Earlier work has investigated the role of PRPF8 in binding RNA as well as the suspected role of lncRNA in retinal degeneration. Genetic correction of the PRPF8 mutation restored the expression of lncRNA to the level of wild-type cells. Future studies will help elucidate the role of this lncRNA in the pathology of splicing factor retinitis pigmentosa. Finally, diseased RPE aberrantly express REC8, which is thought to regulate the G0/G1 to S phase transition, and a disproportionately large population of diseased RPE are in the G0/G1 phase as determined by DNA mass.

IV. Differentiation of Induced Pluripotent Stem Cell-Derived Retinal Organoids for Modeling Autosomal Dominant and Autosomal Recessive Retinitis Pigmentosa

ABSTRACT

Retinitis pigmentosa can be inherited in autosomal dominant and recessive patterns. Specifically, mutations in ubiquitously expressed splicing factor proteins are known to cause an autosomal dominant form of the disease, whereas mutations in the retina-specific crumbs 1 (CRB1) protein cause an autosomal recessive form of the disease. In this study, we investigated the use of stem cell-derived retinal organoids for modeling two forms of retinitis pigmentosa. We show that retinal organoids produced from patient-derived induced pluripotent stem cells are morphologically similar to wild-type retinal organoids *in vitro*. Furthermore, we demonstrate that retinal organoids produced from wild-type stem cells express CRB1. Expression of neural retina-specific proteins, including vimentin and rhodopsin, were observed. Functionally, the diseased and gene-corrected retinal organoids were able to achieve organoid growth rates comparable to those seen in wild-type retinal organoids. These studies show that patient-derived and wild type stem cells are able to differentiate into retinal organoids that recapitulate *in vivo* development, including expression of proteins that are known to cause retinitis pigmentosa.

A. Autosomal dominant splicing factor retinitis pigmentosa: PRPF8

1. Introduction

The human retina consists of not just a few types of neurons, but rather is made up of around 55 different cell types. Masland et al. 2001 describes the added complexities of the primate retina, which unlike some simpler mammals, consists of two types of horizontal cells, twenty-nine types of amacrine cells, between ten and fifteen different retinal ganglion cells, and so on[1]. The inherent complexity of the retina has made it challenging to develop retinal organoids that recapitulate the native retina. The success of existing disease models suggests it is not necessary to produce all of these cell types in a way that mimics the positions and proportions they are found *in vivo.* Instead, protocols have focused on development of the two most commonly affected cell types: photoreceptors and RPE. Production of neural retina has been approached in both two-dimensional [49,50] and three-dimensional methods [51-54]. Various methods for directing differentiation of neural retina in both two-dimensional and three-dimensional cultures for human and mouse stem cells has been thoroughly reviewed from 2006 through 2017 [55].

Here we describe the process used to establish a three-dimensional retinal organoid model from patient-derived iPSC. The iPSC result from a novel method of simultaneous reprogramming and gene-correction, making this is the first report of retinal organoids produced from such cells and from a patient with PRPF8 splicing factor retinitis pigmentosa.

2. Materials and Methods

Differentiation of pluripotent cells to retinal organoids

PRPF8 iPSCs and wild type MyCell iPSCs and H9 hESCs were seeded onto Matrigel-coated 6 well plates (Corning) and cultured for 3 to 7 days before passage by Versene to micro-space 96 well plate (Elplasia, Tokyo, Japan, http://www.elplasia.com) for embryoid body formation. Neural induction and retinal differentiation were performed as described in Zhong et al. 2014 [52]. Media formulations included neural induction media (NIM) and retinal differentiation media 1, 2, and 3. NIM consisted of 1:1 DMEM:F12, 1 X N2, 1 X NEAA, and 2 μg/mL heparin (STEMCELL Technologies). RDM1 was used from day 16 to day 28 and consisted of 3:1 DMEM:F12 1 X B27 without Vitamin A, 1 X NEAA. RDM2 consisted of 3:1 DMEM:F12, 1X B27, 1X NEAA, and RDM3 consisted of 3:1 DMEM:F12, 1 X B27, 1 X NEAA, 10% fetal bovine serum (Atlanta Biologicals), 100 μM taurine, and 2 μM GlutaMAX (Fisher Scientific).

Cryosectioning

Retinal organoids (ROs) were removed from suspension culture between days 40 and 180. Individual ROs were placed in single wells of a 24 well plate and fixed in 4% paraformaldehyde (PFA) in 0.1M sodium cacodylate buffer, pH 7.4, for 20 minutes at room temperature on an orbital shaker in the dark. Samples were imaged and stored for up to 1 month in 0.1% PFA. Fixed samples were rinsed three times for 5 min in cold PBS and cryoprotected in a sucrose gradient: 10%, 20%, and 30% sucrose in PBS for 1 hr each followed by 40% sucrose in PBS overnight on an orbital shaker.

Samples were placed in disposable plastic molds, embedded in Optimal Cutting Temperature Compound (OCT, Fisher Scientific, Hampton, NH, http://www.fishersci.com/), and frozen on dry ice to store at -80 ˚C. Frozen samples were cut into 10-20 μm sections on a Leica Cryostat CM1850 (Leica, www.leica-microsystems.com) at -20 ˚C and adhered to SuperFrost Plus Microscope Slides (Fisher Scientific).

Immunofluorescence

Retinal organoid samples were washed twice with cold PBS then blocked with 5% bovine serum albumin (BSA) (Millipore Sigma) with 0.2% Triton X-100 to permeabilize the cell membrane. After blocking, ROs were incubated overnight at 4 ˚C with primary antibody. Cells were washed three times with cold PBS, incubated with the corresponding secondary antibody conjugated to AlexaFlour (1:300) (Invitrogen) or Cy2, 3, or 5 (1:200)(Jackson-Immuno) for 1 hr at 4 ˚C, incubated with Hoechst (2 μg/mL)(Invitrogen) for 5 min at room temperature, washed three times with PBS, mounted with 80 μL Prolong Gold Mountant (Invitrogen) and coverslip, and imaged on Olympus IX70 Inverted Compound microscope, Olympus Fluoview 1000 Spectral Confocal microscope (Olympus, www.olympusamerica.com), or Leica SP8 Resonant Confocal microscope (Leica, www.leica-microsystems.com).

3. Results

Characterization of retinal organoids

Patient-derived iPSC were differentiated into retinal organoids based on an established protocol[52]. At day 90, total RNA was harvested from suspension retinal organoids for both the diseased and corrected cell lines. Total RNA was also collected from adherent wild-type iPSC as a control for determining the mean fold change in gene expression using the Livak method. There was no significant difference in expression of neural retina markers (**Figure 17**).

Embryoid bodies were formed in microspace plates to control for the size and plating density at day 28. All six patient-derived cell lines produced embryoid bodies that subsequently produced the signature horseshoe morphology that is used to identify neural retina in adherent culture (**Figure 18**). Retinal organoids were measured in culture from day 41 to day 194 and there was no significant difference between the growth of the diseased and corrected organoids, which the exception of Day 111 and Day 194 (**Figure 19**).

In suspension culture, a sub-population of the organoids developed an outer lamina that implied the presence of an outer retinal layer. Organoids were collected at various time points between day 70 to day 194 for sectioning and immunofluorescence. Retinal organoids were screened for mature morphology and were shown to express rhodopsin in few of the organoids at what appears to be distal to the outer nuclear layer (**Figure 20**).

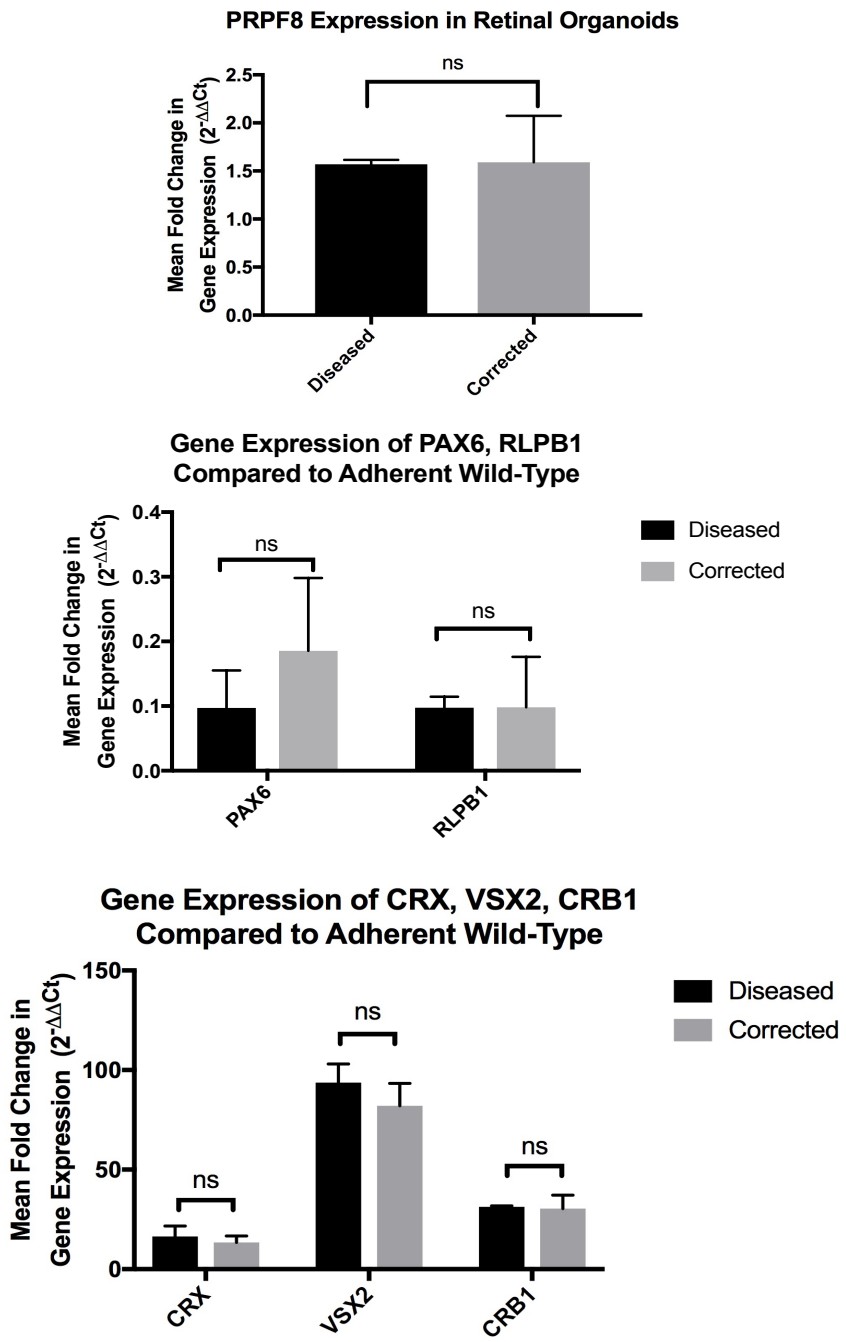

Figure 17. Gene expression in retinal organoids.

Diseased and corrected cells express similar levels of PRPF8 and retina specific genes (PAX6, RLBP1, CRX, VSX2, and CRB1).

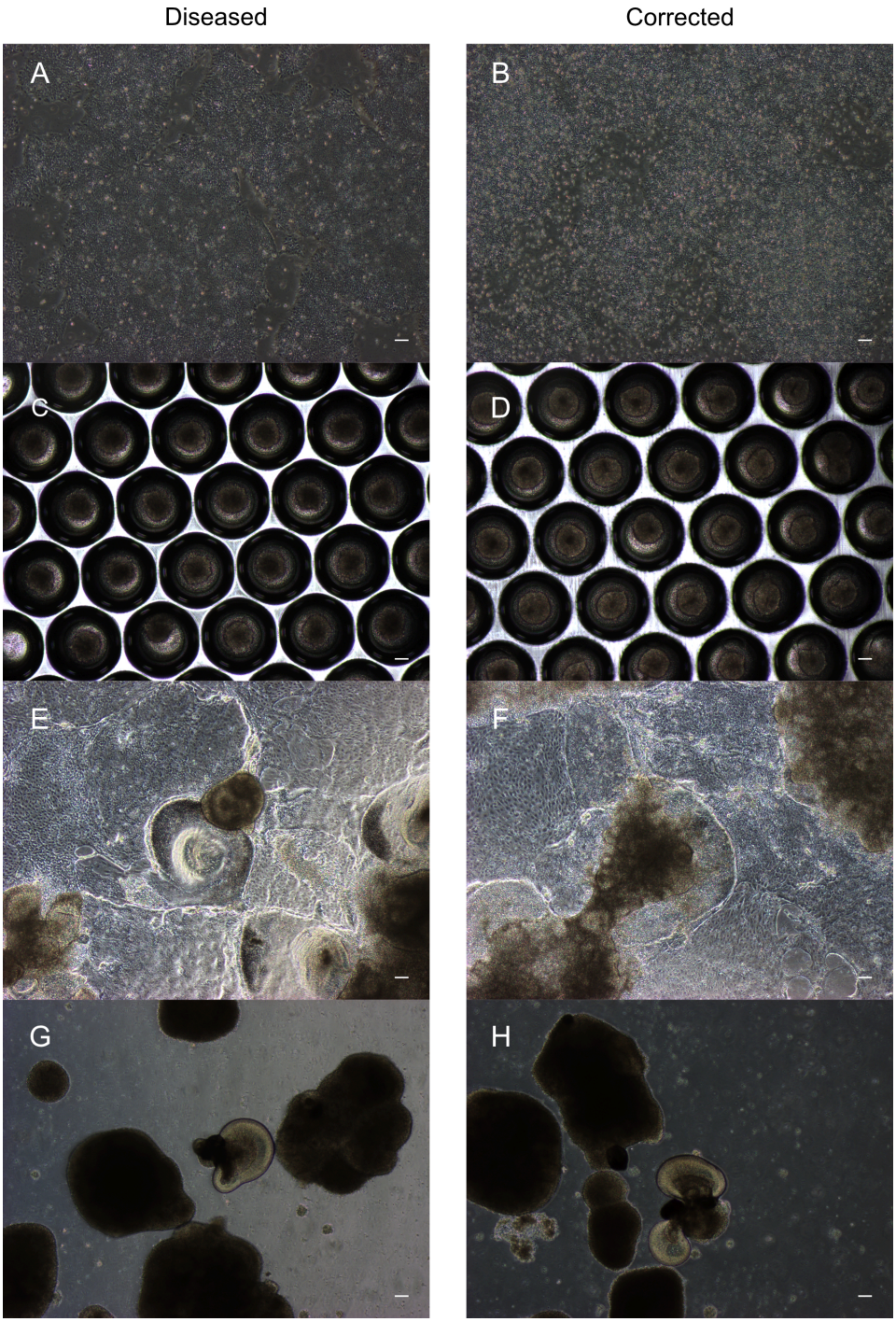

Figure 18. Differentiation process for retinal organoids.

Induced pluripotent stem cells are grown to 75-100% confluence prior to single cell passaging (A-B), Embryoid bodies are formed in microwells for 7 days (C-D), Embryoids are seeded at a density of 20 bodies per cm^2 to allow for the formation of horseshoe morphology (E-F) Retinal organoids are matured for 70 to 200 days (G-H). Scale bar equals 100 μm.

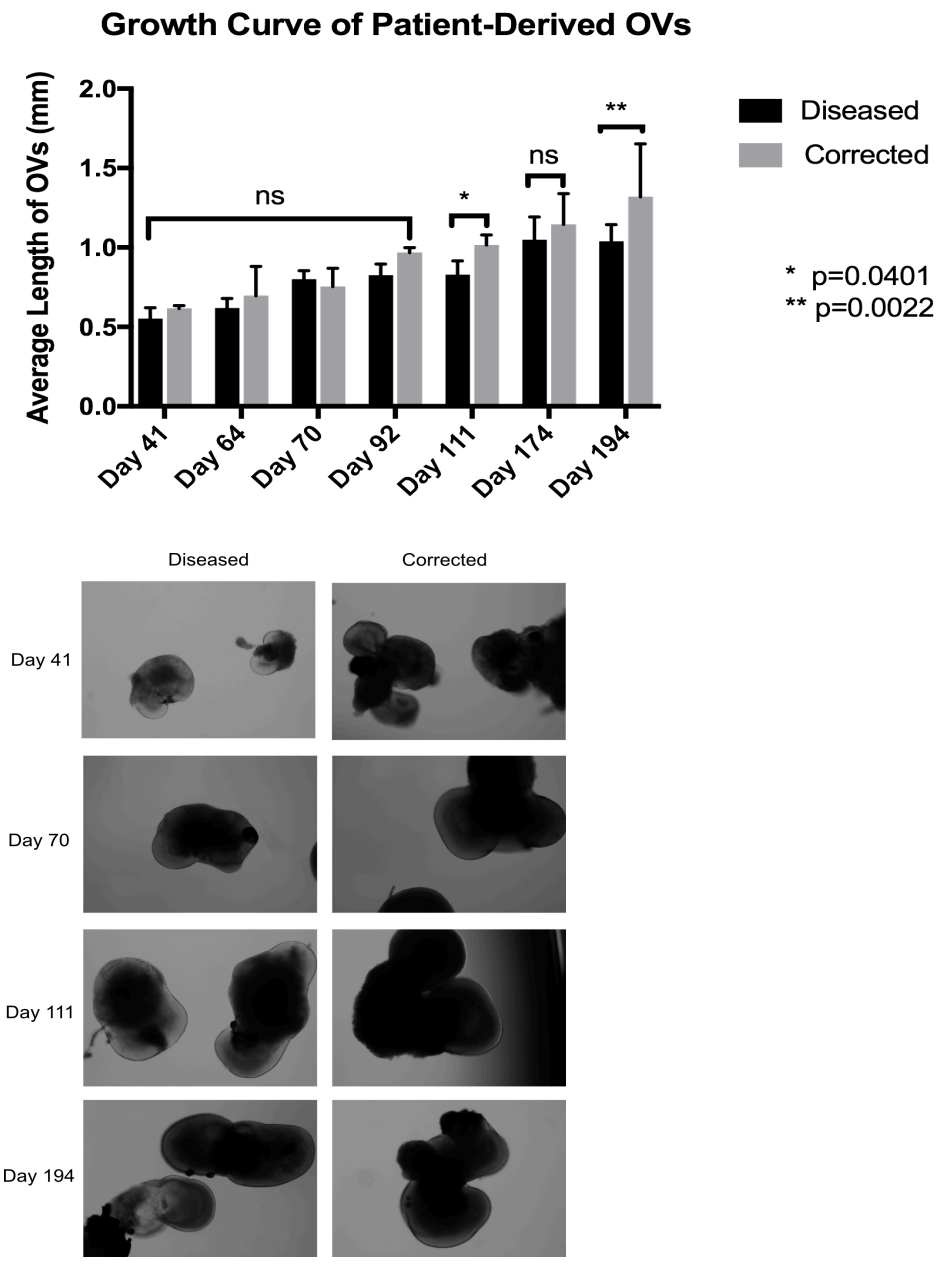

Figure 19. Growth curve for patient-derived retinal organoids.

Retinal organoids were kept in culture for 194 days and imaged regularly to determine growth rate. Each time point consists of 10-20 organoids.

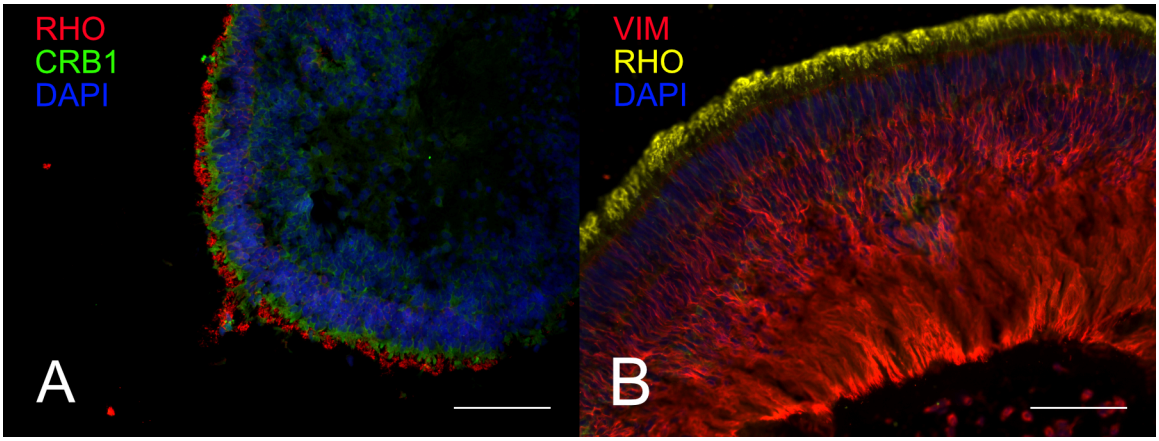

Figure 20. Retinal organoids form rhodopsin-expressing outer segments.

Wild-type human embryonic stem cells are able to produce mature organoids with rhodopsin expression distal to the photoreceptor inner segment as shown by localization of CRB1 (A). Diseased patient-derived cell lines are able to produce Müller glial cells and rhodopsin expression distal to the outer nuclear layer (B). Scale bar equals 100 μm.

4. Discussion

In this study, we show that patient-derived pluripotent cells are able to form retinal organoids that mimic the *in vivo* development of the retina.

The first report of *in vitro* development of an optic-cup structure was reported in 2011[122]. Similar to the development of other organoids, the most incredible feature is the ability of cells to self-organize in a way that mimics *in vivo* tissues. Since the initial report of retinal organoid development, there have been several publications regarding specific methods for differentiation[51–53]. Most protocols involve some combination of adherent and suspension culture, making these methods particularly labor intensive and highly variable. As shown in Figure 18, stem cells begin in adherent culture, proceed to embryoid body suspension culture, return to adherent culture for the identification of neural retina, and finally allowed to grow in suspension for weeks to months at a time.

While we have not quantified this result, we observe that the embryoid bodies tend to develop a large number of neural rosettes and amorphous structures rather than the desirable "horseshoe" morphology. This tendency made it impossible to produce organoids with the same efficiency as a purified cell type such as retinal pigmented epithelial cells. Established protocols call for a specific seeding density of embryoid bodies per cm^2 at day 7 of the procedure (**Figure 18E-F**). We originally used non-adherent tissue culture plates to produce embryoid bodies, but this resulted in varying numbers and sizes of the embryoid bodies. By using the microwells, we were

able to control the size of the embryoid bodies and seed a more precise number of bodies per cm^2 to minimize the variation between cell lines and differentiation batches.

In addition to RNA and protein level expression of retina-specific genes, the organoids also adhered to the growth rate that was demonstrated in wild-type cells[52]. In this analysis, we only considered the size of organoids with laminated exteriors and excluded amorphous, opaque organoids that are removed from culture in most retinal organoid protocols. Given the results of cell cycle arrest in the functional analysis of RPE in chapter III, we hypothesized that the diseased retinal organoids may grow at a slower rate. Although the corrected organoids were significantly larger at day 111 and day 194, these results were limited to only two of the time points measured (**Figure 19**).

In previous iPSC disease models of retinitis pigmentosa, retinal organoids were screened for morphological differences related to the disease. In the case of splicing factor retinitis pigmentosa, morphological affects remain largely unknown. Our results demonstrate potential problems with cell cycle progression, which may be related to ciliogenesis. Retinitis pigmentosa caused by a number of mutations have been identified as ciliopathies in both photoreceptors and RPE. The data presented here suggest that retinal organoids produced from PRPF8 mutants should be examined for indications of ciliopathy. Future studies may help identify morphological differences that were not immediately detectable in the retinal organoids produced during this study.

B. Autosomal recessive retinitis pigmentosa: CRB1

1. Introduction

The crumbs homologue 1 (CRB1) gene encodes for an apical transmembrane protein, which functions in cell-cell interactions and establishment of cell polarity. The human protein was first discovered as a homologue to the CRB protein in Drosophila melanogaster and was determined to be the causative gene involved in RP12, a severe form of autosomal recessive retinitis pigmentosa[123]. CRB1 is critical in the morphogenesis of photoreceptors and is located on the inner segment of mammalian photoreceptors[124]. Genetic screening of autosomal recessive retinitis pigmentosa patients has identified novel missense mutations shown to cause RP12 and Leber congenital amaurosis, the earliest onset and most severe inherited retinal dystrophy[125,126].

Due to the conservation across species, investigation of RP12 in non-human models may provide relevant pathological information (**Figure 21**). A mouse model of RP12, referred to as retinal degeneration 8 (rd8), was established by introducing a one base pair deletion in CRB1 that causes a frame shift mutation and premature stop codon[127]. Gene transfer of CRB2 targeted to photoreceptors and Müller glial cells rescued the structure of photoreceptors in the rd8 mouse, which provided the first pre-clinical evidence of gene therapy in RP12[128]. CRB1, CRB2, and CRB3 are part of a crumbs complex in the retina that connects photoreceptors and glial cells. Although there has been success in using CRB2 to treat CRB1 deficient mice, the crumbs complex is drastically different in mice versus humans. Most notably, CRB1 is a

transmembrane protein in both photoreceptors and glial cells in humans, whereas CRB2 is a membrane associated protein in both cell types in mice. Due to these differences in cellular anatomy, it is critical to model RP12 in human retinal cells to accurately recapitulate normal human development and disease.

Stem cell-derived retinal organoids provide a tool for studying the localization and function of CRB1 *in vitro*. Differentiation methods demonstrate the development of functioning photoreceptor outer segments in culture[49–54]. Previous studies have not tested for the expression of CRB1 in the inner segment of the resulting retinal organoids. We have access to a RP12 patient with two novel missense mutations, one on each allele: Cys698Arg and Leu878Pro (unpublished). Missense mutations including W675C, C891G, and N894S have all been shown to cause RP12[123,129,130]. Prior to gene editing of the patient stem cells, we established the ability to study the crumbs complex in stem cell-derived retinal organoids from wild-type cells.

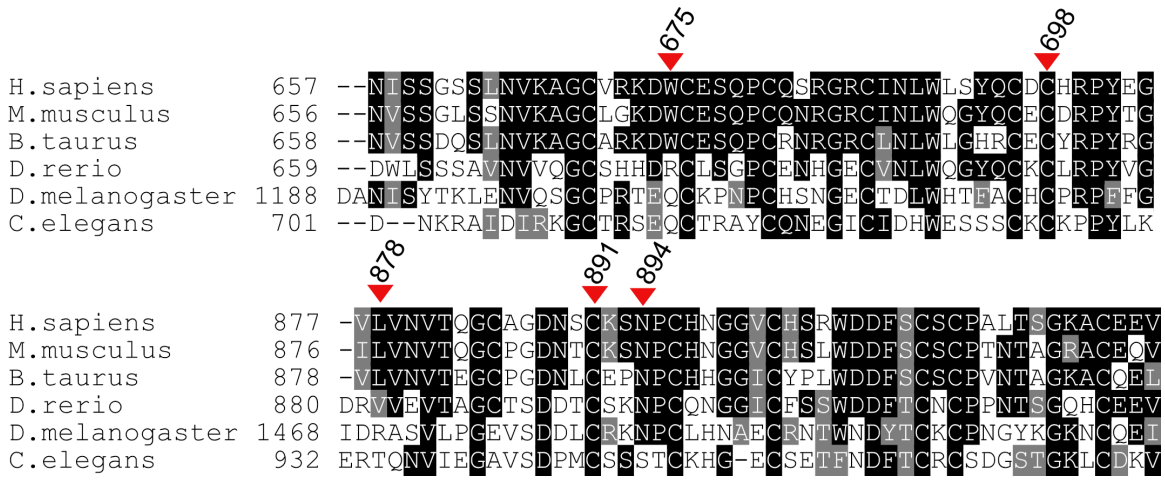

Figure 21. RP12 causative mutations in CRB1.

Multiple sequence alignment for CRB1 demonstrates the conservation of CRB1 in mammals with less consensus among non-mammals. Amino acids at positions 675, 891, and 894 are known causative mutations, whereas mutations at positions 698 and 878 are novel.

2. Materials and Methods

Differentiation of pluripotent stem cells to retinal organoids

H9 human embryonic stem cells were seeded onto Matrigel-coated 6 well plates (Corning) and cultured for 3 to 7 days before passage by Versene for embryoid body formation. Neural induction and retinal differentiation were performed as described in Zhong et al. 2014 [52]. Media formulations included neural induction media (NIM) and retinal differentiation media 1, 2, and 3. NIM consisted of 1:1 DMEM:F12, 1 X N2, 1 X NEAA, and 2 μg/mL heparin (STEMCELL Technologies). RDM1 was used from day 16 to day 28 and consisted of 3:1 DMEM:F12 1 X B27 without Vitamin A, 1 X NEAA. RDM2 consisted of 3:1 DMEM:F12, 1X B27, 1X NEAA, and RDM3 consisted of 3:1 DMEM:F12, 1 X B27, 1 X NEAA, 10% fetal bovine serum (Atlanta Biologicals), 100 μM taurine, and 2 μM GlutaMAX (Fisher Scientific).

Cryosectioning

Retinal organoids (ROs) were removed from suspension culture at day 120. Individual ROs were placed in single wells of a 24 well plate and fixed in 4% paraformaldehyde (PFA) in 0.1M sodium cacodylate buffer, pH 7.4, for 20 minutes at room temperature on an orbital shaker in the dark. Samples were imaged and stored for up to 1 month in 0.1% PFA. Fixed samples were rinsed three times for 5 min in cold PBS and cryoprotected in a sucrose gradient: 10%, 20%, and 30% sucrose in PBS for 1 hr each followed by 40% sucrose in PBS overnight on an orbital shaker. Samples were placed in disposable plastic molds, embedded in Optimal Cutting Temperature Compound (OCT, Fisher Scientific, Hampton, NH, http://www.fishersci.com/), and

frozen on dry ice to store at -80 ˚C. Frozen samples were cut into 10-20 μm sections on a Leica Cryostat CM1850 (Leica, www.leica-microsystems.com) at -20 ˚C and adhered to SuperFrost Plus Microscope Slides (Fisher Scientific).

Immunofluorescence

Retinal organoid samples were washed twice with cold PBS then blocked with 5% bovine serum albumin (BSA) (Millipore Sigma) with 0.2% Triton X-100 to permeabilize the cell membrane. After blocking, ROs were incubated overnight at 4 ˚C with primary antibody. Cells were washed three times with cold PBS, incubated with the corresponding secondary antibody conjugated to AlexaFlour (1:300) (Invitrogen) or Cy2, 3, or 5 (1:200)(Jackson-Immuno) for 1 hr at 4 ˚C, incubated with Hoechst (2 μg/mL)(Invitrogen) for 5 min at room temperature, washed three times with PBS, mounted with 80 μL Prolong Gold Mountant (Invitrogen) and coverslip, and imaged on Olympus IX70 Inverted Compound microscope, Olympus Fluoview 1000 Spectral Confocal microscope (Olympus, www.olympusamerica.com), or Leica SP8 Resonant Confocal microscope (Leica, www.leica-microsystems.com).

3. Results

Characterization of retinal organoids

Retinal organoids were differentiated from human embryonic stem cells according to published protocol[52]. Localization of CRB1 in wild-type hESC-derived retinal organoids was observed using immunofluorescence (**Figure 22**). Figure 23 shows in all three organoids that were examined, CRB1 was properly localized on what is presumably the inner segment of a photoreceptor precursor. The organoids expressed varying amounts of rhodopsin, which is expected based on previous reports[52]. CRB1 co-localized with the Müller glial cells as indicated by vimentin, which is expected as both photoreceptors and Müller glial cells express CRB1.

Retinal organoids were examined for gene expression of CRB1 at day 90 of development. In this work, the diseased and corrected cells correspond to the patient-derived cells used for studying autosomal dominant RP13. In comparison to adherent, wild-type iPSCs that were grown in the same media for 90 days, the suspension retinal organoids highly expressed CRB1. Although these cell lines do not correspond to the gene-corrected cells targeting CRB1, this demonstrates that CRISPR-edited stem cells can produce mature retinal organoids with similar expression of CRB1 (**Figure 24**).

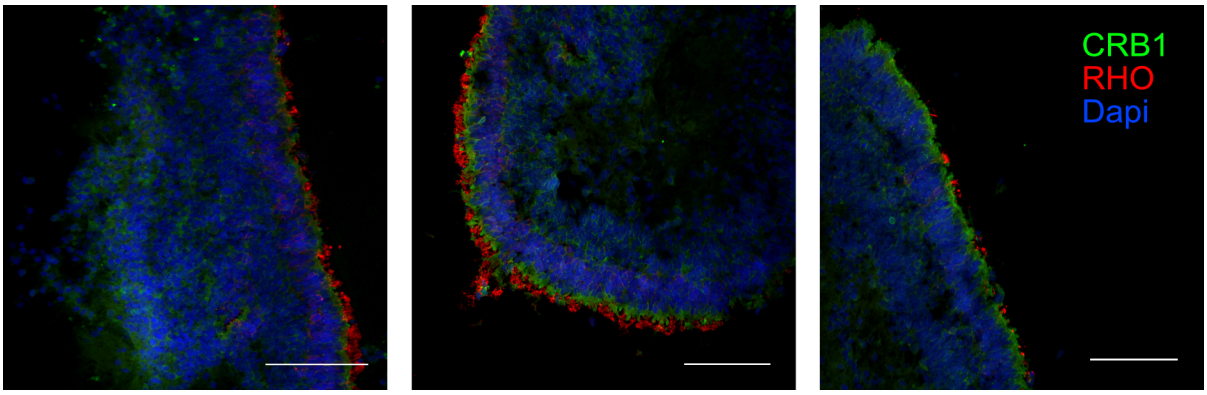

Figure 22. Photoreceptors within hESC-derived retinal organoids.

CRB1 is properly localized proximal to the rhodopsin expressing outer segment. N=3. Scale bars, 100 µm.

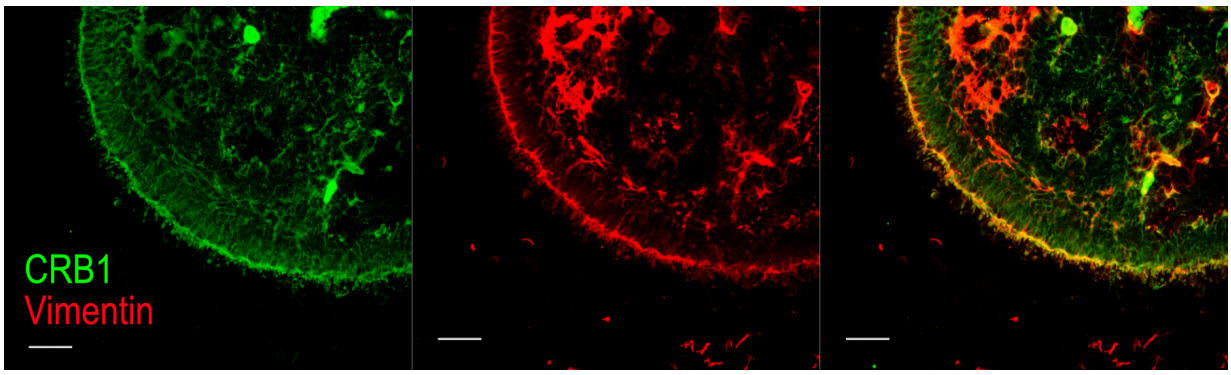

Figure 23. Müller glial cells within hESC-derived retinal organoids.

CRB1 is co-localized with vimentin expressing glial cells. N=3. Scale bars equals 100 µm.

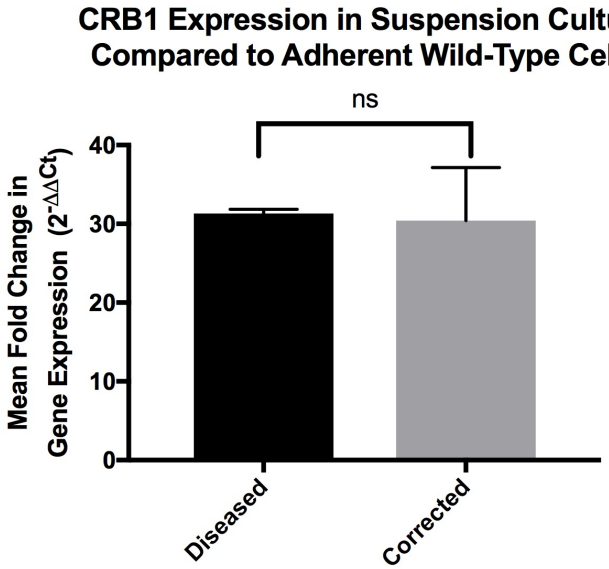

Figure 24. Expression of CRB1 RNA.

Suspension culture of patient-derived retinal organoids express significantly higher levels of CRB1 than adherent cultures.

4. Discussion

In these experiments, we show that CRB1 is expressed at the transcript and protein level in retinal organoids and is correctly localized to the photoreceptor inner segment in suspension culture. This is the first demonstration that CRB1 co-localizes to vimentin in retinal organoids. This implies that CRB1 may be expressed in both the photoreceptor inner segment as well as Müller glial cells.

In disease modeling, the correction of a mutation in a patient-derived line and subsequent functional rescue can demonstrate the necessity of a mutation. In contrast, the introduction of a mutation into wild-type stem cells and subsequent pathology can demonstrate the sufficiency of a mutation (**Figure 1**). This distinction is especially useful in the case of the current patient that has two different recessive mutations. To address the issue of sufficiency, CRISPR-induced mutations have been introduced into wild-type alleles at amino acid positions 698 or 878. Although there has been significant progress in gene-correction using CRISPR/Cas9, it is only just recently that detailed protocols have been provided for obtaining gene-corrected cells[115]. The gene-corrected clones produced thus far have resulted in truncated versions of the CRB1 protein rather than the introduction of a specific point mutation.

Although the CRISPR-edited lines for the CRB1 RP12 patient cells have not been useful thus far, the gene-corrected lines from the PRPF8 RP13 patient provide an opportunity to observe the genetic expression of CRB1 in unedited and CRISPR-edited cell lines. As expected, the suspension retinal organoids expressed high levels of CRB1 transcript relative to the wild-type adherent neural retina. Wild-type iPSCs

were left in adherent culture to ensure ample amounts of RNA to include in all PCR experiments as a control. As the yield of the production of retinal organoids is improved, it may be possible to collect sufficient amounts of RNA from suspension culture to serve as a wild-type control.

With regards to protein expression and localization of CRB1, we hypothesized that the mutated CRB1 would result in abnormal CRB1 localization or complete absence in the Müller glia and photoreceptors. This was based on speculation from three current mouse models *Crb1*$^{-/-}$, *Crb1*$^{C294W/-}$, *Crb1*^{rd8} that demonstrated the loss of adherens junctions at the outer limiting membrane[131]. Initial immunofluorescence analysis showed there was not a complete loss of CRB1 expression at the inner segment of the photoreceptors. However, the truncated version of the protein may not mimic the patient-specific mutation. Furthermore, the crumbs complex in mice is vastly different than that found in humans, indicating that results from the mouse model may not be an accurate representation of the human retina.

C. Conclusions

Our findings demonstrate that PRPF8 patient-derived cells can produce retinal organoids. In addition, we show that retinal organoids express CRB1 protein. Earlier work has shown the ability to differentiate stem cells into neural retina organoids, and it is vital to show the reproducibility of the differentiation process across diseased and wild-type stem cells. While morphological differences were not identified or quantified for the PRPF8 diseased retinal organoids, the presence of CRB1 and the functional role of CRB1 in cell-to-cell junctions provide an avenue for future morphological studies in disease modeling of autosomal recessive retinitis pigmentosa.

V. Reference List

1. Masland, R. H. The fundamental plan of the retina. *Nat. Neurosci.* **4,** 877–886 (2001).

2. Hartong, D. T., Berson, E. L. & Dryja, T. P. Retinitis pigmentosa. *Lancet* 1795–1809 (2006).

3. Kostic, C. & Arsenijevic, Y. Animal modelling for inherited central vision loss. *J. Pathol.* **238,** 300–310 (2016).

4. Van Cruchten, S. *et al.* Pre- and Postnatal Development of the Eye: A Species Comparison. *Birth Defects Res.* **109,** 1540–1567 (2017).

5. Wiley, L. A. *et al.* Patient-specific induced pluripotent stem cells (iPSCs) for the study and treatment of retinal degenerative diseases. *Prog. Retin. Eye Res.* **44,** (2015).

6. Daiger, S. P., Sullivan, L. S. & Bowne, S. J. Genes and mutations causing retinitis pigmentosa. *Clin. Genet.* **84,** 132–141 (2013).

7. Daiger, S. P., Bowne, S. J. & Sullivan, L. S. Genes and Mutations Causing Autosomal Dominant Retinitis Pigmentosa. *Cold Spring Harb Perspect Med* **5,** 17129 (2014).

8. Farkas, M. H. *et al.* Mutations in Pre-mRNA processing factors 3, 8, and 31 cause dysfunction of the retinal pigment epithelium. *Am. J. Pathol.* **184,** 2641–2652 (2014).

9. Jin, Z. B. *et al.* Modeling retinal degeneration using patient-specific induced pluripotent stem cells. *PLoS One* **6,** (2011).

10. Jin, Z.-B., Okamoto, S., Xiang, P. & Takahashi, M. Integration-free induced pluripotent stem cells derived from retinitis pigmentosa patient for disease modeling. *Stem Cells Transl. Med.* **1,** 503–9 (2012).

11. Yoshida, T. *et al.* The use of induced pluripotent stem cells to reveal pathogenic gene mutations and explore treatments for retinitis pigmentosa. *Mol. Brain* **7,** 45 (2014).

12. Tucker, B. A. *et al.* Patient-specifc iPSC-derived photoreceptor precursor cells as a means to investigate retinitis pigmentosa. *Elife* **2013,** 1–18 (2013).

13. McGee, T. L., Seyedahmadi, B. J., Sweeney, M. O., Dryja, T. P. & Berson, E. L. Novel mutations in the long isoform of the USH2A gene in patients with Usher syndrome type II or non-syndromic retinitis pigmentosa. *J. Med. Genet.*

47, 499–506 (2010).

14. Tucker, B. A. *et al.* Exome sequencing and analysis of induced pluripotent stem cells identify the cilia-related gene male germ cell-associated kinase (MAK) as a cause of retinitis pigmentosa. *Proc. Natl. Acad. Sci.* **108,** E569–E576 (2011).

15. Arno, G. *et al.* Mutations in REEP6 Cause Autosomal-Recessive Retinitis Pigmentosa. *Am. J. Hum. Genet.* **99,** 1305–1315 (2016).

16. Li, Y. *et al.* Gene therapy in patient-specific stem cell lines and a preclinical model of retinitis pigmentosa with membrane frizzled-related protein defects. *Mol. Ther.* **22,** 1688–1697 (2014).

17. Schwarz, N. *et al.* Translational read-through of the RP2 Arg120stop mutation in patient iPSC-derived retinal pigment epithelium cells. *Hum. Mol. Genet.* **24,** 972–986 (2015).

18. Schwarz, N. *et al.* Arl3 and RP2 regulate the trafficking of ciliary tip kinesins. *Hum. Mol. Genet.* **26,** 2480–2492 (2017).

19. Lukovic, D. *et al.* Human iPSC derived disease model of MERTK-associated retinitis pigmentosa. *Sci. Rep.* **5,** 1–11 (2015).

20. Ramsden, C. M. *et al.* Rescue of the MERTK phagocytic defect in a human iPSC disease model using translational read-through inducing drugs. *Sci. Rep.* **7,** 51 (2017).

21. Sharma, T. P. *et al.* Patient-specific induced pluripotent stem cells to evaluate the pathophysiology of TRNT1 -associated Retinitis pigmentosa. *Stem Cell Res.* **21,** 58–70 (2017).

22. Megaw, R. *et al.* Gelsolin dysfunction causes photoreceptor loss in induced pluripotent cell and animal retinitis pigmentosa models. *Nat. Commun.* **8,** (2017).

23. Yu, J. *et al.* Induced pluripotent stem cell lines derived from human somatic cells. *Science (80-.).* **318,** 1917–20 (2007).

24. Takahashi, K. *et al.* Induction of Pluripotent Stem Cells from Adult Human Fibroblasts by Defined Factors. *Cell* **131,** 861–872 (2007).

25. Hu, K. *et al.* Efficient generation of transgene-free induced pluripotent stem cells from normal and neoplastic bone marrow and cord blood mononuclear cells. *Blood* **117,** 109–119 (2011).

26. Zhou, T. *et al.* Generation of Induced Pluripotent Stem Cells from Urine. *J. Am.*

Soc. Nephrol. **22,** 1221–1228 (2011).

27. Phillips, M. J. *et al.* Modeling human retinal development with patient-specific induced pluripotent stem cells reveals multiple roles for visual system homeobox 2. *Stem Cells* **32,** 1480–1492 (2014).

28. Phillips, M. J. *et al.* Blood-derived human iPS cells generate optic vesicle-like structures with the capacity to form retinal laminae and develop synapses. *Invest. Ophthalmol. Vis. Sci.* **53,** 2007–2019 (2012).

29. Hu, Q., Friedrich, A. M., Johnson, L. V. & Clegg, D. O. Memory in induced pluripotent stem cells: Reprogrammed human retinal-pigmented epithelial cells show tendency for spontaneous redifferentiation. *Stem Cells* **28,** 1981–1991 (2010).

30. Howden, S. E. *et al.* A Cas9 Variant for Efficient Generation of Indel-Free Knockin or Gene- Corrected Human Pluripotent Stem Cells. *Stem Cell Reports* **7,** 1–12 (2016).

31. Wiley, L. A. *et al.* cGMP production of patient-specific iPSCs and photoreceptor precursor cells to treat retinal degenerative blindness. *Nat. Publ. Gr.* 22–24 (2016).

32. Kim, H. & Kim, J. S. A guide to genome engineering with programmable nucleases. *Nat. Rev. Genet.* **15,** 321–334 (2014).

33. Jinek, M. *et al.* A Programmable Dual-RNA-Guided DNA Endonuclease in Adaptive Bacterial Immunity. *Science (80-.).* **337,** 816–821 (2012).

34. Burnight, E. R. *et al.* Using CRISPR-Cas9 to Generate Gene-Corrected Autologous iPSCs for the Treatment of Inherited Retinal Degeneration. *Mol. Ther.* **25,** 1999–2013 (2017).

35. Burnight, E. R. *et al.* CEP290 gene transfer rescues Leber congenital amaurosis cellular phenotype. *Gene Ther.* **21,** 662–672 (2014).

36. Parfitt, D. A. *et al.* Identification and Correction of Mechanisms Underlying Inherited Blindness in Human iPSC-Derived Optic Cups. *Cell Stem Cell* **18,** 769–781 (2016).

37. Shimada, H. *et al.* In vitro modeling using ciliopathy patient-derived cells reveals distinct cilia dysfunctions caused by CEP290 mutations. *Cell Rep.* **20,** 384–396 (2017).

38. Greenwald, D. L., Cashman, S. M. & Kumar-Singh, R. Engineered zinc finger nuclease-mediated homologous recombination of the human rhodopsin gene.

Investig. Ophthalmol. Vis. Sci. **51,** 6374–6380 (2010).

39. Zhang, Z. *et al.* CRISPR/Cas9 Genome-Editing System in Human Stem Cells: Current Status and Future Prospects. *Mol. Ther. - Nucleic Acids* **9,** 230–241 (2017).

40. Guo, D. *et al.* Creating a patient carried Men1 gene point mutation on wild type iPSCs locus mediated by CRISPR/Cas9 and ssODN. *Stem Cell Res.* **18,** 67–69 (2017).

41. Howden, S. E. *et al.* Simultaneous Reprogramming and Gene Correction of Patient Fibroblasts. *Stem Cell Reports* **2,** 810–824 (2014).

42. Veres, A. *et al.* Low Incidence of Off-Target Mutations in Individual CRISPR-Cas9 and TALEN Targeted Human Stem Cell Clones Detected by Whole-Genome Sequencing. *Cell Stem Cell* **15,** 27–30 (2014).

43. Schaefer, K. A. *et al.* Unexpected mutations after CRISPR – Cas9 editing in vivo Digenome-seq web tool for profiling CRISPR specificity. *Nature* **14,** 547–548 (2017).

44. Klimanskaya, I. *et al.* Derivation and Comparative Assessment of Retinal Pigment Epithelium from Human Embryonic Stem Cells Using Transcriptomics. *Cloning Stem Cells* **6,** 217–245 (2004).

45. Leach, L. L. & Clegg, D. O. Concise Review: Making Stem Cells Retinal: Methods for Deriving Retinal Pigment Epithelium and Implications for Patients with Ocular Disease. *Stem Cells* **33,** 2363–2373 (2015).

46. Maruotti, J. *et al.* Small-molecule–directed, efficient generation of retinal pigment epithelium from human pluripotent stem cells. *Proc. Natl. Acad. Sci.* **112,** 10950–10955 (2015).

47. Leach, L. L. *et al.* Induced Pluripotent Stem Cell-Derived Retinal Pigmented Epithelium: A Comparative Study Between Cell Lines and Differentiation Methods. *J. Ocul. Pharmacol. Ther.* **32,** jop.2016.0022 (2016).

48. Choudhary, P. *et al.* Directing Differentiation of Pluripotent Stem Cells Toward Retinal Pigment Epithelium Lineage. **00602,** 75–86 (2016).

49. Lamba, D. A., Karl, M. O., Ware, C. B. & Reh, T. A. Efficient generation of retinal progenitor cells from human embryonic stem cells. *Proc. Natl. Acad. Sci. U. S. A.* **103,** 12769–74 (2006).

50. Osakada, F. *et al.* Toward the generation of rod and cone photoreceptors from mouse, monkey and human embryonic stem cells. *Nat. Biotechnol.* **26,** 215–224

(2008).

51. Ohlemacher, S. K., Iglesias, C. L., Sridhar, A., Gamm, D. M. & Meyer, J. S. Generation of Highly Enriched Populations of Optic Vesicle − Like Retinal Cells from Human Pluripotent Stem Cells. *Curr. Protoc. Stem Cell Biol.* 1–20 (2015).

52. Zhong, X. *et al.* Generation of three-dimensional retinal tissue with functional photoreceptors from human iPSCs. *Nat. Commun.* (2014).

53. Nakano, T. *et al.* Self-formation of optic cups and storable stratified neural retina from human ESCs. *Cell Stem Cell* **10,** 771–785 (2012).

54. Lowe, A., Harris, R., Bhansali, P., Cvekl, A. & Liu, W. Intercellular Adhesion-Dependent Cell Survival and ROCK-Regulated Actomyosin-Driven Forces Mediate Self-Formation of a Retinal Organoid. *Stem Cell Reports* **6,** 1–9 (2016).

55. Llonch, S., Carido, M. & Ader, M. Organoid technology for retinal repair. *Developmental Biology* **433,** 132–143 (2017).

56. Capowski, E. E. *et al.* Regulation of WNT Signaling by VSX2 During Optic Vesicle Patterning in Human Induced Pluripotent Stem Cells. *Stem Cells* 417–426 (2016).

57. Chen, H. Y., Kaya, K. D., Dong, L. & Swaroop, A. Three-dimensional retinal organoids from mouse pluripotent stem cells mimic in vivo development with enhanced stratification and rod photoreceptor differentiation. *Mol. Vis.* **22,** 1077–1094 (2018).

58. Browne, A. W. *et al.* Structural and Functional Characterization of Human Stem-Cell-Derived Retinal Organoids by Live Imaging. *Invest. Ophthalmol. Vis. Sci.* (2017).

59. May-Simera, H. L. *et al.* Primary Cilium Mediated Retinal Pigment Epithelium Maturation is Retarded in Ciliopathy Patient Cells. *Cell Rep.* 189–205 (2018).

60. Ortmann, D. & Vallier, L. Variability of human pluripotent stem cell lines. *Curr. Opin. Genet. Dev.* **46,** 179–185 (2017).

61. Tuson, M., Garanto, A., Gonzàlez-Duarte, R. & Marfany, G. Overexpression of CERKL, a gene responsible for retinitis pigmentosa in humans, protects cells from apoptosis induced by oxidative stress. *Mol. Vis.* **15,** 168–180 (2009).

62. Fathinajafabadi, A., Pérez-Jiménez, E., Riera, M., Knecht, E. & Gonzàlez-Duarte, R. CERKL, a retinal disease gene, encodes an mRNA-binding protein that localizes in compact and untranslated mRNPs associated with

microtubules. *PLoS One* **9,** (2014).

63. Vaajasaari, H. *et al.* Toward the defined and xeno-free differentiation of functional human pluripotent stem cell-derived retinal pigment epithelial cells. *Mol. Vis.* **17,** 558–75 (2011).

64. Borooah, S. *et al.* Using human induced pluripotent stem cells to treat retinal disease. *Prog. Retin. Eye Res.* **37,** (2013).

65. Strauss, O. The Retinal Pigment Epithelium in Visual Function. *Physiol Rev* 845–881 (2005).

66. Pennington, B. O. & Clegg, D. O. Pluripotent Stem Cell-Based Therapies in Combination with Substrate for the Treatment of Age-Related Macular Degeneration. *J. Ocul. Pharmacol. Ther.* **32,** 261–271 (2016).

67. Buchholz, D. E. *et al.* Rapid and Efficient Directed Differentiation of Human Pluripotent Stem Cells Into Retinal Pigmented Epithelium. *Stem Cells Transl. Med.* **2,** 384–393 (2013).

68. Clegg, D. O. *et al.* in *Stem Cell Research and Therapeutics* (eds. Shi, Y. & Clegg, D. O.) 1–24 (Springer Netherlands, 2008).

69. Leach, L. L., Buchholz, D. E., Nadar, V. P., Lowenstein, S. E. & Clegg, D. O. Canonical/β-catenin wnt pathway activation improves retinal pigmented epithelium derivation from human embryonic stem cells. *Investig. Ophthalmol. Vis. Sci.* **56,** 1002–1013 (2015).

70. Pennington, B. O., Clegg, D. O., Melkoumian, Z. K. & Hikita, S. T. Defined Culture of Human Embryonic Stem Cells and Xeno-Free Derivation of Retinal Pigmented Epithelial Cells on a Novel, Synthetic Substrate. **4,** 165–177 (2015).

71. Mazzoni, F., Safa, H. & Finnemann, S. C. Understanding photoreceptor outer segment phagocytosis: Use and utility of RPE cells in culture. *Experimental Eye Research* **126,** 51–60 (2014).

72. Sonoda, S. *et al.* A protocol for the culture and differentiation of highly polarized human retinal pigment epithelial cells. *Nat. Protoc.* **4,** 662–673 (2009).

73. Lane, A. *et al.* Engineering Efficient Retinal Pigment Epithelium Differentiation From Human Pluripotent Stem Cells. *Stem Cells Transl. Med.* **3,** 1295–1304 (2014).

74. Thomson, J. A. Embryonic Stem Cell Lines Derived from Human Blastocysts. *Science (80-.).* **282,** 1145–1147 (1998).

75. Amit, M. & Itskovitz-Eldor, J. Derivation and spontaneous differentiation of

human embryonic stem cells. *Journal of Anatomy* **200,** 225–232 (2002).

76. Kent, L. Culture and Maintenance of Human Embryonic Stem Cells. *J. Vis. Exp.* 3–5 (2009).

77. Croze, R. H. *et al.* ROCK Inhibition Extends Passage of Pluripotent Stem Cell-Derived Retinal Pigmented Epithelium. *Stem Cells Transl. Med.* **3,** 1066–1078 (2014).

78. Lin, H. & Clegg, D. O. Integrin av/35 Participates in the Binding of Photoreceptor Rod Outer Segments during Phagocytosis by Cultured Human Retinal Pigment Epithelium. *Invest Ophthalmol Vis Sci* **39,** 1703–1712 (1998).

79. Cao, H. *et al.* Temporal and tissue specific regulation of RP-Associated splicing factor genes PRPF3, PRPF31 and PRPC8-implications in the pathogenesis of RP. *PLoS One* **6,** (2011).

80. Grainger, R. J. Prp8 protein: At the heart of the spliceosome. *RNA* **11,** 533–557 (2005).

81. Garcia-Blanco, M. A., Anderson, G. J., Beggs, J. & Sharp, P. A. A mammalian protein of 220 kDa binds pre-mRNAs in the spliceosome: a potential homologue of the yeast PRP8 protein. *Proc Natl Acad Sci U S A* **87,** 3082–3086 (1990).

82. Whittaker, E., Lossky, M. & Beggs, J. D. Affinity purification of spliceosomes reveals that the precursor RNA processing protein PRP8, a protein in the U5 small nuclear ribonucleoprotein particle, is a component of yeast spliceosomes. *Proc Natl Acad Sci U S A* **87,** 2216–2219 (1990).

83. Pinto, A. L. & Steitz, J. A. The mammalian analogue of the yeast PRP8 splicing protein is present in the U4/5/6 small nuclear ribonucleoprotein particle and the spliceosome. *Proc Natl Acad Sci U S A* **86,** 8742–8746 (1989).

84. Boon, K.-L. *et al.* prp8 mutations that cause human retinitis pigmentosa lead to a U5 snRNP maturation defect in yeast. *Nat. Struct. Mol. Biol.* **14,** 1077–1083 (2007).

85. Trifunović, D. *et al.* A high-resolution RNA expression atlas of retinitis pigmentosa genes in human and mouse retinas. *Investig. Ophthalmol. Vis. Sci.* **49,** 2330–2336 (2008).

86. Bertram, K. *et al.* Cryo-EM Structure of a Pre-catalytic Human Spliceosome Primed for Activation. *Cell* **170,** 701–713.e11 (2017).

87. Will, C. L. & Lührmann, R. Spliceosome structure and function. *Cold Spring*

Harb. Perspect. Biol. **3,** 1–2 (2011).

88. Pena, V., Liu, S., Bujnicki, J. M., Lührmann, R. & Wahl, M. C. Structure of a Multipartite Protein-Protein Interaction Domain in Splicing Factor Prp8 and Its Link to Retinitis Pigmentosa. *Mol. Cell* **25,** 615–624 (2007).

89. Zhang, L. *et al.* Crystal structure of the C-terminal domain of splicing factor Prp8 carrying retinitis pigmentosa mutants. *Protein Sci.* **16,** 1024–1031 (2007).

90. Liu, M. M. & Zack, D. J. Alternative splicing and retinal degeneration. *Clinical Genetics* **84,** 142–149 (2013).

91. Mordes, D. *et al.* Pre-mRNA splicing and retinitis pigmentosa. *Mol. Vis.* **12,** 1259–71 (2006).

92. Martínez-Gimeno, M. *et al.* Mutations in the pre-mRNA splicing-factor genes PRPF3, PRPF8, and PRPF31 in Spanish families with autosomal dominant retinitis pigmentosa. *Investig. Ophthalmol. Vis. Sci.* **44,** 2171–2177 (2003).

93. McKie, A. B. *et al.* Mutations in the pre-mRNA splicing factor gene PRPC8 in autosomal dominant retinitis pigmentosa (RP13). *Hum. Mol. Genet.* **10,** 1555–1562 (2001).

94. Testa, F. *et al.* Clinical phenotype of an Italian family with a new mutation in the PRPF8 gene. *Eur J Ophthalmol* **16,** 779–781 (2006).

95. Ziviello, C. *et al.* Molecular genetics of autosomal dominant retinitis pigmentosa (ADRP): a comprehensive study of 43 Italian families. *J. Med. Genet.* **42,** e47–e47 (2005).

96. Mali, P. *et al.* RNA-guided human genome engineering via Cas9. *Science* **339,** 823–6 (2013).

97. Sander, J. D. & Joung, J. K. CRISPR-Cas systems for editing, regulating and targeting genomes. *Nature Biotechnology* **32,** 347–350 (2014).

98. Kung, J. T. Y., Colognori, D. & Lee, J. T. Long Noncoding RNAs: Past, Present, and Future. *Genetics* **193,** 651–669 (2013).

99. Au, E. D., Fernandez-Godino, R., Kaczynksi, T. J., Sousa, M. E. & Farkas, M. H. Characterization of lincRNA expression in the human retinal pigment epithelium and differentiated induced pluripotent stem cells. *PLoS One* **12,** 1–17 (2017).

100. Li, F., Wen, X., Zhang, H. & Fan, X. Novel Insights into the Role of Long Noncoding RNA in Ocular Diseases. *Int J Mol Sci* **17,** 478 (2016).

101. Zhu, W., Xing, Q., Tao, J. & Lu, J. Identification of lncRNAs involved in biological regulation in early age-related macular degeneration. 7589–7602 (2017).

102. Beers, J. *et al.* Passaging and colony expansion of human pluripotent stem cells by enzyme-free dissociation in chemically defined culture conditions. *Nat. Protoc.* **7,** 2029–2040 (2013).

103. Maminishkis, A. *et al.* Confluent monolayers of cultured human fetal retinal pigment epithelium exhibit morphology and physiology of native tissue. *Investig. Ophthalmol. Vis. Sci.* **47,** 3612–3624 (2006).

104. Foltz, L. P. & Clegg, D. O. Rapid, Directed Differentiation of Retinal Pigment Epithelial Cells from Human Embryonic or Induced Pluripotent Stem Cells. *J. Vis. Exp.* **9,** 2–7 (2017).

105. Livak, K. J. & Schmittgen, T. D. Analysis of Relative Gene Expression Data Using Real-Time Quantitative PCR and the 2−ΔΔCT Method. *Methods* **25,** 402–408 (2001).

106. Love, M. I., Anders, S. & Huber, W. *Differential analysis of count data - the DESeq2 package*. *Genome Biology* **15,** (2014).

107. Chen, Y., Mccarthy, D., Robinson, M. & Smyth, G. K. edgeR : differential expression analysis of digital gene expression data User ' s Guide. (2015).

108. Osterreicher, C. H. *et al.* Fibroblast-specific protein 1 identifies an inflammatory subpopulation of macrophages in the liver. *Proc. Natl. Acad. Sci.* **108,** 308–313 (2011).

109. Johnson, A. A. *et al.* Bestrophin 1 and retinal disease. *Prog. Retin. Eye Res.* **58,** 45–69 (2017).

110. Robinson, M. D. & Oshlack, A. A scaling normalization method for differential expression analysis of RNA-seq data. *Genome Biol.* **11,** (2010).

111. Hogan, M. J., Wood, I. & Steinberg, R. H. Phagocytosis by pigment epithelium of human retinal cones. *Nature* **252,** 305–307 (1974).

112. Carr, A.-J. *et al.* Molecular characterization and functional analysis of phagocytosis by human embryonic stem cell-derived RPE cells using a novel human retinal assay. *Mol. Vis.* **15,** 283–95 (2009).

113. Mao, Y. & Finneman, S. C. Analysis of Photoreceptor Outer Segment Phagocytosis by RPE Cells in Culture. *Methods Mol Biol.* 285–295 (2014).

114. Mao, Y. & Finnemann, S. C. Analysis of Photoreceptor Outer Segment

Phagocytosis by RPE Cells in Culture. *Methods Mol. Biol.* **935,** 285–295 (2013).

115. Howden, S. E., Thomson, J. A. & Little, M. H. Simultaneous Reprogramming and Gene Editing of Human Fibroblasts. *Nat. Protoc.* **13,** 875–898 (2018).

116. Ferrè, F., Colantoni, A. & Helmer-Citterich, M. Revealing protein-lncRNA interaction. *Brief. Bioinform.* **17,** 106–116 (2016).

117. Goff, L. A. & Rinn, J. L. Linking RNA biology to lncRNAs. *Genome Res.* **25,** 1456–1465 (2015).

118. Yu, J. *et al.* REC8 functions as a tumor suppressor and is epigenetically downregulated in gastric cancer, especially in EBV-positive subtype. *Oncogene* **36,** 182–193 (2017).

119. Wheway, G., Parry, D. A. & Johnson, C. A. The role of primary cilia in the development and disease of the retina. *Organogenesis* **10,** 69–85 (2014).

120. Wheway, G. *et al.* An siRNA-based functional genomics screen for the identification of regulators of ciliogenesis and ciliopathy genes. *Nat. Cell Biol.* **17,** 1074–1087 (2015).

121. Hyun, J. *et al.* Genome-wide screen identifies novel machineries required for both ciliogenesis and cell cycle arrest upon serum starvation. *BBA - Mol. Cell Res.* **1863,** 1307–1318 (2016).

122. Eiraku, M. *et al.* Self-organizing optic-cup morphogenesis in three-dimensional culture. *Nature* **472,** 51–58 (2011).

123. Den Hollander, A. I. *et al.* Mutations in a human homologue of Drosophila crumbs cause retinitis pigmentosa (RP12). *Nat. Genet.* **23,** 217–221 (1999).

124. Pellikka, M. *et al.* Crumbs, the Drosophlia homologue of human CRB1/RP12, is essential for photoreceptor morhogenesis. *Nature* **416,** (2002).

125. Li, L. *et al.* Detection of variants in 15 genes in 87 unrelated Chinese patients with Leber congenital amaurosis. *PLoS One* **6,** 5–10 (2011).

126. Jinda, W. *et al.* Whole exome sequencing in Thai patients with retinitis pigmentosa reveals novel mutations in six genes. *Invest. Ophthalmol. Vis. Sci.* **55,** 2259–68 (2014).

127. Mehalow, A. K. *et al.* CRB1 is essential for external limiting membrane integrity and photoreceptor morphogenesis in the mammalian retina. *Hum. Mol. Genet.* **12,** 2179–2189 (2003).

128. Pellissier, L. P. *et al.* Gene therapy into photoreceptors and Müller glial cells

restores retinal structure and function in CRB1 retinitis pigmentosa mouse models. *Hum. Mol. Genet.* **24,** 3104–3118 (2014).

129. Bernal, S. *et al.* Study of the involvement of the RGR, CRPB1, and CRB1 genes in the pathogenesis of autosomal recessive retinitis pigmentosa. *J Med Genet* **40,** e89 (2003).

130. Henderson, R. H. *et al.* Phenotypic variability in patients with retinal dystrophies due to mutations in CRB1. *Br. J. Ophthalmol.* **95,** 811–817 (2011).

131. Quinn, P. M., Pellissier, L. P. & Wijnholds, J. The CRB1 complex: Following the trail of crumbs to a feasible gene therapy strategy. *Front. Neurosci.* **11,** (2017).

132. Deng, W. L. *et al.* Gene Correction Reverses Ciliopathy and Photoreceptor Loss in iPSC-Derived Retinal Organoids from Retinitis Pigmentosa Patients. *Stem Cell Reports* **10,** 1–15 (2018).

133. Lustremant, C. *et al.* Human induced pluripotent stem cells as a tool to model a form of Leber congenital amaurosis. *Cell. Reprogram.* **15,** 233–46 (2013).

134. Tucker, B. A. *et al.* Using patient specific iPSCs to interrogate the pathogenicity of a novel RPE65 cryptic splice site mutation and confirm eligibility for enrollment into a clinical gene augmentation trial. *Transl. Res.* **166,** 48–56 (2015).

135. Howden, S. E. *et al.* Genetic correction and analysis of induced pluripotent stem cells from a patient with gyrate atrophy. *Proc. Natl. Acad. Sci.* **108,** 6537–6542 (2011).

136. Meyer, J. S. *et al.* Optic Vesicle-like Structures Derived from Human Pluripotent Stem Cells Facilitate a Customized Approach to Retinal Disease Treatment. *Stem Cells* **29,** 1206–1218 (2012).

137. Sangermano, R. *et al.* Photoreceptor Progenitor mRNA Analysis Reveals Exon Skipping Resulting from the ABCA4 c.5461-10T→C Mutation in Stargardt Disease. *Ophthalmology* **123,** 1375–1385 (2016).

138. Aukrust, I. *et al.* The intronic ABCA4 c.5461-10T>C variant, frequently seen in patients with Stargardt disease, causes splice defects and reduced ABCA4 protein level. *Acta Ophthalmol.* **95,** 240–246 (2017).

139. Singh, R. *et al.* iPS cell modeling of best disease: Insights into the pathophysiology of an inherited macular degeneration. *Hum. Mol. Genet.* **22,** 593–607 (2013).

140. Li, Y. *et al.* Patient-specific mutations impair BESTROPHIN1's essential role in

mediating Ca 2+ -dependent Cl- currents in human RPE. *Elife* 1–23 (2017).

VI. Appendix

Table 1. Primary Antibodies

Target Protein	Clonality/ Immunoglobulin	Host	Source/ Catalog Number
RPE65	monoclonal/IgG1	mouse	Millipore/MAB5428
PMEL	monoclonal	mouse	Dako/ M0634
PRPF8	polyclonal	rabbit	abcam/ ab87433, ab79237
ZO-1	polyclonal	rabbit	abcam/ ab59720
BEST1	monoclonal/ IgG1	mouse	abcam/ ab2182
BRN3a	polyclonal	rabbit	Millipore/ AB5945
CRB1	polyclonal/ IgG	rabbit	abcam/ ab156282
RCVRN	monoclonal	mouse	abcam/ ab31928
RHO	monoclonal/ IgG1	mouse	Millipore/ MAB5316
VIM	polyclonal	chicken	Millipore/ AB5733
GAPDH	monoclonal/ IgG1	mouse	ThermoFisher/ MA5-15738

Table 2. Secondary Antibodies

Target	Fluorophore/ Immunoglobulin	Host	Source/ Catalog Number
anti-chicken	Cy3 / IgY, IgG (H+L)	donkey	Jackson Immuno/703-165-155
anti-mouse	Cy5 / IgG (H+L)	donkey	Jackson Immuno/715-175-150
anti-rabbit	Cy2 / IgG (H+L)	donkey	Jackson Immuno/711-225-152
anti-mouse	Cy3	donkey	Jackson Immuno/715-165-150
anti-rabbit	Cy3	donkey	Jackson Immuno/711-165-752
anti-mouse	800CW	donkey	LI-COR/ 925-32212
anti-rabbit	680RD	donkey	LI-COR/ 925-68073

Script 1. Differential Expression Analysis of RNA-Seq raw count data

```
# DE Analysis of RNA-seq data

# Load libraries
library(edgeR)
library(DESeq2)
library(limma)
library(Biobase)
library(org.Hs.eg.db)

# Reading in the data
rawdata <- read.delim("/Users/lfoltz/Desktop/DE_analysis/AllcountsV1_rearrange.txt", head=T)
head(rawdata)
rownames(rawdata)=rawdata[,1]
GeneSymbols = select(org.Hs.eg.db,keys=rownames(rawdata),columns="SYMBOL")
rawdata1=cbind(GeneSymbols, rawdata[,3:8])
colnames(rawdata1)=c("EntrezID","GeneSymbol","3","3_5","3_80","3_16","3_8","3_86_1")
group = c(1,1,1,2,2,2)

#Create DGE object
y <- DGEList(counts=rawdata1[,3:8], genes=rawdata1[,1:2], group=group)
y$samples

# Filtering out lowly expressed genes
keep <- rowSums(cpm(y)>1) >= 2
y <- y[keep, , keep.lib.sizes=FALSE]

# Normalization
y <- calcNormFactors(y)
y$samples

# Estimating Dispersions
y <- estimateCommonDisp(y)
y <- estimateTagwiseDisp(y)

#Plots
plotBCV(y)
plotMDS(y, top=100)

# Testing for DE genes
et <- exactTest(y)
topTags(et)
summary(de <- decideTestsDGE(et, p=.05))

results_edgeR <- topTags(et)
head(results_edgeR$table)
sum(results_edgeR$table$FDR < .05)
plotSmear(et, de.tags = rownames(results_edgeR)[results_edgeR$table$FDR < .05])
abline(h = c(-2, 2), col = "blue")
summary(dt <- decideTestsDGE(et))


# Data exploration
plotMDS(y, top=100)

plotMD(cpm(y, log=TRUE), column=1)
abline(h=0, col="red", lty=2, lwd=2)
```

Table 1. Retinitis Pigmentosa

Publication	iPSC source	Reprogramming method	Control iPSC; Rescue Yes/No	Gene; Mutation	# of patients	Cell type; Findings
[9]	skin biopsy/ fibroblast	retroviral transduction	wild-type; No	Axonemal Microtubule Associated (RP1); 721Lfs722X Pim-1 Kinase Associated Protein (RP9); H137L Peripherin 2 (PRPH2); W316G Rhodopsin (RHO); G188R	5	2D rod photoreceptor cells; expressed markers of cellular stress
[14]	skin biopsy/ fibroblast	lentiviral transduction	wild-type control & non-MAK RP iPSC control; No	Male germ cell-associated kinase (MAK); Alu insert	2	2D retinal progenitor cells; discovered pathogenic insertion
[10]	skin biopsy/ fibroblast	non-integrating Sendai-virus	wild-type; No	Rhodopsin (RHO); G188R	1	2D rod photoreceptor cells; ER stress, rod degeneration
[12]	keratinocytes	non-integrating Sendai-virus	wild-type and patient control; No	Usherin (USH2A); IVS0, Arg4192His	2	3D retinal organoid; demonstrated pathogenicity

[11]	skin biopsy/ fibroblast	retroviral transduction	wild-type; Yes, HDAdV	Rhodopsin (RHO); E181K	1	2D rod photoreceptor cells; ER stress and apoptosis
[16]	skin biopsy/ fibroblast	lentiviral transduction	wild-type; Yes AAV8	Membrane frizzle-related protein (MFRP); IVS10 +5G>A, 1-bp del 492C	2	RPE; actin disorganization
[17]	skin biopsy/ fibroblast	non-integrating episomal vectors	healthy, sex-matched control; Yes, TRID	ARL3 GTPase Activating Protein (RP2) (c.519C>T; p.R120X)	1	RPE; restored RP2 using TRID**
[19]	skin biopsy/ fibroblast	Sendai virus	healthy control; No	MER receptor tyrosine kinase (MERTK) (Ser331Cysfs*5)	1	RPE; phagocytosis defect
[15]	skin biopsy/ fibroblast	episomal plasmid vectors	wild-type; No	Receptor expression-enhancing protein 6 (REEP6) (various, incl. p.Leu135Pro)	7	3D retinal organoid; identified variants
[20]	skin biopsy/ fibroblast	episomal vectors	wild-type; Yes, TRID	MER receptor tyrosine kinase (MERTK) (61+1G>A, 1951C>T; biallelic)	1	RPE; restored MERTK, functional rescue of phagocytosis
[18]	skin biopsy/ fibroblast	non-integrating episomal vectors	healthy, sex-matched control Yes, TRID	ARL3 GTPase Activating Protein (RP2) (c.519C>T; p.R120X)	1	3D retinal organoid; restored RP2 using TRIDs**, rescue of Kif7 in cilia

[21]	skin biopsy/ fibroblast	Non-integrating Sendai virus	healthy, age-matched control; No	tRNA nucleotidyl transferase, CCA-adding 1 (TRNT1), various indels	3	3D retinal organoid; autophagy defect in retinal organoids, oxidative stress
[22]	skin biopsy/ fibroblast	lentiviral transduction	healthy sex-matched control; Yes; overexpression of gelsolin	X-linked retinitis pigmentosa GTPase regulator (RPGR) (g.ORF15+689−692del4)	2	3D retinal organoid; abnormal actin polymerization and rhodopsin mislocalization
[132]	urinary cells	lentiviral transduction	healthy control; Yes; CRISPR/Cas9	X-linked retinitis pigmentosa GTPase regulator (RPGR) (various frameshift)	3	RPE and 3D retinal organoid; rescued photoreceptor structure and electrophys.

Table 2. Leber Congenital Amaurosis

Publication	iPSC source	Reprogramming method	Control iPSC; Rescue Yes/No	Gene & Mutation	# of patients	Cell type; Findings
[133]	skin biopsy/ fibroblast	retroviral transduction	wild-type; No	unknown	2	2D neurons, RPE; identified differentially expressed genes
[35]	skin biopsy/ fibroblast	lentiviral transduction	JK1 fibroblast-like control; Yes, lentiviral transduction of CEP290	Centrosomal protein 290kDa (CEP290) (IVS26 (c.2991 + 1665A>G), various deletions)	4	Fibroblast; rescued ciliogenesis defect in fibroblasts
[134]	skin biopsy/ fibroblast	Non-integrating Sendai virus vector	wild-type iPSC; No	Retinal pigment epithelium-Specific 65kDa, retinoid isomerohydrolase (RPE65) (L408P, IVS3-11 A>G)	1	RPE; identified novel mutation
[36]	skin biopsy/ fibroblast	episomal vector, electroporation	wild-type; Yes, antisense oligonucleotide	Centrosomal protein 290kDa (CEP290) (IVS26 c.2991 + 1665A>G)	1	3D retinal organoid; functional rescue and improved ciliation
[37] (LCA and Joubert syndrome)	skin biopsy/ fibroblast	Non-integrating Sendai virus vector	4 healthy controls; No	Centrosomal protein 290kDa (CEP290) (2 heterozygotes, 1 homozygote (IVS26+1655A>G))	3	3D retinal organoid; observed ciliogenesis defects

[59] (Joubert syndrome)	skin biopsy/ fibroblast	Non-integrating Sendai virus vector	healthy sibling control; No	Centrosomal protein 290kDa (CEP290) (c.2495_2512, c. 5668 G>T; biallelic)	1	RPE; observed defective primary cilia

Table 3. Gyrate Atrophy

Publication	iPSC source	Reprogramming method	Control iPSC; Rescue Yes/No	Gene & Mutation	# of patients	Cell type; Findings
[135]	fibroblast (Coriell)	episomal vector	Yes, BAC-based vector	Ornithine-□-aminotransferase (OAT) (677C>T)	1	iPS; reduced mutational load
[136]	fibroblast (Coriell)	lentiviral vector	wild-type; Yes, BAC-mediated homologous recombination	Ornithine-□-aminotransferase (OAT) (A226V)	1	RPE; rescued OAT activity upon correction

Table 4. Stargardt macular dystrophy

Publication	iPSC source	Reprogramming method	Control iPSC; Rescue Yes/No	Gene & Mutation	# of patients	Cell type; Findings
[137]	skin biopsy/ fibroblast	lentiviral vector	healthy control, No	ATP-binding cassette transporter type A4 (ABCA4) (c.5461-10T → C)	17 total, 3 iPSC lines	2D photoreceptors; exon skipping
[138]	skin biopsy/ fibroblast	N/A	healthy control, No	ATP-binding cassette transporter type A4 (ABCA4) (c.5461-10T>C)	4	Fibroblasts; splice defects and reduction of ABCA4

Table 5. Best vitelliform macular dystrophy

Publication	iPSC source	Reprogramming method	Control iPSC; Rescue Yes/No	Gene & Mutation	# of patients	Cell type; Findings
[139]	skin biopsy/ fibroblast	lentiviral delivery	2 sibling controls; No	Bestrophin 1 (BEST1), A146K, N296H	2	RPE; observed disrupted fluid flux and POS handling
[140]	skin biopsy/ fibroblast	Non-integrating Sendai virus vector	age-matched controls; Yes, baculoviral vector	Bestrophin 1 (BEST1), P274R, I201T	2	RPE; restored BEST1 mediation of Cl^- current